Influence of Argon on Static Charge Mitigation in Pressurized Gas-Solid Fluidized Bed Reactors at Varying Temperatures and Concentrations

Talha Syed

Thesis submitted to the University of Ottawa
in partial fulfillment of the requirements for the
Master's Degree in Applied Science

Department of Chemical and Biological Engineering
Faculty of Engineering
University of Ottawa

Abstract

Electrostatic charge generation is inherent to gas-solid systems, including fluidized beds, due to repeated particle contacts with surrounding surfaces. In industrial solids processing operations, such as gas-phase polyethylene production, electrostatic charging is generated from particle interactions with each other and with the reactor wall, promoting particle agglomeration and wall adhesion of highly charged particles, leading to operational issues. These occurrences pose safety risks and necessitate reactor shutdowns and maintenance with substantial operational costs. This thesis investigates the impact of adding argon gas on mitigating electrostatic charge buildup in polyethylene gas-solid fluidized bed reactors under industrially relevant temperatures (up to 70°C) and pressures (up to 2600 kPa). Argon, which has a much lower dielectric strength than gases like nitrogen, was expected to help lower static charge buildup in the fluidized bed because of its ability to break down, leading to the dissipation of surface charge on polyethylene particles. A multi-scale experimental approach was employed, including gas dielectric strength measurement, bench-scale shake tests, and pilot-scale pressurized gas-solid fluidization experiments, to investigate the influence of argon gas breakdown behavior on the degree of static buildup and the resulting fluidized bed wall fouling for a commercially produced polyethylene resin at various concentrations and temperatures.

Bench-scale single-particle and multiple-particle shake tests were employed to simulate charging arising from particle-wall and particle-particle interactions within the fluidized bed, respectively. Tests using the polyethylene resin under nitrogen and argon at 23 and 65°C (± 2.5°C) showed that argon consistently resulted in lower saturation charge levels than nitrogen, while increasing temperature significantly reduced charge accumulation only for nitrogen, indicating gas-dependent charge dissipation behavior with temperature. A breakdown voltage measurement device was built in-house, and the dielectric strength of pure argon and nitrogen, and their mixtures (20, 50, 75, and 90 vol.%), were measured from atmospheric pressure up to 2600 kPa and temperatures of 25, 70, and 110°C (± 2°C). For all gases, dielectric strength increased with increasing pressure up to 2600 kPa, with argon consistently exhibiting a lower dielectric strength than nitrogen across all testing conditions. Minimal variation in dielectric strength with temperature between 25 and 70°C was seen, followed by a pronounced decrease for the pure gases at 110°C. In addition, argon-nitrogen mixtures exhibited intermediate dielectric behavior, with even 25 vol.% argon showing a

substantial reduction of approximately 40-45% in dielectric strength relative to pure nitrogen. Moreover, the dielectric strength data obtained in this work fill a critical gap, particularly at high temperature and pressure, and can be used as a reference for future studies.

Gas-solid fluidization at 2600 kPa and 25 ± 2°C and 68 ± 2°C demonstrated that increasing argon concentration and temperature reduced electrostatic charge accumulation in the bulk of the bed and the fouled layer on the column wall, resulting in mitigation of column wall fouling, with the influence of temperature diminishing under argon-rich conditions. Pure argon reduced wall fouling by approximately 70% compared to nitrogen at 2600 kPa and 68°C. Even at a low argon concentration of 25 vol.%, an approximately 30% reduction in wall fouling at 68°C was obtained. Importantly, the observed reduction trend in fouling with argon concentration strongly correlated with the dielectric strength trends for the gases, indicating the role of gas ionization in facilitating surface charge neutralization of the fluidizing particles.

Overall, the results obtained in this thesis confirmed that argon gas, even at low concentrations of approximately 25 vol.%, can be utilized in industrial gas-phase polyethylene fluidized bed reactors to mitigate static buildup and consequently reduce the wall sheeting occurrences. Beyond the specific system studied, the results of this thesis may also be relevant to other gas-solid handling and processing systems susceptible to static charge generation.

Résumé

La génération de charges électrostatiques est inhérente aux systèmes gaz-solide, y compris aux lits fluidisés, en raison des contacts répétés entre les particules et les surfaces environnantes. Dans les opérations industrielles de traitement des solides, telles que la production de polyéthylène en phase gazeuse, des charges électrostatiques sont générées par les interactions entre les particules elles-mêmes et avec la paroi du réacteur, favorisant l'agglomération des particules et l'adhésion pariétal de particules fortement chargées, ce qui entraîne des problèmes opérationnels. Ces phénomènes présentent des risques pour la sécurité et nécessitent des arrêts de réacteur et des opérations de maintenance impliquant des coûts d'exploitation importants. Cette thèse étudie l'impact de l'ajout de gaz argon sur l'atténuation de l'accumulation de charges électrostatiques dans des réacteurs de lit fluidisé gaz-solide de polyéthylène, dans des conditions industrielles pertinentes de température (jusqu'à 70°C) et de pression (jusqu'à 2600 kPa). L'argon, dont la rigidité diélectrique est beaucoup plus faible que celle de gaz tels que l'azote, était supposé contribuer à réduire l'accumulation de charges statiques dans le lit fluidisé grâce à sa capacité de claquage, conduisant à la dissipation des charges de surface sur les particules de polyéthylène. Une approche expérimentale multi-échelle a été mise en œuvre, comprenant des mesures de rigidité diélectrique des gaz, des essais de secouage à l'échelle du laboratoire et des expériences de fluidisation gaz-solide pressurisées à l'échelle pilote, afin d'étudier l'influence du comportement de claquage de l'argon sur le degré d'accumulation électrostatique et l'encrassement de la paroi du lit fluidisé pour une résine de polyéthylène commerciale, à différentes concentrations et températures.

Des essais de secouage à l'échelle du laboratoire, impliquant une seule particule ou plusieurs particules, ont été utilisés pour simuler respectivement les phénomènes de charge résultant des interactions particule-paroi et particule-particule au sein du lit fluidisé. Les essais réalisés avec la résine de polyéthylène sous azote et sous argon à 23 ± 2,5 et 65 ± 2,5°C ont montré que l'argon conduisait systématiquement à des niveaux de charge de saturation plus faibles que l'azote, tandis que l'augmentation de la température réduisait significativement l'accumulation de charges uniquement dans le cas de l'azote, indiquant que l'effet de la température sur la dissipation des charges dépend du type de gaz. Un dispositif de mesure de la tension de claquage a été conçu en interne, et la rigidité diélectrique de l'argon pur, de l'azote pur et de leurs mélanges (20, 50, 75 et 90% vol.) a été mesurée depuis la pression atmosphérique jusqu'à 2600 kPa, et à des températures de 25, 70 et 110°C (± 2°C). Pour tous les gaz, la rigidité diélectrique augmentait avec la pression

jusqu'à 2600 kPa, l'argon présentant systématiquement une rigidité diélectrique plus faible que l'azote pour l'ensemble des conditions expérimentales. Une variation minimale de la rigidité diélectrique avec la température entre 25 et 70°C a été observée, suivie d'une diminution marquée pour les gaz purs à 110°C. En outre, les mélanges argon-azote ont montré un comportement diélectrique intermédiaire, avec une réduction substantielle d'environ 40 à 45 % de la rigidité diélectrique par rapport à l'azote pur, même pour une teneur en argon de seulement 25% vol. La fluidisation gaz-solide à 2600 kPa et à 25 ± 2 et 68 ± 2°C a démontré que l'augmentation de la concentration en argon et de la température réduisait l'accumulation de charges électrostatiques dans le volume du lit et dans la couche encrassée sur la paroi de la colonne, conduisant à une atténuation de l'encrassement des parois, l'influence de la température diminuant dans des conditions riches en argon. L'argon pur a réduit l'encrassement des parois d'environ 70% par rapport à l'azote à 2600 kPa et 68°C. Même à une faible concentration d'argon de 25% vol., une réduction d'environ 30% de l'encrassement des parois à 68°C a été obtenue. Fait important, la tendance observée de réduction de l'encrassement avec l'augmentation de la concentration en argon était fortement corrélée aux tendances de rigidité diélectrique des gaz, indiquant le rôle de l'ionisation du gaz dans la facilitation de la neutralisation des charges de surface des particules fluidisées.

Dans l'ensemble, les résultats obtenus dans cette thèse confirment que le gaz argon, même à de faibles concentrations d'environ 25% vol., peut être utilisé dans des réacteurs industriels de lit fluidisé en phase gazeuse pour la production de polyéthylène afin d'atténuer l'accumulation de charges statiques et, par conséquent, de réduire les phénomènes d'encrassement pariétal. Au-delà du système spécifique étudié, les résultats de cette thèse peuvent également être pertinents pour d'autres systèmes de manipulation et de traitement gaz-solide susceptibles de générer des charges électrostatiques.

Statement of Contribution of Collaborators

All chapters presented in this thesis were written by me, with editorial comments and guidance provided by my supervisor, Professor Poupak Mehrani. The research team at Univation Technologies, LLC (USA) provided valuable insight to ensure the industrial relevance and applicability of the results to polyethylene reactor systems.

Chapter 2 is compiled as a manuscript submitted for publication in a peer-reviewed academic journal. The majority of the experimental work, data analysis, and writing were performed by me. The relative humidity experiments included in this chapter were conducted by PhD student Grissel Myrtle Fernandes, with one additional set of experiments performed by MASc student Nikhil Sridhar. The experimental methodology and results sections corresponding to the humidity experiments were written by Grissel Myrtle Fernandes, while the remaining sections of the chapter were written by me. Editorial comments were provided by Professor Poupak Mehrani. All contributors are listed as co-authors on the manuscript.

Chapter 3 is compiled as a manuscript to be submitted for publication in a peer-reviewed academic journal. All experiments were designed and performed by me, with experimental assistance provided by postdoctoral fellow Dr. Mohsen I. Nimvari and PhD student Benjamin Hotte. Data analysis and writing of the chapter were done solely by me, with editorial comments provided by Professor Poupak Mehrani. Professor Mehrani and Dr. Nimvari are listed as co-authors on the manuscript.

Chapter 4 is compiled as a manuscript to be submitted for publication in a peer-reviewed academic journal. All experiments were designed and performed by me, with experimental assistance provided by postdoctoral fellow Dr. Mohsen I. Nimvari. Data analysis and writing were conducted solely by me, with editorial comments provided by Professor Poupak Mehrani, who is listed as a co-author.

Acknowledgements

I would like to express my sincere gratitude to my supervisor, Professor Poupak Mehrani, for her continuous guidance, encouragement, and support throughout my Master's program. Her commitment to mentorship, constructive feedback, and high academic standards consistently pushed me to perform at my best, and her supervision played a pivotal role in shaping this research.

I am also grateful to the team at Univation Technologies, LLC (USA), in particular Mr. John Szul, Dr. Kishori Deshpande, and Mr. David Pearson, for their valuable technical insight and for providing the experimental materials used in this study. Their contributions helped ensure the industrial relevance of the work presented in this thesis.

I would like to acknowledge the support and collaboration of my peers and colleagues, including postdoctoral fellows Dr. Mohsen I. Nimvari and Dr. Mizuki Shoyama, as well as PhD students Grissel Myrtle Fernandes, Benjamin Hotte, and Otome Obukohwo, whose discussions and assistance were greatly appreciated.

I also extend my appreciation to the staff of the Department of Chemical and Biological Engineering, particularly Franco Ziroldo, Patrick Pageau, Gérard Nina, and Frantz Célestin, for their technical support and assistance throughout the course of my research.

The financial support provided by the Natural Sciences and Engineering Research Council of Canada (NSERC) and Univation Technologies, LLC is gratefully acknowledged.

Lastly, I would like to convey my sincere gratitude to my family and friends for their unwavering encouragement and support throughout my Master's journey.

Table of Contents

List of Figures

List of Tables

Nomenclature

A	Gas constant
B	Gas constant
C	Capacitance, F
d	Gap/distance between electrodes, m
d_p	Particle diameter, m
d_{p50}	Median particle diameter, m
e	Electron Charge, -1.602×10^{-19} C
E	Electric field, V/m
$E_{conduction}$	Conduction band energy, J
$E_{valence}$	Valence band energy, J
E/P	Reduced electric field, V/mPa
i_0	Saturation charge, A
L/D	Column height-to-diameter ratio
n	Energy level
P	Gas pressure, Pa
P-value	Probability associated with statistical test
pd	Gas pressure-electrode distance product, Torr.cm, bar.mm
pd_{min}	Paschen minimum, Torr.cm
q	Surface charge, C
Q/m	Specific charge expressed as net charge over mass, nC/g
RH	Relative humidity, %
r_0	Equilibrium distance, m
T	Temperature, ºC
t	Time, s
U_{mf}	Minimum fluidization velocity, m/s
V	Voltage, V
V_B	Breakdown voltage, V
V_B/d	Dielectric strength, V/m
V_C	Contact charge potential, V

α	Townsend's first ionization coefficient
γ	Townsend's second ionization coefficient
ε_0	Permittivity of free space, C/Vm
λ	Mean free path, m
φ	Work function, eV, J

Chapter 1 Introduction

Industries that involve solids processing and handling often report electrostatic charge generation in their processes. These charges are a result of solids' contact with each other and nearby surfaces. This charge generation can often become a nuisance for efficient operation by causing challenges such as particle agglomeration and wall fouling. In some cases, these challenges can play a significant role in the operation and incur large economic losses to the industry.

One such process where electrostatic charge generation is regularly seen is gas-solid fluidization. In this process, gas is passed through a bed of solid particles, which can cause the bed to render a fluid-like state. The gas flow causes vigorous mixing of particles, which builds up charge on the particles as they collide with each other and the column wall. An example of an industrial process that employs gas-solid fluidization is the gas phase polymerization of ethylene into polyethylene. In this process, the catalyst and polyethylene particles are the sources of charge generation as they collide with each other and with the reactor wall. The charged particles then stick to the reactor wall, leading to wall fouling. Due to the exothermic nature of the reaction, the fouled particles melt over time and form "sheets" [1]. These sheets, if left unchecked, can fall and block the distributor plate, which necessitates reactor shutdown for many days, sometimes even exceeding months, depending on the severity of sheeting. Many parameters have been considered to affect the charge generation in these reactors, prompting various measures to mitigate the charge. However, to better deal with the issue of charge generation in gas-solid fluidized beds, it is important to first understand the mechanisms behind the charge generation inside these reactors.

1.1. Electrostatic fundamentals

This part of the thesis focuses on the mechanisms of how charges are generated and transferred between solids, specifically in gas-solid fluidized beds. Understanding the basics of charge generation and transfer would aid in developing mitigation techniques for charge generation in fluidized beds.

1.1.1 Charge generation

Electrostatic charge generation in solids is generally classified into three types: contact, frictional, and induction charging.

Solids, when in contact with each other, generate charges on each other's surfaces. The charges occur on the surface of the solids upon contact and separation. Solids can either just briefly come into contact with each other (Figure 1.1a) or have a rubbing motion (Figure 1.1b) to transfer charge. The latter case is also referred to as frictional charging. However, due to the difficulty in distinguishing the type of contact between solids, contact and frictional charging are collectively referred to as triboelectrification [2-5].

Induction charging (Figure 1.1c) occurs when a charged object (e.g., an insulator) is brought near a neutral conductor. Due to the proximity of the charged object to the conductor, the charge carriers in the conductor redistribute in such a way that the side facing the object acquires an opposite polarity charge. If the conductor is then grounded, charges of similar polarity to the charged object on the conductor would disperse to the ground, and the conductor would attain a charge opposite in polarity to the charged object. As a result, the charged object holds the opposite polarity charge on the conductor through the "image force". Unlike triboelectrification, induction charging does not require direct contact between the charged object and the conductor [2].

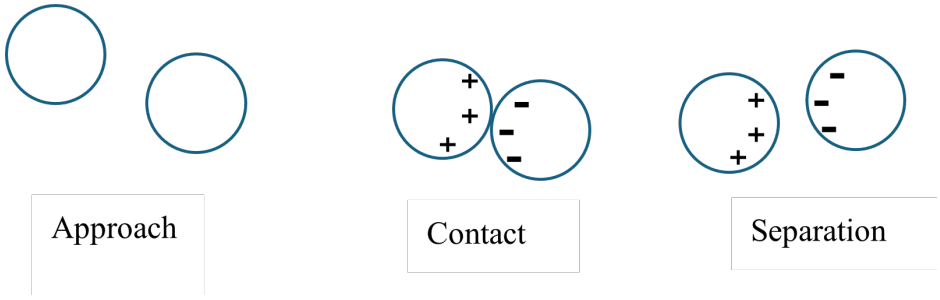

(a)

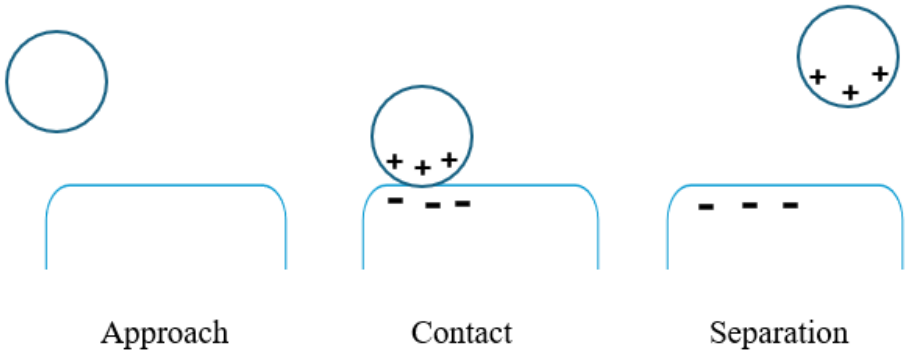

(b)

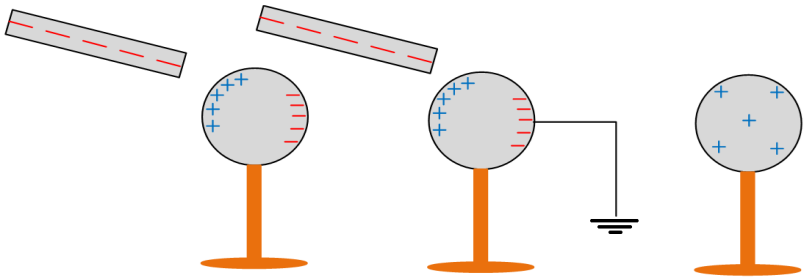

(c)

Figure 1.1: (a) Contact charging; (b) Frictional charging; (c) Induction charging

1.1.2. Electron energies

In an isolated atom, electrons occupy discrete energy levels or orbitals (Figure 1.2a), whose energy is determined based on their distance from the nucleus. Each orbital has a specific energy and can hold a fixed number of electrons. The electronic configuration of a material determines how these levels are filled and varies between different materials. However, in solids, many atoms are packed closely. This forces the electrons to interact with each other, resulting in an overlap of their respective energy levels (Figure 1.2b). These levels, after overlapping, form energy bands (Figure 1.2c), which the electrons can occupy [4].

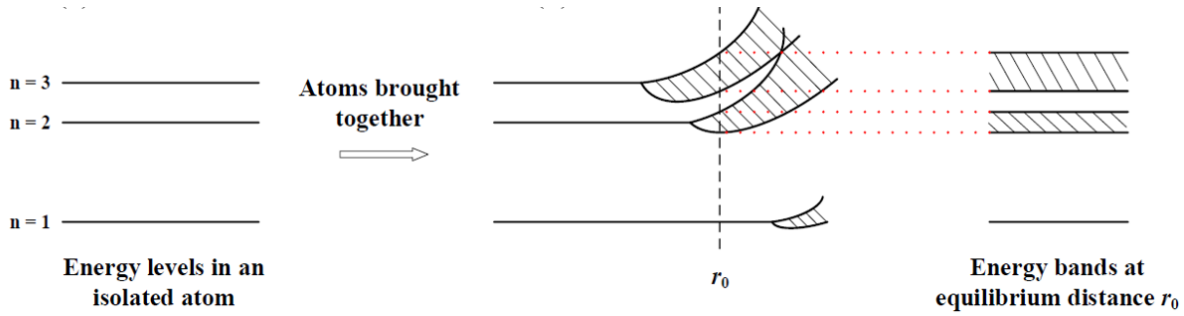

(a) (b) (c)

Figure 1.2: (a) Energy levels in an isolated atom; (b) variation in energies; (c) energy band at an equilibrium distance (copied from *[4]*).

The inner-shell electrons interact minimally with electrons from neighbouring atoms and form narrower bands, while the outer electrons overlap more with electrons in neighbouring atoms, forming a wider band, known as the valence band. Each energy band represents a range of allowed energies for electrons in a solid. The electrons in the valence band can get excited and move to the conduction band, which contains higher energy states. The distance between the valence and

conduction bands is known as the forbidden gap. The size of this band gap determines the conductivity of the substance.

Metals have a partially filled valence band which overlaps with the conduction band, making it easier for the electrons to gain energy and jump to the conduction band, making metals good conductors (Figure 1.3a). On the other hand, the valence band in insulators is filled and has a large forbidden gap (Figure 1.3b). The energy requirement for electrons to jump to the conduction band is quite high in the case of insulators. Semiconductors fall between these two extremes, possessing a smaller band gap than insulators that can be overcome through thermal, optical, or electrical excitation (Figure 1.3c).

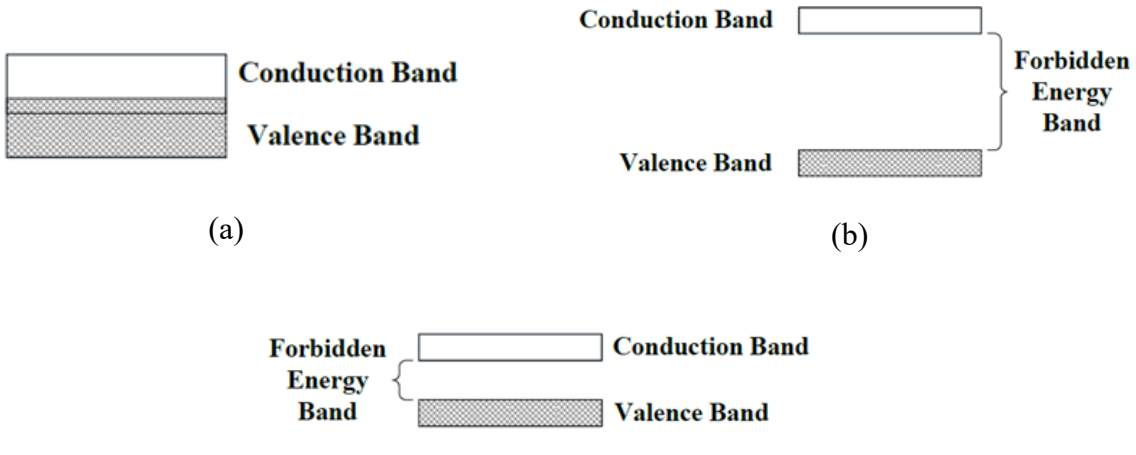

Figure 1.3: Energy band in (a) conductors; (b) insulators; (c) semi-conductors (copied from [4]).

1.1.3. Charge transfer mechanisms

The transfer of charge during solids charging arises through several underlying mechanisms, depending on whether the materials involved are metals or insulators. The type of contacts can be categorized as metal-metal, metal-insulator, and insulator-insulator. Each case follows a different dominant charge transfer mechanism, including electron transfer, ion transfer, and material transfer.

1.1.3.1. Electron transfer

This mechanism is primarily applicable to metal-metal type contacts, and to a lesser extent, to contacts involving insulators. In metals, this charge transfer is dominant due to a difference in their

work function. Work function is the energy required to move an electron from the material into a vacuum [4]. When two metals are brought into contact, the electrons will flow from the metal with a lower work function (i.e., higher Fermi level) to the one with a higher work function (i.e., lower Fermi level) until equilibrium is established. This mechanism is illustrated in Figure 1.4. This causes the metal to lose an electron to gain a positive charge, while the one accepting the electron to gain a negative charge [6]. The resulting contact potential, V_c, is then given by:

$$V_c = -\frac{\phi_1 - \phi_2}{e} \qquad \text{(Eq. 1.1)}$$

Where ϕ denotes the work function of the respective metals and e is the elementary charge (1.602×10^{-19} C).

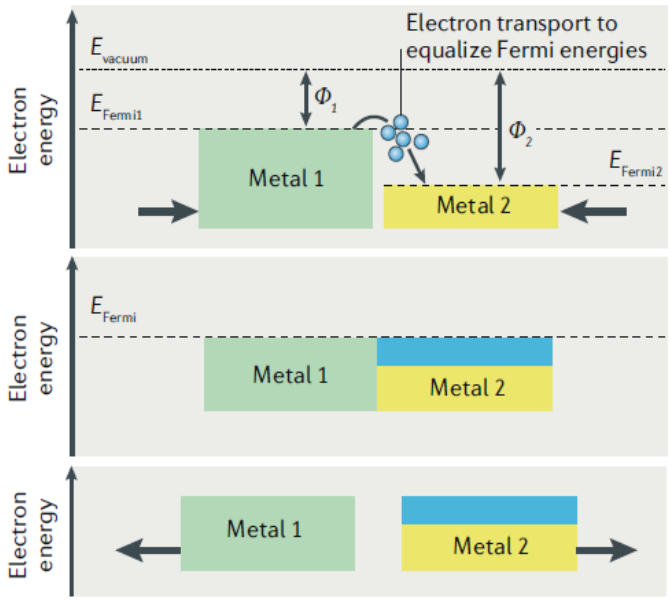

Figure 1.4: Electron transfer in metal-metal contacts (copied from *[6]*).

In metal-insulator and insulator-insulator contacts, electron transfer is less straightforward due to the absence of mobile electrons. However, an effective work function can be assigned to insulators.

$$V_c = -\frac{\phi_E - \phi_M}{e} \qquad \text{(Eq. 1.2)}$$

Here, ϕ_E refers to the effective work function of the insulator, and ϕ_M is the work function of the metal. Since insulators do not have any electrons in the conduction band, electron transfer between insulators and insulator-metal contacts is explained through the surface state models. These models

propose that electron transfer is mediated by energy states localized at the surface of the insulator, rather than through bulk conduction, as shown in Figure 1.5. The energy levels available for electron transfer are present only at the surface, called surface states [6]. Another possible theory is the existence of surface defects, such as highly strained bonds, that act as an intermediate energy level between the valence and conduction band, allowing electron transfer to take place [7].

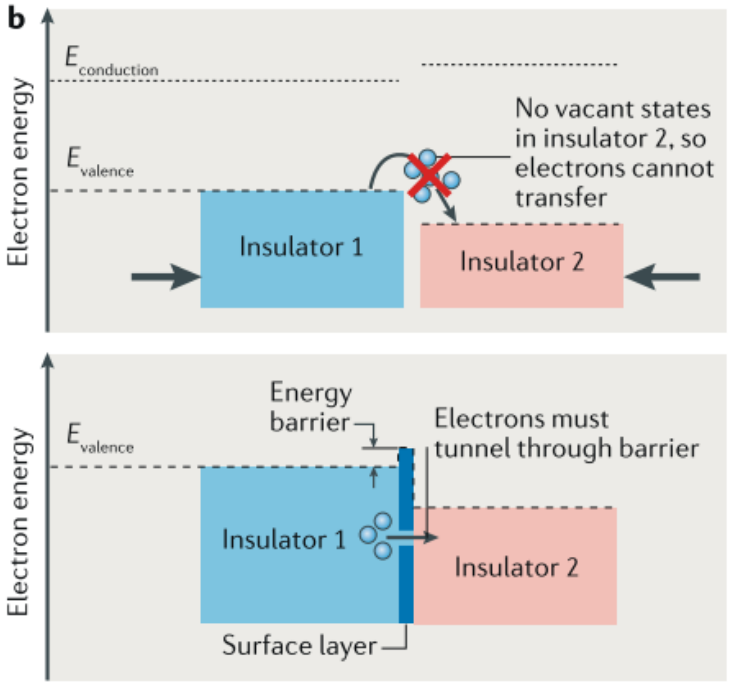

Figure 1.5: Electron transfer in insulator-insulator contacts (copied from *[6]*).

1.1.3.2. Ion transfer

According to this mechanism, the charge transfer occurs due to the transfer of ions from one material to the other upon contact. An ion is a charged atom or molecule where the number of electrons differs from the number of protons. Mobile ions from the surface of an ionic material can dissociate and attach to a different material upon contact, as shown in Figure 1.6 [6].

It was found that the polarity of triboelectric charge on glass could be altered by treating the surface with acids or alkali. This was suspected due to the adsorption of H^+ or OH^- ions on the glass surface. Furthermore, H^+ or OH^- ions can adsorb or desorb from surfaces during contact, especially in humid conditions [6].

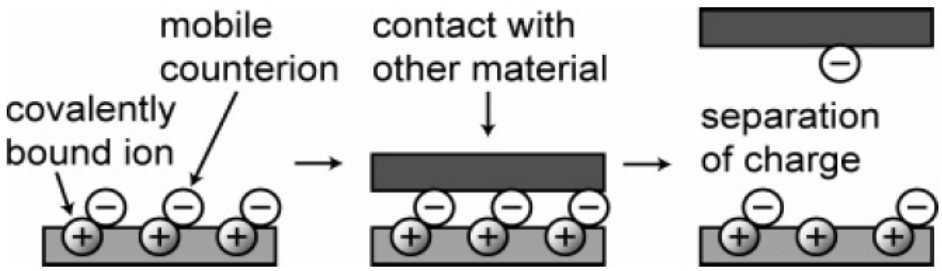

Figure 1.6: Illustration of ion transfer mechanism (copied from *[8]*).

1.1.3.3. Material transfer

Charge transfer can also result from the transfer of material fragments between surfaces during contact. These fragments carry a charge with them as they deposit on the surface of the contacting material, contributing to charge accumulation. Techniques such as Kelvin Force Microscopy (KFM) have identified changes in surface roughness and exchange of patches between contacting solids (Figure 1.7a), as reported by Baytekin et al. [9]. This is also illustrated by Pandey et al. [10] (Figure 1.7b), which depicts contact-induced cleavage and material transfer between dissimilar polymer surfaces, leading to localized charge retention after separation.

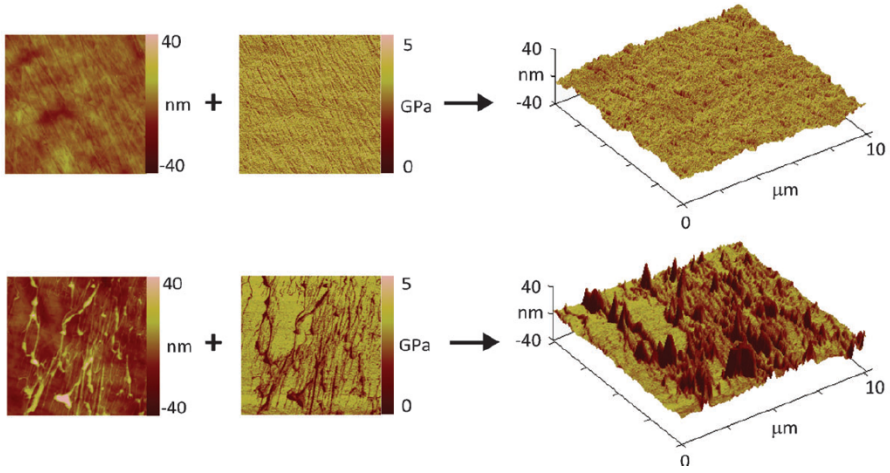

(a)

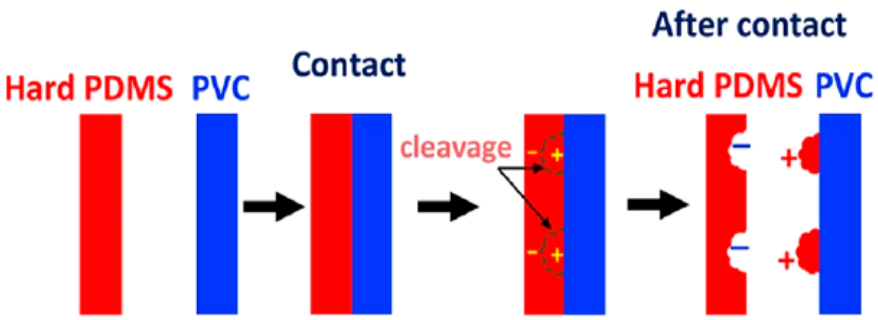

(b)

Figure 1.7: (a) KFM images depicting changes in surface roughness after PS surface contact with PTFE *[9]*; (b) transfer of material after bond cleavage (copied from *[10]*).

1.1.4. Triboelectric series

The triboelectric series is an empirical list that predicts triboelectric charge polarity between insulators. In this series, materials are arranged in a way that the ones that are higher in the list are more likely to charge positively when contacted against the ones lower in the list (Figure 1.8a) [4]. For instance, if silk were brought into contact with paper, silk would charge positively, while the paper would charge negatively, according to this series. However, materials such as silk, zinc, glass, cotton, and paper exhibit a cyclic triboelectric series (Figure 1.8b), deviating from the conventional linear series [11].

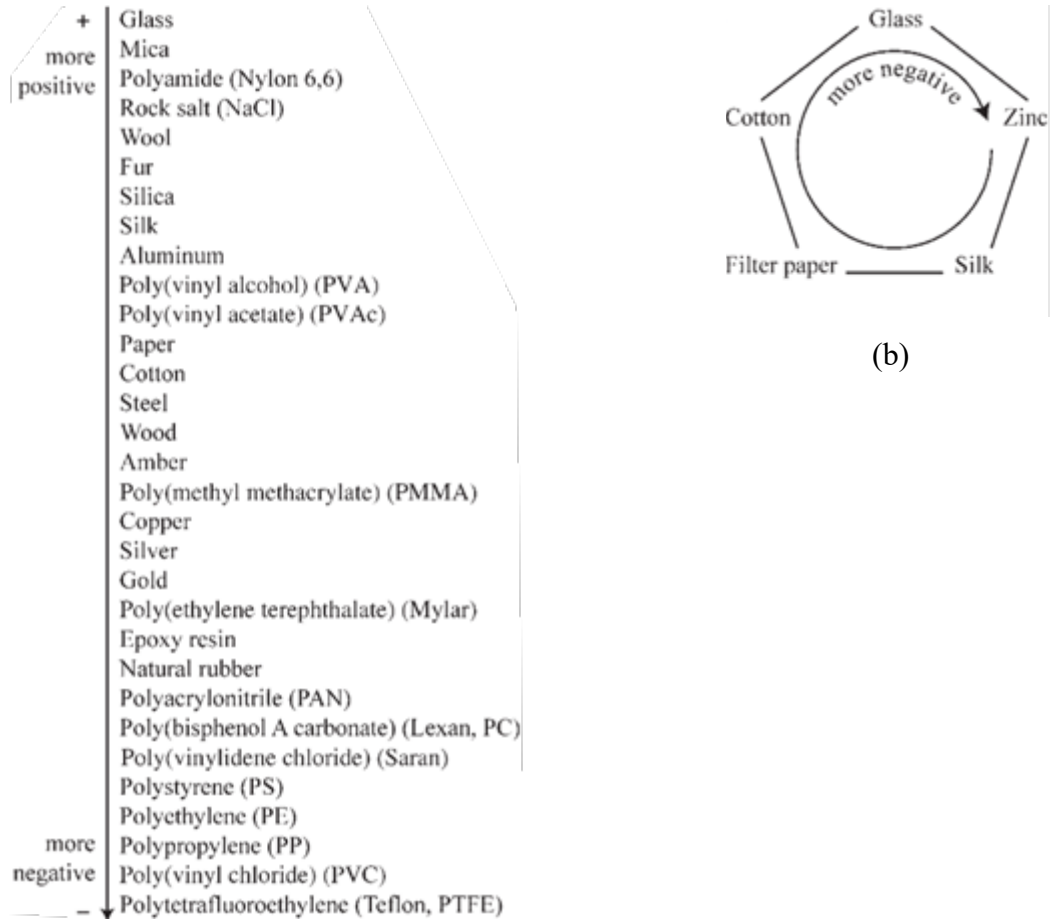

Figure 1.8: (a) A linear triboelectric series; (b) a cyclic triboelectric series (copied from *[11]*).

1.1.5. Charge measurement techniques

Two commonly used charge measurement techniques, which work on the principle of induction charging, are: (a) the Faraday cup, and (b) the electrostatic probe.

1.1.5.1. Faraday cup

As illustrated in Figure 1.9, a Faraday cup consists of an inner shell and an outer shell, both made from highly conductive material such as copper. The inner shell is the charge collector, while the outer shell acts as an electrical shield for the inner cup from external fields that could affect charge measurement. The inner and the outer shells are separated from each other through an insulating pad. When a charged object falls into the inner cup, an image charge is generated on the inner surface of the shell. Consequently, the charges similar to the object accumulate on the outer surface of the shell. With the help of a grounded electrometer connected to the inner shell, electrons flow

to or from the ground to the cup depending on the polarity and magnitude of the charged particle. The electrometer reads this flow of electrons as current and converts it into a charge reading [4].

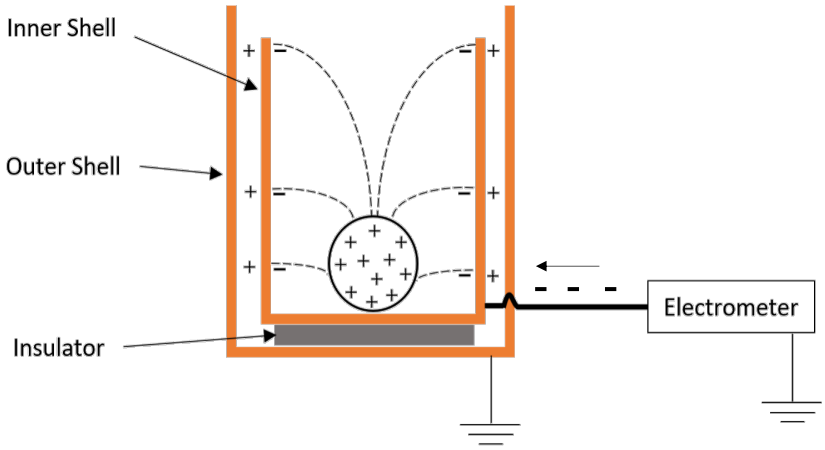

Figure 1.9: Faraday cup measurement technique.

1.1.5.2. Electrostatic probe

The electrostatic probe is another charge measurement device. As shown in Figure 1.10, the probe consists of an inner metal rod that is separated from an outer grounded shield through an insulator. When a charged object comes into the vicinity of the probe, it induces an image charge on the inner rod on the side closer to the object. This charge is read by an electrometer connected to the other end of the inner rod. An example of the application of such probes is in commercial polyethylene fluidized bed reactors, where the electrostatic probe is mounted on the reactor wall. Due to its measurement technique, the probe is only able to measure charge in a localized area. In order to get a good representation of charge generation within a large area, such as the commercial polyethylene fluidized bed reactors, multiple electrostatic probes may be required. Furthermore, the charged particles can adhere to the probe itself, due to electrostatic charge, reducing the potential measured by the probe. The particles in the bed could also acquire additional charge by colliding with the probe itself [12].

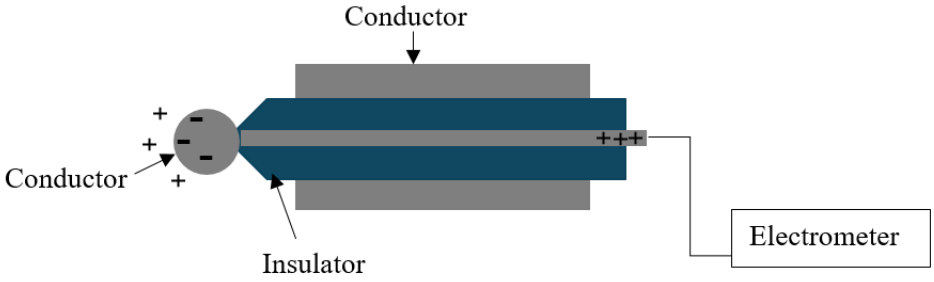

Figure 1.10: Electrostatic probe measurement technique.

1.2. Gas breakdown

Gases are typically insulating under normal conditions due to the absence of free charge carriers. However, in certain cases, such as in the presence of a strong high electric field, gas molecules can get ionized through collisions with energized free electrons. This ionization process can be represented as:

$$A + e^- \rightarrow A^+ + 2e^- \quad \text{(Eq. 1.3)}$$

Where a neutral gas molecule A collides with an electron possessing kinetic energy and breaks into a positive ion and an additional electron. As this process repeats, these charge carriers multiply until eventually the gas breaks down and becomes conductive [13]. In triboelectric systems, this breakdown plays a critical role in limiting charge accumulation. To understand this further, we will examine the role of gas breakdown in triboelectric systems and the underlying principles behind gas breakdown.

1.2.1. Gas breakdown in triboelectrification

The maximum charge that can be accumulated on an insulator surface is governed by two limiting factors. First, the resultant electric field due to triboelectric charging creates a repulsive energy barrier that opposes further charge transfer. Second, as charged surfaces separate, the surrounding gas may undergo electrical breakdown [14]. The latter is heavily dependent on the type of gas and its dielectric strength, which is a unique property of each gas. It refers to the maximum field that a gas can withstand without undergoing complete gas ionization. In the case of triboelectric charging, the separation of the surfaces leads to an increase in capacitive voltage as shown in Eq. 1.4,

$$V_C = \frac{qd}{A\varepsilon_0} \quad \text{(Eq. 1.4)}$$

Where V_C is the capacitive voltage, q is the surface charge, A is the contacting surface area, d is the distance between the charged surfaces, and ε_0 is the permittivity of free space. As shown, the voltage increases proportionally with the gap distance between the charged surfaces. When this voltage exceeds the breakdown threshold of the surrounding gas, the ions and electrons generated from the ionization process can partially neutralize the nearby surface charges. This breakdown happens in cycles until the remaining surface charge on the particle cannot disengage further breakdown events. For atmospheric air, it was found that the breakdown events initiate in the first few micrometers of separation [14].

Various studies have shown that the gas environment in a triboelectric system can significantly influence both the magnitude of charge accumulation and dissipation. Miura [15, 16] conducted a study on the charging behavior between metals and insulators under different gas environments, noting that a metal sliding on a quartz disc accumulated charge without dissipation in a vacuum. In contrast, in an argon environment, the charge dissipated rapidly. Miura observed that air and nitrogen exhibited slower dissipation rates compared to argon. Similarly, Zhang and Ciampi [17] conducted a study where they rubbed various materials, such as PTFE, PDMS, PVC, PMMA, nylon, and glass, with dry ice in both air and argon environments. Their study aimed to study the triboelectric charging behavior of solid carbon dioxide (CO_2) in different environments for CO_2 fire extinguisher applications. Their findings showed consistently lower charge generation in argon across all tested materials compared to air. Additionally, Matsuyama and Yamamoto [18, 19] examined the charging behavior of Teflon, nylon, Delrin, and polystyrene particles upon collisions with titanium, chromium, and nickel plates in different gas environments, confirming that the particles acquired a lower charge in argon compared to air. Further supporting these findings, Liu and Sundaresan [20] investigated the charging due to 10 min vibration of soda-line glass (1.46 - 2.2 mm) and polyethylene particles (>2.1 mm) in a 4.5” high and 2” wide PMMA vibratory bed in nitrogen and argon environments. They observed that the magnitude of charge for polyethylene particles was 50% lower, and that for glass particles was 70% lower in argon than in nitrogen. Therefore, all the aforementioned studies display argon’s static mitigation ability across a wide range of materials and setups.

1.2.2. Gas breakdown fundamentals

The major factor governing argon's static mitigation ability is its lower dielectric strength as compared to other gases. In other words, the threshold for electrical breakdown is much lower in argon than it is for most other gases. Table 1.1 presents the dielectric strength of common gases under ambient temperature and atmospheric conditions.

Table 1.1: Dielectric strength of different gases at 20°C and 1 atm *[21]*.

Gas type	**Dielectric strength (kV/mm)**
Neon	0.05
Argon	0.6
Hydrogen	1.6
Air	3.25
Nitrogen	3.4
Sulfur hexafluoride	8.86
Hydrocarbons	> 3.8

The electrical breakdown, known as breakdown voltage, is found by applying a potential difference across a pair of metal electrodes separated by a fixed gap until a spark is achieved. This pair of electrodes is housed within a chamber filled with a gas of known composition, temperature, and pressure. The dielectric strength of a gas is defined as the breakdown voltage evaluated for a specific electrode gap. The geometry of the electrodes plays a significant role in breakdown measurements, with commonly used configurations including parallel plates, spherical, and concentric cylindrical electrodes, each producing electric fields of varying uniformity and consequently different breakdown voltages. Examples of apparatus used to determine the dielectric strength of a gas are shown in Figure 1.11.

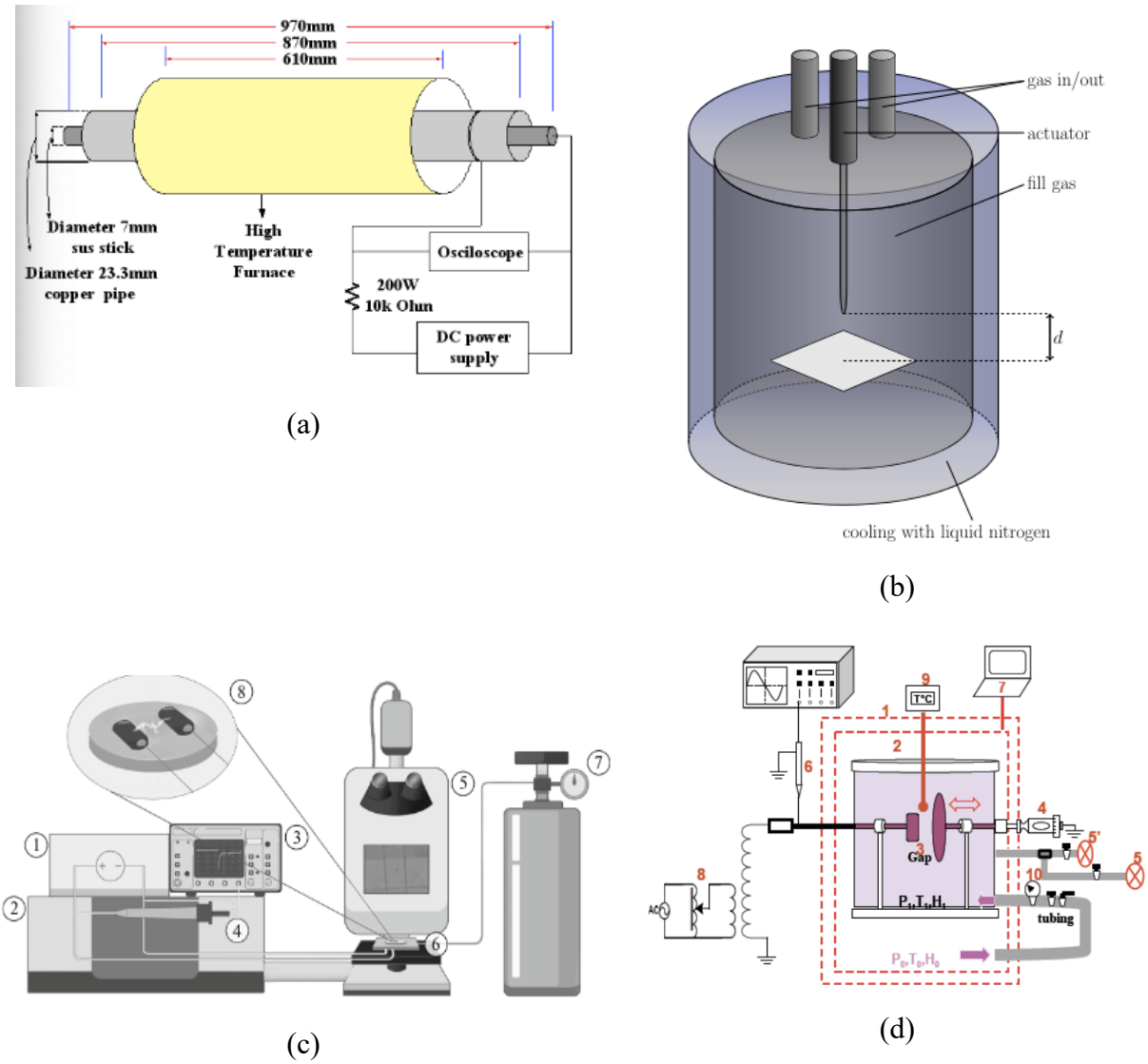

Figure 1.11: Breakdown voltage measurement setups for (a) copied from *[22]*; (b) copied from *[23]*; (c) copied from *[24]*; (d) copied from *[25]*.

The measured breakdown voltage is influenced by several factors, including the electrode material due to variations in work function, pressure, gas type, and electrode gap. This relationship between the breakdown voltage of a gas and the above-mentioned factors is shown below, in the form of an equation, as developed by Friedrich Paschen in 1889 [13]:

$$V_B = \frac{Bpd}{ln(Apd) - ln\left\{ln\left(1 + \frac{1}{\gamma}\right)\right\}} \qquad \text{(Eq. 1.5)}$$

Where "p" represents gas pressure and "d" is the distance between electrodes. A and B are gas-specific constants, and γ accounts for Townsend's secondary electron emission coefficient. Values for A and B for some common gases are presented in Table 1.2.

Table 1.2: Values for A and B and their range of validity for different gases *[13]*.

Gas	***A*** **(Torr.cm)$^{-1}$**	***B*** **(V/Torr.cm)**	***E/P*** **(V/Torr.cm)**
Air	14.6	365	100-800
Nitrogen	12	342	100-600
Argon	13.6	235	100-600
Hydrogen	5.1	138.8	20-600

Paschen's law is also presented graphically (Figure 1.12), famously known as the Paschen curve, which is a unique curve for each gas but has a characteristic shape. The curve has a minimum breakdown voltage value at $(pd)_{min}$, known as the Paschen minimum. The breakdown voltage increases steeply on either side with the variation in pd. On the left side of the minimum, breakdown voltage increases with a decrease in pressure for a fixed gap due to fewer molecules available for ionization. As for the right side of the minimum, there are enough molecules for ionization, hence the mean free path of the charge carriers becomes important. The mean free path is the average distance an electron travels before undergoing a collision. When the pressure is high, it translates into a dense population of gas molecules, which results in the reduction of the mean free path. As a result, electrons and ions do not gain enough energy to cause ionization between collisions [13].

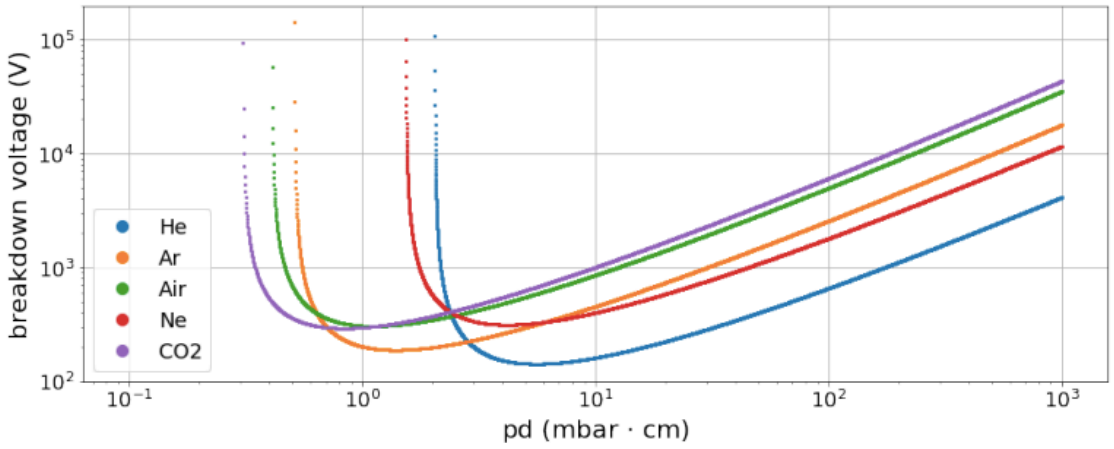

Figure 1.12: Example of Paschen curves for different gases with stainless-steel electrodes (copied from *[26]*).

Temperature also affects the breakdown voltage, although in contrast to pressure and gap distance. This effect is not directly visible in Paschen's equation, as the traditional equation was developed as a function of pressure. Deviations were observed in the Paschen's curve as temperature was altered, leading to temperature corrections such as the Peek and Dunbar corrections [25, 27]. These corrections at a higher temperature, alongside the conventional Paschen curve at room temperature, are shown in Figure 1.13 [27]. Peek correction altered the voltage by a factor of T_0/T, where T_0 is the ambient temperature, and T is the new temperature. This correction lowers the Paschen's curve at higher temperatures. In the Dunbar correction, the pressure is adjusted by a factor of T_0/T, pushing the curve to the right for higher temperatures [25, 27]. With these corrections, the original Paschen law gets modified as

$$V_B^{Peek} = \left[\frac{Bpd}{ln(Apd) - ln\left\{ln\left(1+\frac{1}{\gamma}\right)\right\}}\right] \times \frac{T_0}{T} \qquad \text{(Eq. 1.6)}$$

$$V_B^{Dunbar} = \frac{B(p\frac{T_0}{T})d}{ln\left(A(p\frac{T_0}{T})d\right) - ln\left\{ln\left(1+\frac{1}{\gamma}\right)\right\}} \qquad \text{(Eq. 1.7)}$$

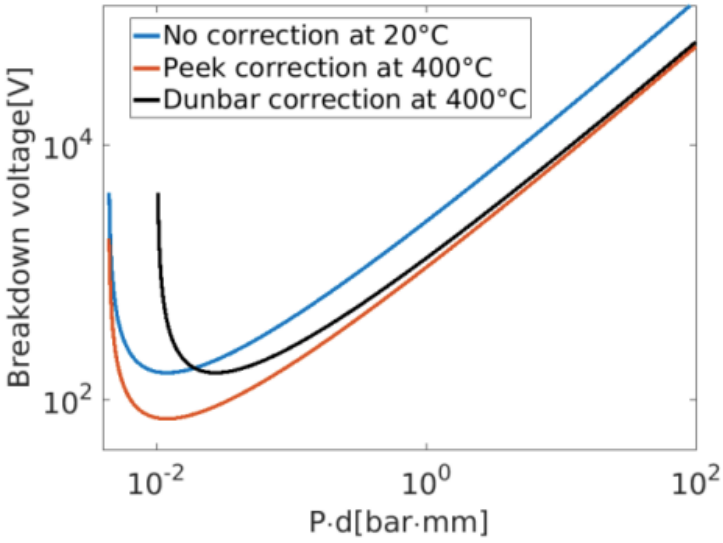

Figure 1.13: Peek and Dunbar corrections at 400°C plotted along with the standard Paschen curve (copied from *[27]*).

Physically, higher temperatures increase the kinetic energy of gas molecules, leading to more frequent collisions and ionization events. Conversely, as the gas density decreases, the mean free path increases, resulting in fewer collisions and fewer ionization events. The increase in the mean free path allows the excited species to gain enough energy to ionize other molecules before collisions [25]. Overall, energy for ionization is reduced, thus lowering the breakdown voltage. Uhm et al. [22] investigated this effect of temperature on breakdown voltage in stainless-steel and copper coaxial cylindrical electrodes containing air, nitrogen, and oxygen from 27°C to 300°C (Figure 1.11a). For all gases studied, an increase in temperature resulted in a decrease in breakdown voltage, as shown for nitrogen in Figure 1.14a, where the solid line depicts the values based on the theoretical model, while the red and black solids represent their experimental data. The authors proposed a modified form of Paschen's law incorporating the Peek correction, in which the breakdown voltage is scaled by a factor of T_0/T. Borodulina et al. [24] also studied the variation of breakdown voltage with temperature using a parallel-plate electrode configuration over the temperature range of -193 to 22°C (Figure 1.11c). They reported a 50% decline in breakdown voltage for nitrogen in comparison to a 36% decline in argon (Figure 1.14b). However, in the case of elegas (SF_6), they found that the breakdown voltage did not decrease consistently in the temperature range of testing. Therefore, their results indicated a gas-dependent decline of breakdown voltage with temperature.

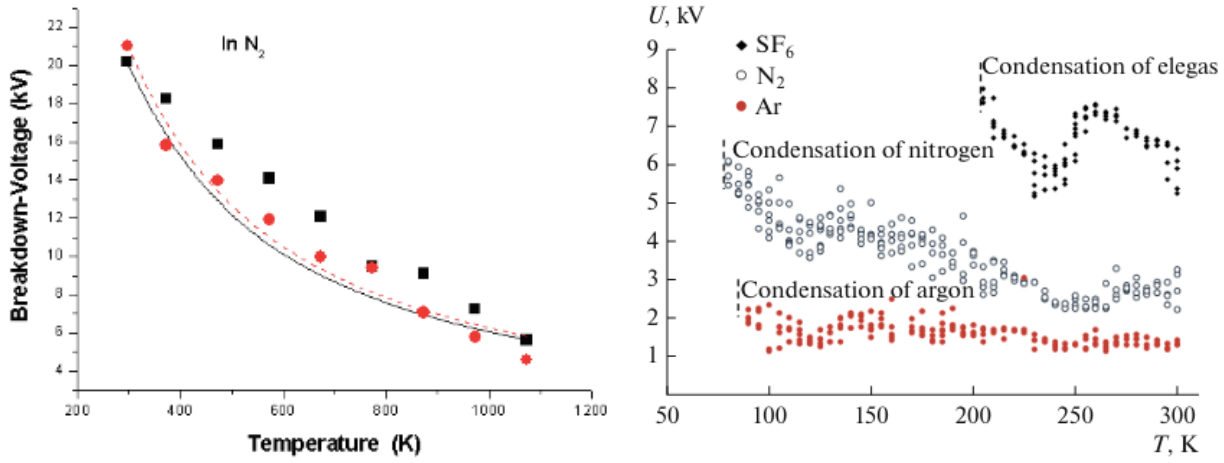

(a) (b)

Figure 1.14: Breakdown voltage variation with temperature at atmospheric pressure for (a) nitrogen as seen in *[22]*; and (b) nitrogen, argon, and elegas as seen in *[24]*.

Massarczyk et al. [23] examined temperature-dependent breakdown behavior in neon, nitrogen, argon, and xenon using a pin-plate electrode configuration at atmospheric pressure (Figure 1.11b). They found that when the temperature was increased from -193°C to 22°C, the breakdown voltage decreased for all the gases, which is evident in their experimental Paschen data at different temperatures for nitrogen and argon, shown in the Figure 1.15a and Figure 1.15b, respectively. Based on these results, the authors concluded that temperature effects should be incorporated into Paschen's law through the gas density, replacing the conventional *pd* term with gas density (*pd/T*), thereby modifying the equation to the following,

$$V_B = \frac{B\left(\frac{pd}{T}\right)}{ln\left(A\left(\frac{pd}{T}\right)\right) - ln\left\{ln\left(1+\frac{1}{\gamma}\right)\right\}} \quad \text{(Eq. 1.8)}$$

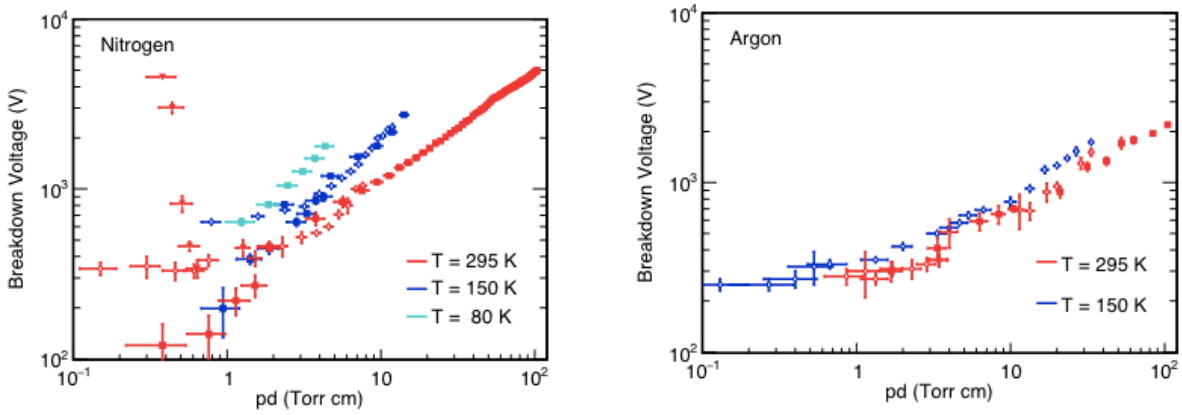

(a) (b)

Figure 1.15: Experimental Paschen data at different temperatures for (a) nitrogen and (b) argon as seen in *[23]*.

Similarly, Sili et al. [25] investigated the variation in breakdown voltage of air with temperature using stainless-steel plate electrodes housed in a climatic chamber, examining temperatures of 50, 100, and 125°C over a pressure range extending from low (vacuum) pressures up to atmospheric conditions (Figure 1.11d). Their results showed that the temperature dependence of breakdown voltage was pressure-dependent, with breakdown voltage decreasing with increasing temperature to the right of the Paschen minimum and increasing with temperature to the left of the minimum (Figure 1.16). Notably, at atmospheric pressure, the breakdown voltage decreased from approximately 3 kV at 50°C to 1 kV at 100°C. Based on their experimental observations, the authors proposed an empirical modification to Paschen's law by introducing a correction factor to account for temperature-induced changes in gas density.

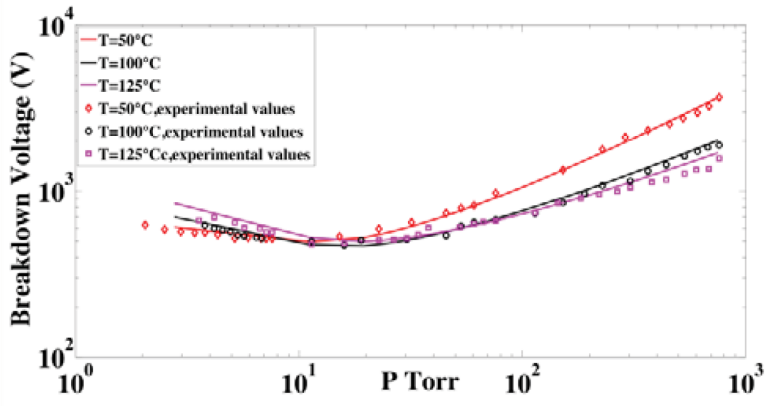

Figure 1.16: Experimental Paschen data at different temperatures for air (copied from *[25]*).

1.2.3. Breakdown mechanisms

1.2.3.1. Townsend breakdown theory

The most foundational explanation of gas breakdown comes from the Townsend breakdown theory. In this model, the free electrons that are initially present and the secondary electrons emitted from the cathode are accelerated by the electric field between the two electrodes. The electrons collide with neutral gas molecules as they move through the gap, possessing kinetic energy and ionize them, which generates further electrons. Moreover, the positive ions generated from ionization travel to the cathode, where they generate more electrons from the cathode surface. These additionally generated electrons can create further ionization events, triggering a cascade effect known as an electron avalanche. For a self-sustaining ionization to occur, electrons must gain sufficient kinetic energy between collisions. This kinetic energy is dictated by the strength of the electric field applied and the mean free path of the electrons. If the mean free path is too short, electrons may not gain sufficient energy between collisions to cause ionization. On the contrary, if the mean free path is too long, there will not be enough collisions for ionization to sustain itself. To quantify this, Townsend introduced two main parameters: Townsend's first ionization coefficient (α), which represents the number of ionizing collisions per unit distance travelled by an electron, and the secondary electron emission coefficient (γ), which accounts for the number of electrons emitted from the cathode per incident ion. Complete gas breakdown occurs when the number of secondary electrons generated at the cathode becomes sufficient to sustain the avalanche

initiated by the first ionization [13, 28, 29]. Figure 1.17 schematically illustrates the Townsend breakdown mechanism, showing electron multiplication through successive ionization events and secondary emission at the cathode that collectively lead to self-sustaining gas breakdown under a sufficiently strong electric field [30].

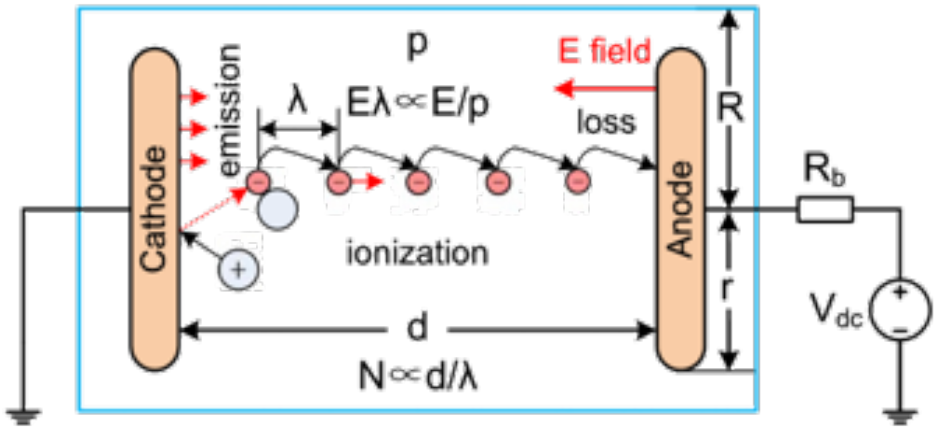

Figure 1.17: Illustration of the Townsend breakdown mechanism (copied from *[30]*).

Mathematically, this criterion is described by the Townsend criterion,

$$\alpha d = ln\,(1 + \frac{1}{\gamma}) \qquad \text{(Eq. 1.9)}$$

This criterion forms the foundation of Paschen's law, which was seen in the earlier section.

The relationship between current and applied voltage for a Townsend-type discharge is shown in Figure 1.18 [13]. Initially, as the voltage is increased up to V_0, the current increases and reaches a saturation value at i_0. Now, as the voltage is increased up to V_1, there is no increase in current. However, at V_1, the current begins to increase exponentially as the electrons cause ionizing collisions, generating more electrons. At V_2, current increases even more rapidly due to the generation of secondary electrons from the cathode [13, 28].

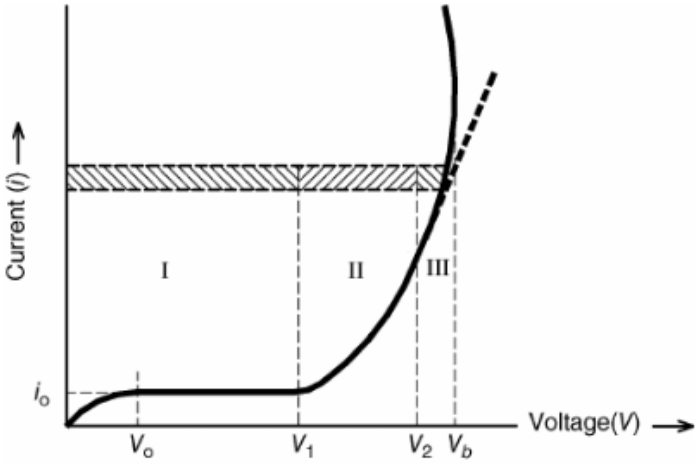

Figure 1.18: Current-Voltage relationship during gas discharge (copied from *[13]*).

1.2.3.2. Streamer theory

Although Townsend's theory works well for low-pressure gases and small gaps in a uniform field, it fails to describe breakdown for higher-pressure gases or large gaps. Under such conditions, the streamer mechanism becomes dominant. Unlike Townsend breakdown, where the applied field causes the avalanche to continue, streamer breakdown occurs when the avalanche itself generates an electric field strong enough to sustain further ionization. As the avalanche is developed, the electrons accelerate towards the anode, leaving the larger positive ions behind. This charge separation, especially near the avalanche head, results in a localized electric field. If the avalanche becomes densely populated with charges, this localized field can even exceed the applied electric field and give rise to secondary avalanches, which eventually form a conductive stream between the anode and cathode. This process of streamer development is depicted schematically in Figure 1.19.

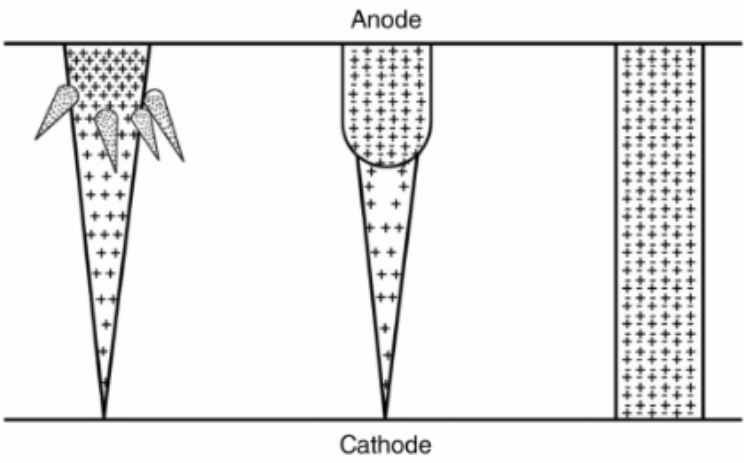

Figure 1.19: Streamer breakdown mechanism (copied from *[13]*).

The Meek-Raether [13, 28, 29] criterion provides a condition for when the streamer mechanism occurs, as shown below,

$$\alpha d \sim 18 - 21 \qquad \text{(Eq. 1.10)}$$

Where α is Townsend's first ionization coefficient, and d is the electrode gap. In simpler words, this criterion states that if enough ionizations have occurred in the gap, the field generated by the avalanche becomes strong enough to sustain ionization, irrespective of the applied voltage.

1.3. Gas-solid fluidization

Gas-solid fluidization was first seen in 1922 by Winkler for the gasification of coal. After that, fluidized beds were extensively used during World War II by the petroleum industry for catalytic cracking. Since then, fluidized beds have been widely used in various industrial applications involving polymerization, combustion, and coating due to their enhanced mixing and heat and mass transfer characteristics. Their use spread across various industries, including pharmaceuticals, petrochemicals, and so on [31].

In a typical setup, a fluidizing gas is introduced from the bottom of a column, flowing upwards through a distributor plate into a packed bed of particles. The distributor plate ensures even distribution of gas into the solid bed. The flowing gas exerts a drag force on the particles, which increases with the increase in gas velocity. At a certain velocity, known as the minimum fluidization velocity (U_{mf}), the combination of drag force and buoyancy force acting upwards balances the downward gravitational force, rendering the bed a fluid-like state. If the velocity is increased beyond this point, the excess gas turns into bubbles at the distributor and rises through

the bed and bursts at the surface. This is known as the bubbling flow regime. The bubbles grow with further increase in gas velocity, sometimes approaching the column diameter, known as the slugging flow regime. The flow regime becomes turbulent when the gas velocity increases even more, at which point the bed surface becomes indistinct and particle entrainment becomes significant. At extremely high velocities, fast fluidization and pneumatic transport occur, where solids are carried out of the column [31, 32]. These different flow regimes in a gas-solid fluidized bed are depicted below in Figure 1.20.

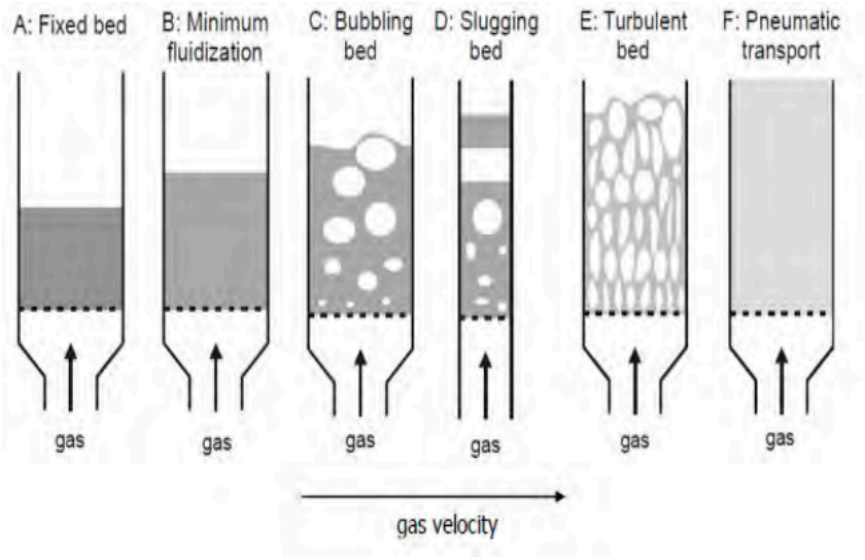

Figure 1.20: Schematic of different fluidization regimes with increasing gas superficial velocity (copied from *[31]*).

The behavior of particles in the fluidized bed depends strongly on their size and density. Geldart used these factors to classify different particles based on their fluidization behavior, shown in Geldart's powder classification chart in Figure 1.21. Group C particles are the smallest in size and are extremely difficult to fluidize due to dominant interparticle attraction forces (Van der Waals and electrostatic forces). Group A particles are larger in size and density, meaning lesser cohesive forces exist. The main feature of these particles is that at the minimum fluidization velocity, the bed fluidizes smoothly. Bubble formation, in this case, takes place at a higher velocity known as the minimum bubbling velocity (U_{mb}). Group B and D particles are much larger, with negligible interparticle forces. For group B particles, bubble formation happens at the point of minimum fluidization, while group D particles are too large to fluidize and are used in spouting beds [32].

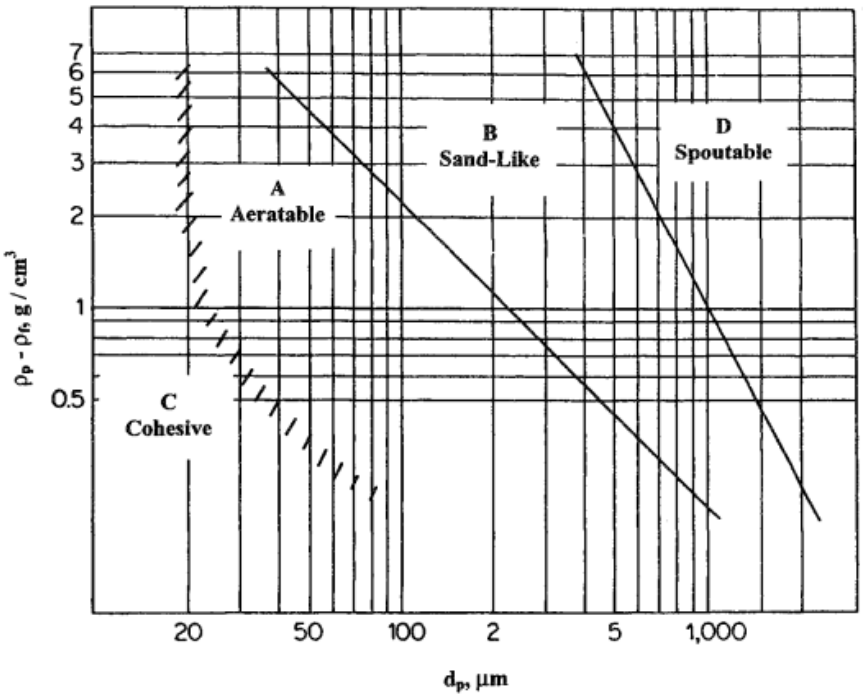

Figure 1.21: Geldart classification of powders (copied from *[32]*).

1.3.1. Polyethylene process

Polyethylene (PE) is one of the most widely used polymers in the world, with applications in sectors such as packaging, construction, consumer goods, textiles, and automotive components. Products made from polyethylene include films, pipes, containers, reusable bags, insulation materials, and plastic items used domestically and in industries. Depending on the product use, PE can be fabricated using techniques such as blow molding, injection molding, and extrusion. As a result, a wide spectrum of products can be derived from PE, ranging from lightweight packaging bags to rigid storage tanks [33].

The performance and application of polyethylene are strongly linked to its chemical structure and method of processing. One of the key attributes used to classify polyethylene is density, which signifies its degree of crystallinity and chain packing of the polymer. The American Society for Testing and Materials (ASTM) has categorized polyethylene into four groups based on density. Groups I (0.910-0.925 g/cm^3) and II (0.926-0.940 g/cm^3) are commonly referred to as low-density polyethylene (LDPE), while groups III (0.941-0.959 g/cm^3) and IV (≥0.960 g/cm^3) are known as high-density polyethylene (HDPE). Linear low-density polyethylene (LLDPE) is a distinct linear

polyethylene with density values within the LDPE range and is characterized by reduced long-chain branching compared to the conventional LDPE [34].

Polymerization of ethylene monomers in the presence of comonomers and catalysts leads to the formation of polyethylene. The choice of comonomers and catalysts determines the final properties of the polymer. Common comonomers such as 1-butene, 1-hexene, and 1-octene help in the adjustment of short-chain branching, which influences the density and crystallinity of the polymer [35]. Moreover, hydrogen is added as a chain transfer agent to control the polymer's molecular weight [36]. Different catalysts utilized in commercial processes include Ziegler-Natta (titanium-based), Phillips (chromium-based), and metallocene (single-site) catalysts [37].

Commercially, the polyethylene production process takes place in a gas-solid fluidized bed reactor, like the one shown in Figure 1.22. Ethylene gas is introduced into the reactor from the bottom while the catalyst and cocatalyst (such as trialkyl aluminum) are fed into the reactor above the distributor plate. Catalyst injection is done pneumatically, using inert gases such as nitrogen, or through a slurry [38]. The polymerization reaction occurs on the catalyst surface, where the polyethylene chains grow on the active sites. The process is highly exothermic, and the resulting heat is constantly removed through the flow of cold ethylene gas to prevent runaway reactions. As polyethylene resin forms and settles towards the bottom, it is continuously removed from the reactor. Polyethylene reactors typically operate at pressures ranging between 1800 and 3000 kPa and temperatures between 70-110ºC. The residence time for the product is approximately 1-2 hours [37].

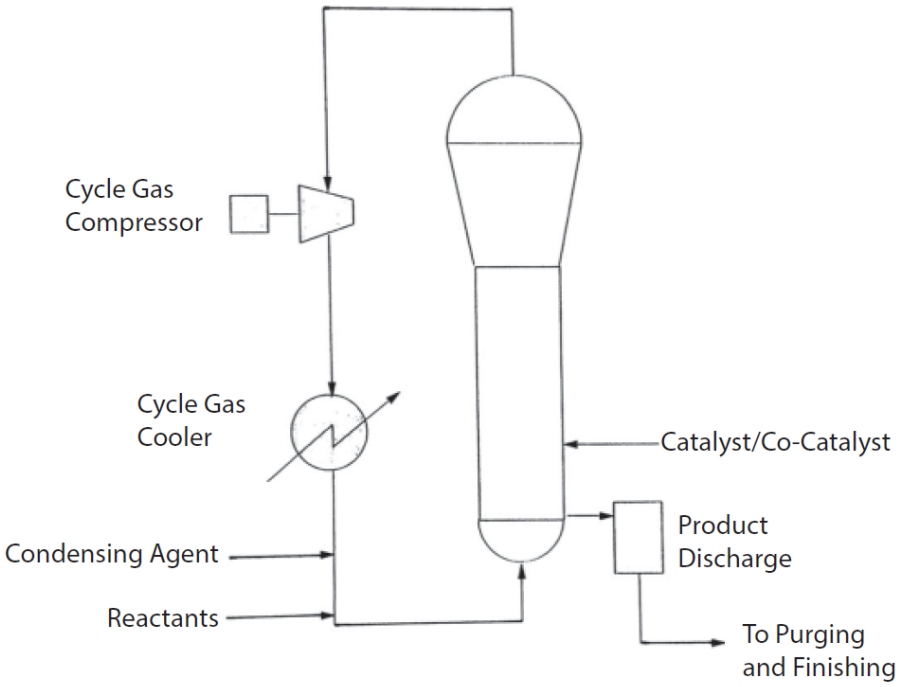

Figure 1.22: Schematic of UNIPOL™ process (copied from *[37]*).

1.3.2. Electrostatic charging in PE fluidized beds

In gas-phase polyethylene production, both polyethylene and catalyst particles are insulating in nature. As a result, vigorous mixing inside the fluidized bed gives rise to triboelectric charging. Charge is generated due to frequent particle-particle and particle-wall collisions, leading to operational challenges. The additional interparticle force due to electrostatic charging causes the particles' agglomeration and particle adhesion to the reactor walls. The fouled particles on the wall may continue to polymerize in place, especially if the catalyst is fouled as well. This is particularly concerning due to the exothermic nature of the polymerization reaction, as the fouled particles are unable to effectively dissipate heat. As a result, local temperatures near the fouled regions increase, and the adhered particles melt and fuse, forming polymer "sheets" [1]. Sheeting is found to be more prone in critical areas such as the fluidization zone, expanded section, or the dome of the reactor, as shown in Figure 1.23.

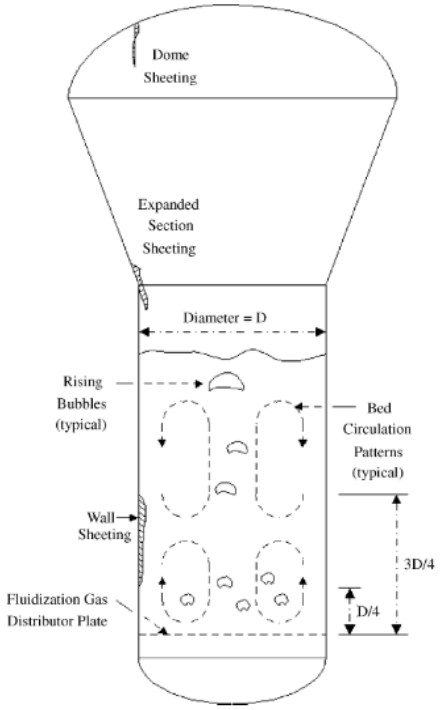

Figure 1.23: Common sheeting locations in a commercial polyethylene reactor (copied from *[1]*).

These sheets are typically categorized as either warm or cold sheets, depending on the source particles and wall temperature. Warm sheets form when fine catalyst-rich particles stick to the wall and continue to react. This creates a hot reaction zone on the wall, which cools down as the reaction front moves away. The outer layer of these sheets consists of granular particles, while the core is composed of fused polymer. Cold sheets, in contrast, form when polymer particles adhere to the wall and undergo slow polymerization. The local temperature increases slowly and reaches the sintering point, the adhered particles fuse and form a dense, smooth layer, different from that of warm sheets [1].

As sheets grow thicker, they act as thermal insulators, and the reactor skin temperature decreases. Eventually, the sheets detach from the wall and fall onto the distributor plate, obstructing gas flow. The consequences include the generation of dead zones in the bed and reduced fluidization quality. Moreover, the dislodged sheets mandate reactor shutdown, often between 2 and 30 days, for cleanup and maintenance. Reactor shutdown results in significant economic losses for the polyethylene industry, approximated to be USD 2 million per day for a large-scale LLDPE reactor.

The mitigation and control of electrostatic charge generation within polyethylene fluidized beds has become a critical challenge for the industry. Commercial strategies such as the use of antistatic agents and reactor wall surface treatments have been implemented; however, their effectiveness is limited, and hence the issue remains unsolved.

1.3.3. Parameters affecting charge generation in fluidized beds

Numerous studies, including those from this research group and others, have identified key parameters that influence charge generation in gas-solid polyethylene fluidized beds. These include particle size and distribution [39], fluidizing gas flow regime [40-42], operating pressure [42, 43] and temperature [42, 44], gas humidity [45], fluidization gas type [46], and the use of continuity additives [47]. From these studies, it was found that an increase in gas velocity (transition from bubbling to turbulent flow regime) and pressure promoted charge generation, while temperature increase was able to suppress charge generation within the fluidized bed [41-44]. The addition of continuity additives, if used in the right concentration, was found useful in mitigating charging within the bed [47].

1.3.3.1. Effect of pressure and temperature

Operating temperature and pressure, apart from being critical to the process, also influence electrostatic charge behavior. Experimental studies have shown a contrasting effect between pressure and temperature on charge generation. For instance, in a study by Moughrabiah et al. [42] involving polyethylene resin and glass beads fluidized with compressed air, it was found that increasing the pressure from 100 to 800 kPa led to a greater charge accumulation, while raising the temperature from 18 to 60°C resulted in reduced particle charging. In their study, small particle samples were taken from three different ports in the column, and their net charges were measured using a Faraday cup. However, no quantifying fouling data was collected in their study.

The quantification of particle fouling was done in a later study by Song and Mehrani [43], where they conducted fluidization experiments with LLDPE resin using nitrogen at pressures ranging from atmospheric conditions to 2600 kPa. Their setup included Faraday cages at the top and bottom of a pilot-scale gas-solid fluidized bed, enabling comprehensive charge measurements of both entrained fines and particles within the column. Their findings indicated that increasing pressure from 100 to 600 kPa doubled the extent of wall fouling, with only a marginal increase beyond that.

The underlying reason was found to be linked with changes in bed hydrodynamics, as bubble size reduced while their frequency increased, promoting collisions within the bed.

Using the same apparatus, Mohsen et al. [44] later examined the impact of temperature on wall fouling for fluidization of LLDPE resin using nitrogen gas. Operating temperatures were varied between 24 and 58°C, which revealed a decrease in wall fouling at higher temperatures due to lower charge generation. This reduction was attributed to the decreased resistivity of the resin with increasing temperature, with temperature predominantly affecting particle-particle interactions rather than particle-wall collisions.

1.3.3.2. Effect of gas type

Another important but less explored factor influencing triboelectrification is the type of gas used for fluidization. As mentioned earlier, particles undergo frequent collisions with other particles and surfaces in the fluidized bed, acquiring charge through contact and building potential as they separate post contact. Once the potential between them reaches the breakdown voltage of the fluidizing gas, ionization occurs, which helps in surface charge dissipation of the particles, limiting the charge generated in the bed. While most fluidized bed studies have used nitrogen or air, recent research has explored the role of inert gases such as argon as potential static charge suppressors. Owing to its lower dielectric strength compared to nitrogen (Table *1.1*), argon undergoes breakdown at lower electric fields, thereby promoting more effective charge dissipation and limiting charge accumulation in the bed.

Hou et al. [48] were among the first to compare the degree of charging in HDPE and glass beads fluidized with air, nitrogen, and argon. Their results showed that argon significantly reduced the charge-to-mass ratio (Q/m) of both particle types compared to air and nitrogen. However, the sampling for charge analysis was done at a single sampling port, which may not represent the entire charge generation in the column. Moreover, the wall fouling produced because of the charge was not quantified in their study.

Sridhar and Mehrani [49] conducted a more detailed study by measuring the extent of charging and wall fouling in polyethylene fluidized beds with nitrogen, argon, and their binary mixtures. Their experiments at atmospheric pressure demonstrated that replacing nitrogen with argon led to a 90% reduction in wall fouling, and even a 10 vol.% of argon with nitrogen declined wall fouling

by 50%. Furthermore, it was found that when argon was introduced in the bed intermittently after nitrogen, fouling reduction was observed. When similar experiments were conducted by Sridhar and Mehrani [50] at 2600 kPa, they observed a 40% decline in fouling when pure argon was used in place of nitrogen as the fluidizing gas. However, the effectiveness of argon as a static mitigator remains to be explored at 2600 kPa and temperatures of 70°C, which are operating conditions relevant for commercial polyethylene fluidized bed reactors.

1.4. Thesis objectives

The primary objective of this thesis is to investigate a mitigation technique for electrostatic charge generation in gas-solid fluidized bed reactors. As previously discussed, electrostatic charging in gas-solid fluidized beds, especially in the gas-phase polyethylene industry, can lead to operational challenges such as particle agglomeration and reactor wall fouling, leading to undesirable sheeting phenomenon, enforcing unplanned reactor shutdowns, incurring significant economic losses and impacting productivity.

Recent studies have highlighted the influence of fluidizing gas type on the amount of charge buildup within the reactor. Specifically, gases like argon have been observed to diminish charge accumulation. The underlying reason was hypothesized to be the differences in the dielectric strength of the gases. Gases with lower dielectric strength tend to suppress charge accumulation, thereby reducing wall fouling. However, to be relevant to commercial polyethylene reactors, it is essential to study the impact of argon under industrially relevant operating conditions, especially since temperature and pressure affect the dielectric properties of the gases.

Accordingly, the specific objectives of this thesis are:

- To conduct bench-scale shake tests using LLDPE resin with nitrogen and argon at ambient temperature and 65°C, in order to evaluate the extent of charge generation and charge accumulation on the resin at bench-scale.
- To measure the dielectric strength of nitrogen, argon, and their mixtures for pressures up to 2600 kPa and temperatures up to 110°C, and to investigate how dielectric strength for the aforementioned gases varies under these operating conditions.
- To perform gas-solid fluidization experiments using LLDPE resin with nitrogen, argon, and their mixtures as the fluidizing gas at 2600 kPa and temperatures of 25 and 70°C, to

assess the degree of charge accumulation of LLDPE resin and the extent of wall fouling in the fluidization column.

While this research was centered around gas-solid polyethylene fluidized beds, the findings can be applied to other gas-solid handling and processing systems in various industries. Moreover, the dielectric strength data from this work fill a critical gap, particularly at high temperature and pressure, and can be used as a reference for future studies.

1.5. Thesis outline

This thesis comprises five chapters, three of which are prepared in manuscript form for publication in refereed journals.

The second chapter of this thesis presents the results of bench-scale shake tests conducted using a commercially produced LLDPE resin under nitrogen and argon gas at 23 ± 2.5°C and 65 ± 2.5°C. These experiments were designed to quantify electrostatic charge accumulation on the resin under controlled conditions and to examine the influence of gas type and temperature on charge generation at bench-scale. This chapter is a manuscript published in the *Journal of Electrostatics*.

The third chapter presents the results for dielectric strength measurements for nitrogen, argon, and their binary mixtures across a temperature range of 25, 70, and 110°C (± 2°C). The chapter examines how dielectric strength varies with gas composition, pressure, and temperature, providing insight into the breakdown behavior of the gases under conditions relevant to gas-solid fluidized bed experiments in chapter four. This chapter is prepared in manuscript form for submission to the *Journal of Electrostatics*.

The fourth chapter presents the results for gas-solid fluidization experiments conducted using the LLDPE resin fluidized with nitrogen, argon, and their binary mixtures at 25 ± 2°C and 68 ± 2.5°C. The study examined the degree of charge generation and the extent of wall fouling of the resin employing reliable measurement techniques while considering the influence of gas type and temperature on dielectric strength. This chapter is prepared in manuscript form for submission to the *Journal of Powder Technology*.

Lastly, chapter five integrates the key findings from all the experiments and concludes on the hypothesis presented in the thesis objective. Additionally, it proposes future scope and recommendations based on the thesis outcomes.

References

[1] G. Hendrickson, “Electrostatics and gas phase fluidized bed polymerization reactor wall sheeting,” Chem. Eng. Sci., vol. 61, no. 4, pp. 1041–1064, Feb. 2006, doi: 10.1016/j.ces.2005.07.029.

[2] G. E. Klinzing, F. Rizk, R. Marcus, and L. S. Leung, Pneumatic Conveying of Solids: A theoretical and practical approach. in Particle Technology Series. Dordrecht: Springer Netherlands, 2010. doi: 10.1007/978-90-481-3609-4.

[3] P. Mehrani, M. Murtomaa, and D. J. Lacks, “An overview of advances in understanding electrostatic charge buildup in gas-solid fluidized beds,” J. Electrost., vol. 87, pp. 64–78, Jun. 2017, doi: 10.1016/j.elstat.2017.03.005.

[4] J. Cross, Electrostatics: principles, problems and applications. Bristol: Hilger, 1987.

[5] M. Nifuku and H. Katoh, “A study on the static electrification of powders during pneumatic transportation and the ignition of dust cloud,” Powder Technol., vol. 135–136, pp. 234–242, Oct. 2003, doi: 10.1016/s0032-5910(03)00163-3.

[6] D. J. Lacks and T. Shinbrot, “Long-standing and unresolved issues in triboelectric charging,” Nat. Rev. Chem., vol. 3, no. 8, pp. 465–476, Jul. 2019, doi: 10.1038/s41570-019-0115-1.

[7] J. Lowell and A. R. Akande, “Contact electrification-why is it variable?,” J. Phys. Appl. Phys., vol. 21, no. 1, pp. 125–137, Jan. 1988, doi: 10.1088/0022-3727/21/1/018.

[8] L. S. McCarty, A. Winkleman, and G. M. Whitesides, “Electrostatic self-assembly of polystyrene microspheres by using chemically directed contact electrification,” Angew. Chem. Int. Ed., vol. 46, no. 1–2, pp. 206–209, Jan. 2007, doi: 10.1002/anie.200602914.

[9] H. T. Baytekin, A. Z. Patashinski, M. Branicki, B. Baytekin, S. Soh, and B. A. Grzybowski, “The mosaic of surface charge in contact electrification,” Science, vol. 333, no. 6040, pp. 308–312, Jul. 2011, doi: 10.1126/science.1201512.

[10] R. K. Pandey, H. Kakehashi, H. Nakanishi, and S. Soh, “Correlating material transfer and charge transfer in contact electrification,” J. Phys. Chem. C, vol. 122, no. 28, pp. 16154–16160, Jul. 2018, doi: 10.1021/acs.jpcc.8b04357.

[11] L. S. McCarty and G. M. Whitesides, “Electrostatic charging due to separation of ions at interfaces: contact electrification of ionic electrets,” Angew. Chem. Int. Ed., vol. 47, no. 12, pp. 2188–2207, Mar. 2008, doi: 10.1002/anie.200701812.

[12] Fujino Mitsuo, ;, Ogata Sumitoshi, ;, and Shinohara Hisashi, “Electric potential distribution profile in a naturally charged fluidized bed and its effects,” Int. Che. Eng., vol. 25, no. 1, pp. 149–159, 1985.

[13] J. Lehr and P. Ron, Foundations of Pulsed Power Technology, 1st ed. Wiley, 2017. doi: 10.1002/9781118886502.

[14] H. Tao and J. Gibert, “Measuring gas discharge in contact electrification,” Nat. Commun., vol. 14, no. 1, Dec. 2023, doi: 10.1038/s41467-023-43721-1.

[15] T. Miura and I. Arakawa, “Gas discharge caused by triboelectricity around a contact during friction between insulators,” IEEE Trans. Dielectr. Electr. Insul., vol. 14, no. 3, pp. 560–565, Jun. 2007, doi: 10.1109/TDEI.2007.369513.

[16] T. Miura, “Observation of charge separation and gas discharge during sliding friction between metals and insulators,” J. Phys. Conf. Ser., vol. 646, p. 012057, Oct. 2015, doi: 10.1088/1742-6596/646/1/012057.

[17] J. Zhang and S. Ciampi, “The position of solid carbon dioxide in the triboelectric series,” Aust. J. Chem., vol. 72, no. 8, p. 633, 2019, doi: 10.1071/ch19239.

[18] T. Matsuyama and H. Yamamoto, “Charge relaxation process dominates contact charging of a particle in atmospheric conditions,” J. Phys. Appl. Phys., vol. 28, no. 12, pp. 2418–2423, Dec. 1995, doi: 10.1088/0022-3727/28/12/005.

[19] T. Matsuyama and H. Yamamoto, “Charge-relaxation process dominates contact charging of a particle in atmospheric condition: II. The general model,” J. Phys. Appl. Phys., vol. 30, no. 15, pp. 2170–2175, Aug. 1997, doi: 10.1088/0022-3727/30/15/008.

[20] X. Liu and S. Sundaresan, “The effect of gas on tribocharging of particles in a vibrated bed,” Powder Technol., vol. 401, p. 117272, Mar. 2022, doi: 10.1016/j.powtec.2022.117272.

[21] K. P. Brand, “Dielectric strength, boiling point and toxicity of gases - different aspects of the same basic molecular properties,” IEEE Trans. Electr. Insul., vol. EI-17, no. 5, pp. 451–456, Oct. 1982, doi: 10.1109/tei.1982.298489.

[22] S. Uhm, S. J. Jung, and H. S. Kim, “Influence of gas temperature on electrical breakdown in cylindrical electrodes,” J. Korean Phys. Soc., vol. 42, pp. S989–S993, Feb. 2003.

[23] R. Massarczyk, P. Chu, C. Dugger, S. R. Elliott, K. Rielage, and W. Xu, “Paschen’s law studies in cold gases,” J. Instrum., vol. 12, no. 06, pp. P06019–P06019, Jun. 2017, doi: 10.1088/1748-0221/12/06/P06019.

[24] A. V. Borodulina, O. V. Minakova, and S. L. Veber, “Breakdown voltage in argon, nitrogen, and sulfur hexafluoride gases as a function of temperature,” Russ. J. Coord. Chem., vol. 48, no. 7, pp. 452–455, Jul. 2022, doi: 10.1134/S1070328422070028.

[25] E. Sili and J. P. Cambronne, “A new empirical expression of the breakdown voltage for combined variations of temperature and pressure,” Mar. 2012, doi: 10.5281/ZENODO.1079916.

[26] B. Gerke et al., “Suppression of electrical breakdown phenomena in liquid TriMethyl Bismuth based ionization detectors,” J. Instrum., vol. 17, no. 09, p. P09029, Sep. 2022, doi: 10.1088/1748-0221/17/09/p09029.

[27] G. Galli et al., “Paschen’s law in extreme pressure and temperature conditions,” IEEE Trans. Plasma Sci., vol. 47, no. 3, pp. 1641–1647, Mar. 2019, doi: 10.1109/tps.2019.2896352.

[28] J. M. Meek, J. D. Craggs, and J. M. Meek, Eds., Electrical breakdown of gases. in Wiley series in plasma physics. Chichester: Wiley, 1978.

[29] L. Norman, K. Silva, B. J. P. Jones, A. D. McDonald, M. R. Tiscareno, and K. Woodruff, “Dielectric strength of noble and quenched gases for high pressure time projection chambers,” 2021, doi: 10.48550/ARXIV.2107.07521.

[30] Y. Fu, P. Zhang, J. P. Verboncoeur, and X. Wang, "Electrical breakdown from macro to micro/nano scales: a tutorial and a review of the state of the art," Plasma Res. Express, vol. 2, no. 1, p. 013001, Feb. 2020, doi: 10.1088/2516-1067/ab6c84.

[31] D. Kunii and O. Levenspiel, Fluidization engineering, 2nd ed. in Butterworth-Heinemann series in chemical engineering. Boston London Singapore (etc.): Butterworth-Heinemann, 1991.

[32] W.-C. Yang, Ed., Handbook of Fluidization and Fluid-Particle Systems, 0 ed. CRC Press, 2003. doi: 10.1201/9780203912744.

[33] "Use and fabrication of polyethylene products," in Handbook of Polyethylene, 0 ed., CRC Press, 2000, pp. 469–518. doi: 10.1201/9781482295467-20.

[34] T. Xie, K. B. McAuley, J. C. C. Hsu, and D. W. Bacon, "Gas phase ethylene polymerization: production processes, polymer properties, and reactor modeling," Ind. Eng. Chem. Res., vol. 33, no. 3, pp. 449–479, Mar. 1994, doi: 10.1021/ie00027a001.

[35] "Commercial development of polyethylene," in Handbook of Polyethylene, 0 ed., CRC Press, 2000, pp. 37–52. doi: 10.1201/9781482295467-4.

[36] S. Horne et al., "Ameripol SN—A Cis-, 4-Polyisoprene," Ind. Eng. Chem., vol. 48, no. 4, pp. 784–791, 1956.

[37] T. E. Nowlin, Business and Technology of the Global Polyethylene Industry: An In-Depth Look at the History, Technology, Catalysts, and Modern Commercial Manufacture of Polyethylene and its Products, 1st ed. Wiley, 2014. doi: 10.1002/9781118946039.

[38] Y. Rao, P. Cai, K. Cann, D. Hussein, W. Mariott, and P. A. Cao, "Supported catalyst with improved flowability," US20190211180A1, 2020

[39] A. Sowinski, "The study of reactor wall fouling in gas-solid fluidized beds caused by electrostatic charge generation," Sep. 2012, doi: 10.20381/RUOR-904.

[40] A. Sowinski, L. Miller, and P. Mehrani, "Investigation of electrostatic charge distribution in gas–solid fluidized beds," Chem. Eng. Sci., vol. 65, no. 9, pp. 2771–2781, May 2010, doi: 10.1016/j.ces.2010.01.008.

[41] D. Song and P. Mehrani, "Comparison of electrostatic charge generation in gas-solid fluidized beds in turbulent versus pre-turbulent flow regime," Powder Technol., vol. 319, pp. 426–433, Sep. 2017, doi: 10.1016/j.powtec.2017.07.013.

[42] W. O. Moughrabiah, J. R. Grace, and X. T. Bi, "Effects of pressure, temperature, and gas velocity on electrostatics in gas−solid fluidized beds," Ind. Eng. Chem. Res., vol. 48, no. 1, pp. 320–325, Jan. 2009, doi: 10.1021/ie800556y.

[43] D. Song and P. Mehrani, "Effect of fluidization pressure on electrostatic charge generation of polyethylene particles," Ind. Eng. Chem. Res., vol. 56, no. 49, pp. 14716–14724, Dec. 2017, doi: 10.1021/acs.iecr.7b04056.

[44] M. I. Nimvari, A. Sowinski, and P. Mehrani, "Effect of temperature on triboelectrifcation of polyethylene particles in a pilot-scale pressurized gas-solid fluidized bed," Powder Technol., vol. 405, p. 117524, Jun. 2022, doi: 10.1016/j.powtec.2022.117524.

[45] A. Giffin and P. Mehrani, “Effect of gas relative humidity on reactor wall fouling generated due to bed electrification in gas-solid fluidized beds,” Powder Technol., vol. 235, pp. 368–375, Feb. 2013, doi: 10.1016/j.powtec.2012.10.037.

[46] N. Sridhar, “Role of dielectric strength of gases on the degree of solids electrostatic charging and fouling in fluidization and pneumatic conveying systems,” Jun. 27, 2023, Université d’Ottawa / University of Ottawa. doi: 10.20381/RUOR-29306.

[47] M. Taghavivand, A. Sowinski, and P. Mehrani, “Triboelectric effects of continuity additives and a silica catalyst support on polyethylene fluidized bed wall fouling,” Chem. Eng. Sci., vol. 245, p. 116882, Dec. 2021, doi: 10.1016/j.ces.2021.116882.

[48] J. Hou et al., “Effect of gas properties and wall materials on particle charging in gas–solid fluidized beds,” Can. J. Chem. Eng., vol. 101, no. 1, pp. 244–255, Jan. 2023, doi: 10.1002/cjce.24568.

[49] N. Sridhar and P. Mehrani, “Utility of argon as a static charge and wall fouling suppressant in atmospheric gas-solid fluidized beds,” Powder Technol., vol. 442, p. 119880, Jun. 2024, doi: 10.1016/j.powtec.2024.119880.

[50] N. Sridhar and P. Mehrani, “Utility of argon as a suppressant of triboelectrification in pressurized Gas-Solid fluidized beds,” Chem. Eng. Sci., vol. 311, p. 121623, Jun. 2025, doi: 10.1016/j.ces.2025.121623.

Chapter 2 Bench-scale Tribocharging of Polyethylene: Role of Gas Type, Temperature, and Relative Humidity

Talha Mukarram Syed, Grissel Myrtle Fernandes, Nikhil Sridhar, Poupak Mehrani

Department of Chemical and Biological Engineering, University of Ottawa

161 Louise Pasteur, Ottawa, ON K1N 6N5, Canada

Manuscript published in the Journal of Electrostatics

Abstract

Bench-scale shake tests were conducted using linear low-density polyethylene (LLDPE) particles in controlled environments of argon, nitrogen, and ambient air to investigate how gas type (argon vs. nitrogen), relative humidity (10-75% RH), and temperature (23 and 65°C) affect charge buildup. Tests involved single and multiple particles in aluminum cups and stainless-steel cups coated with LLDPE resin, respectively. Under low humidity (RH < 3%), charge accumulation with nitrogen was 50% higher than with argon, due to differences in the gases' dielectric strengths. Higher RH (~38%) in ambient air resulted in a saturation charge similar to argon, as increased moisture diminished charge buildup. Across an RH range of 10 to 75%, minimal variation in average particle charge was observed below 40%, but higher relative humidity caused a notable decline in charge accumulation. Elevated temperatures decreased charge buildup under nitrogen, while argon showed no significant change, highlighting a gas-dependent response to temperature.

Keywords: Triboelectrification, Argon, Dielectric strength, Temperature, Relative humidity, Polyethylene

2.1. Introduction

Contact electrification, which occurs when solid surfaces come into contact and separate, is a common occurrence and a persistent challenge in many solid handling and processing industries. During operations such as transportation, mixing, or processing, solids frequently collide with each other and with neighbouring surfaces, leading to charge transfer and accumulation. The buildup of static charge can disrupt process productivity through particle agglomeration and adhesion on contacting surfaces and may even pose a serious risk of electrostatic discharge and subsequent explosions [1]. Among various systems involving solids processing, gas-solid fluidization is particularly susceptible to electrostatic effects [2]. For instance, in the polyethylene (PE) industry, wherein polymerization of ethylene monomers takes place in a gas-phase catalytic fluidized bed reactor, collisions between polymer particles and the polymer and the catalyst contribute to the generation of electrostatic charge inside the reactor [3]. Consequently, charged polymer and catalyst particles foul on the reactor wall, leading to the formation of fused masses called sheets, necessitating reactor shutdowns for cleaning and maintenance. [2]. Given the potential operational challenges linked to electrostatic charging, particularly in industrial settings, it is important to study the factors influencing the degree of charging and determine methods to mitigate the charging effects.

In relation to the gas-solid fluidized beds, several parameters have been shown to strongly affect solids triboelectrification. Among them, studies have shown that gas relative humidity [4-6], fluidization gas type such as argon [7], and elevated temperatures [8, 9] tend to reduce charge generation and accumulation. In particular, temperature has also been found to affect the extent of triboelectrification in other gas-solid systems. Greason [10] examined a metal-insulator contacting system in which a stainless-steel ball was rolled inside cylindrical tubes made of various insulating materials, including glass, PTFE, acrylic, quartz, polycarbonate, and nylon 6/6. He found that for relative humidities below 60%, an increase in temperature from 10 to 30°C led to a decrease in charge magnitude, which was more pronounced at lower humidity levels. This behavior was attributed to a reduction in material resistivity at elevated temperatures, enhancing charge leakage to the ground. In another study, Harris et al. [11] investigated the temperature dependence of contact electrification between nylon and PTFE. In their setup, a PTFE block was placed inside a Faraday cup, and a nylon block was lowered to contact it for 10 seconds while the resulting charge

on the nylon was measured over a range of 24 to 78°C at a controlled humidity level (42-44% RH). They observed that the saturation charge on both insulators approximately halved as the temperature increased. Upon thermogravimetric analysis, they found that the surface moisture had reduced by 40% for nylon from 24 to 78°C, which limited the availability of OH^- ions that the authors claimed to be the charge carriers during contact. Jantac et al. [12] studied triboelectrification through the sliding and shaking of polyethylene particles and glass beads between 22 and 90°C. They reported contrasting trends between the two materials, where the increase in temperature led to an increase in charge on polyethylene, while for glass beads, the charge decreased. The authors attributed this difference to the possible softening of the polyethylene at elevated temperatures, which would increase its effective contact area during collisions, although this was never confirmed in their study. However, the authors suggested that charge leakage dominated in the case of more conductive glass. Nimvari et al. [13] conducted bench-scale shake tests with the linear low-density polyethylene (LLDPE) resin at 23 and 60°C in two stainless-steel cups, where the inner wall of one of the cups was coated with small LLDPE particles. They found that the magnitude of charge generation with the increase in temperature was not affected for the stainless-steel cup, but it was lowered with the coated cup. They also tested the changes in volume resistivity of nylon and polyethylene films at 23 and 60°C. They reported that the volume resistivity declined for both materials at 60°C, indicating that the mobility of charge carriers could increase at higher temperatures.

In addition to temperature, the type of surrounding gas plays an important role in the extent of solids triboelectric charging, as it influences the attainable saturation charge. Under normal conditions, gases are electrical insulators; however, when subjected to sufficiently strong electric fields, they undergo ionization. The resulting free electrons get accelerated by the electric field and collide with neutral gas molecules, leading to the generation of a large number of charge carriers. A conductive pathway is formed between the two surfaces, acting as electrodes across which the electric field is applied, known as gas breakdown [14]. The electric field threshold at which this occurs is the dielectric strength of the gas. Cross [15] proposed that the maximum charge possessable by a particle is limited by this dielectric strength. When two particles collide and attain charges of opposite polarity, a potential difference is developed between them. This potential difference increases as the particles depart from each other until the resultant electric

field approaches the dielectric strength of the gas, at which point gas breakdown occurs. The charge carriers generated can then dissipate some of the accumulated charge [14-16]. Keeping that in mind, it is noteworthy to mention that gases vary widely in their dielectric properties. For instance, at ambient conditions, argon has a relatively lower dielectric strength (~0.6 kV/mm) as compared to other gases such as nitrogen (~3.4 kV/mm) [17]. Consequently, argon gas can break down easily, thereby limiting the allowance for charge buildup to a larger extent than nitrogen in systems prone to static charging and buildup. Matsuyama and Yamamoto [18, 19] in a study using experimentation and modelling reported that the usage of argon reduced the magnitude of impact charging of solids (PTFE, nylon, Delrin, and polystyrene). Their study compared the impact charge gained by a single polymer particle in air and argon after it collides with a metal plate placed at an angle. In a similar study, Miura et al. [20, 21] photographed micro-gap discharge occurring between metal-insulator (stainless steel-quartz) and insulator-insulator (diamond-quartz, diamond-MgO, sapphire-quartz, quartz-quartz) contacts. The study employed a pin-and-disk technique to generate triboelectric charges on either an insulating or conducting pin as it slid on an insulator disk under various gases, including argon, nitrogen, neon, krypton, and air. The authors concluded that gas discharge limits the charge gained by the pin, while also observing that inert gases like argon with low dielectric strength better limit the charges compared to air and nitrogen. Liu and Sundaresan [22] also studied the effect of argon and nitrogen on soda lime and polyethylene particles shaken in a small bench-scale PMMA vibratory bed. Their study concluded that argon appeared to limit the charge on both particles to a lower magnitude.

The dielectric strength of gases is affected by the gas temperature and pressure. In general, an increase in temperature lowers the dielectric strength, although the extent of this drop depends on the gas species and pressure. Mechanistically, increased temperature raises the kinetic energy of gas molecules and electrons, which can accelerate gas ionization and reduce the external voltage requirement to trigger gas breakdown. Additionally, at constant pressure, higher temperature reduces gas density, which lengthens the mean free path of electrons and allows them to gain more energy between collisions, further facilitating breakdown [23]. Several studies have measured breakdown voltage of various gases, such as air, nitrogen, oxygen, argon, neon, etc., under various temperatures, and all have concluded a declining trend [23-26]. This reduction in breakdown voltage with temperature could provide an additional explanation for the reduced charge

accumulation observed in triboelectrification studies that examined the influence of temperature on particle charging. In a previous work, we investigated the influence of fluidizing gas type on the extent of static charging and wall fouling in a polyethylene fluidized bed under both atmospheric pressure [7] and found that the addition of argon resulted in a substantial reduction in wall fouling. These findings reaffirm argon's effectiveness, due to its lower dielectric strength as compared to most other gases, as a static mitigating gas in polyethylene fluidized beds, consistent with the behavior observed for argon in other gas-solid systems discussed earlier.

Although relative humidity is not controlled in industrial polyethylene fluidized bed reactors, its effect on the charging of solids needs to be considered. This is because the relative humidity of the surrounding gas also plays a critical role in determining the extent and persistence of electrostatic charging in solid systems. The impact of relative humidity on solids charging is twofold: some studies report enhanced charging with increased humidity levels, while others demonstrate that humidity promotes charge dissipation. More importantly, humidity's impact on charging is material dependent [27]. Hydrophobic materials tend to retain charge even as humidity increases, whereas hydrophilic materials adsorb moisture that forms conductive films, allowing easier charge dissipation. For instance, Hou et al. [5, 6] investigated the role of relative humidity on charging of HDPE and glass beads in fluidization columns made of stainless-steel, PMMA [5] and copper [6] fluidized with air, nitrogen, and argon. For high-humidity experiments, the inlet gases were passed through a humidifier. In both studies, glass particles exhibited strong charge dissipation as RH increased to 30%, while HDPE particles showed little change. This behavior was reported to stem from the hydrophilic nature of glass particles and the hydrophobic nature of HDPE. Giffin and Mehrani [4] found that relative humidity levels of 60% and above reduced charge generation and subsequent wall fouling in a polyethylene fluidized bed. This reduction was attributed to the hydrophilic nature of the stainless-steel fluidization column walls, which can develop a thin water film under humid conditions, thereby reducing the extent of charge generation and providing a conductive pathway for charge dissipation from PE particles upon particle-wall contacts. Greason [10], in the same study discussed earlier, found that increasing the relative humidity of air from 10 to 70% significantly reduced charge generation on the stainless-steel ball, consistent with enhanced charge leakage at higher humidity. Likewise, Jantac et al. [12] also studied the effect of relative humidity in the same study discussed earlier. Their sliding and shaking apparatus was placed in a

glove box filled with nitrogen with a humidifier to vary the relative humidity. They found that the charge on both polyethylene and glass beads had declined as the humidity level was increased from 10 to 90%. Recent studies demonstrate that the influence of relative humidity on triboelectric charging is non-linear and characterized by a humidity threshold beyond which charge dissipation dominates. Schella et al. [28] investigated polymer-steel contact in an electromagnetic shaker setup over 5% to 100% RH for various polymers, including HDPE, nylon, polyoxymethylene (POM), PMMA, polypropylene (PP), polystyrene (PS), PTFE, and polyvinylchloride (PVC) of diameter 3 mm. The net charge of the particle decreased with increasing humidity and was close to zero when the humidity reached 60%. There was minimal change in the particle net charge at humidities below 30%. Similar trends were observed by Kolehmainen et al. [29], who examined charging of a polyethylene-glass system through controlled single particle-wall collision experiments by using an electromagnetic shaker. Their experimental results, combined with discrete element modelling over an RH range of 20 to 60%, showed that the increasing relative humidity reduces the effective contact potential difference between the particle and the contacting surface. Furthermore, Cruise et al. [30] investigated the charging of PTFE powders of different particle sizes interacting with a grounded stainless-steel container across 10-60% RH by shake tests. The results demonstrated that the RH level at which a sudden decline in charge occurs depends on particle size. Smaller PTFE Particles are discharged at a lower RH than the larger particles because of their higher specific surface area, which enables earlier formation of adsorbed water layers that provide pathways for charge leakage.

As mentioned above, we have carried out pilot-scale investigations in relation to gas-solid fluidization; however, we also realized the necessity to understand, at a small scale, the effect of different gases, relative humidity, and temperature on the generation, accumulation, and saturation of charges on similar particles. Moreover, we found no prior studies that systematically investigated triboelectric charging behavior for LLDPE by varying the gas from nitrogen to argon, along with changes in temperature and relative humidity. To address this gap, the present study employed bench-scale shake tests using LLDPE resin in enclosed containers, one with a bare metal wall and another coated with the same particles. The testing was carried out to replicate relevant contact conditions to the gas-phase polyethylene fluidized bed, namely particle-particle and particle-fluidization column wall collisions. This way, we were able to systematically investigate

the influence of gas environment (argon, nitrogen, and air), temperature, and relative humidity on the triboelectric charging behavior of LLDPE resin particles under controlled conditions. Notably, this study aimed to collect data pertaining to the usage of argon as a static mitigation technique in not only fluidization systems but also other solid-handling and processing operations.

2.2. Materials and methodology

The shake testing was conducted using LLDPE resin directly received from a commercial polyethylene reactor, with a true particle density of 917 kg/m^3. As shown in Figure 2.1, the Scanning Electron Microscope (SEM) image of the resin shows that the particles were non-spherical and had a rough surface. The resin was sieved to obtain particles with diameters of 0.78, 1.2, 2.5, and 5 mm. The 0.78 mm size corresponds to an average particle diameter between 0.71 mm and 0.85 mm sieves, while the larger sizes represent discrete particle diameters. The particles were washed with water to remove any fine particles that might have adhered to their surface during sieving and dried in the oven at 70˚C for 20 hours.

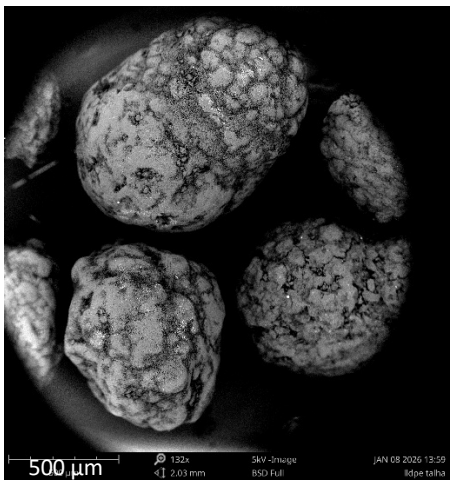

Figure 2.1: SEM image of the LLDPE resin of size 0.78 mm used in the multiple-particle approach.

One set of shake testing was conducted under ambient laboratory air (RH ≈ 38%), while all other experiments were performed inside a glove box equipped with a hygrometer for monitoring humidity and temperature. A schematic and an image of the experimental setup are shown in Figure 2.2. The experiments in the glove box were conducted under controlled humidity and temperature conditions using either nitrogen or argon gas, supplied from a gas cylinder with a 99.9% purity. When the gas type was changed, the glove box was evacuated using a vacuum pump and purged several times with the desired gas until the relative humidity was below 3%. A slight

continuous purge was then maintained overnight. To study the effects at higher RH levels under a nitrogen blanket, a portable humidifier was used inside the glove box to adjust the RH. To achieve equilibrium, the particles and the shaking cup were placed inside the glove box for 48 hours, allowing them to attain identical RH conditions. A temperature of 65°C was selected for the high-temperature trials to approximate the industrial gas-phase polyethylene process conditions, which are typically operated at approximately 70°C. This temperature was achieved by using the orbital shaker (OHAUS® ISLD04HDG) with temperature control, maintained within a tolerance of ± 2.5°C. The shaking cup fixed to the shaker was heated until the desired temperature of 65°C was read by a thermocouple placed inside the cup without touching the cup surface. This temperature was maintained for 30 minutes before the shaking commenced. Before each trial, the shaking cup was grounded, and both the cup and particles were neutralized using a fan-type ionizer (SMC IZF10 R). Charge measurements after shaking were obtained using a Faraday cup connected to a digital electrometer (Keithley® 6514). All experiments were repeated at least twice under identical conditions, and error bars reported in the results represent one standard deviation between repeats.

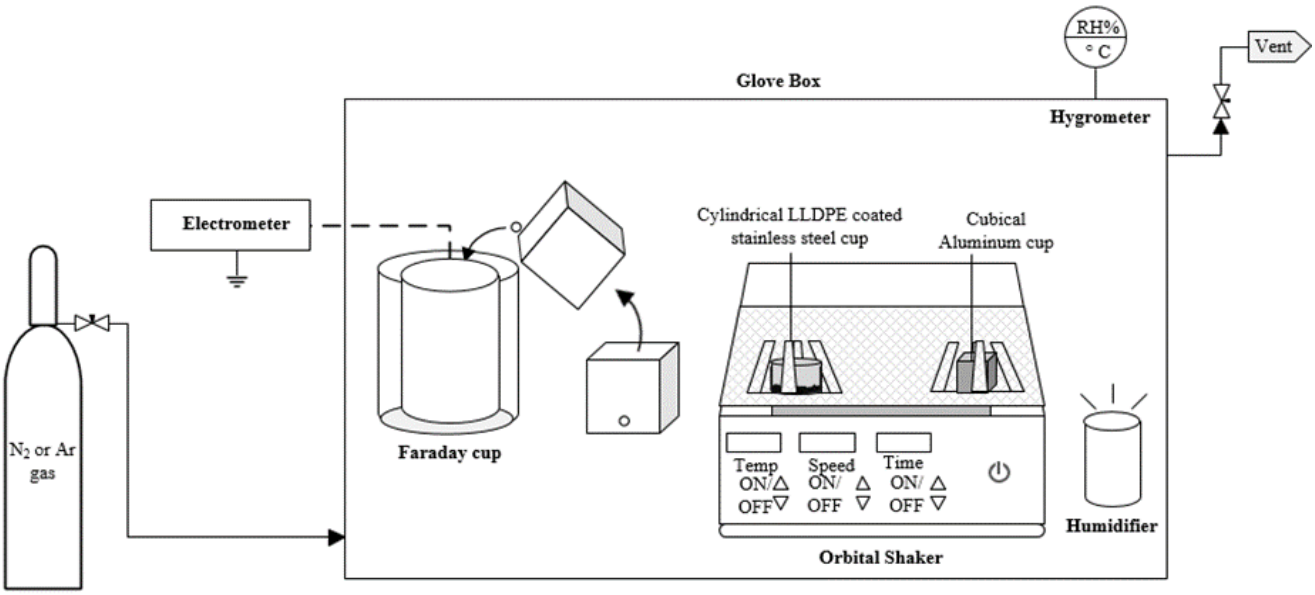

(a)

(b)

Figure 2.2: (a) Schematic diagram of the experimental setup and (b) image of the shaker and the Faraday cage.

Two complementary approaches were employed to investigate contact charging at the bench scale: (i) single-particle shaking, and (ii) multiple-particle shaking. In the single-particle approach, charge generation is dominated by polymer-metal contacts. For this testing, the number of shakes was varied, and the resulting charge values were recorded. In contrast, the multiple-particle approach emphasizes particle-particle interactions, including contacts between bulk particles and smaller wall-adhered particles, representative of conditions encountered in fluidized bed reactors. In this case, a fixed shaking duration was used instead of the number of shakes.

2.2.1 Single-particle approach

The first approach studied the contact charging behavior of a single LLDPE particle of sizes 1.2, 2.5, and 5 mm in contact with a metallic surface. A cubical aluminum container (with a side length of 0.055 m) with a lid was used for these tests (Figure 2.3a). The shake test was conducted manually in an up-and-down motion at different numbers of shakes, ranging from 15 to 240, with each shake representing 2 collisions between the particle and the container wall. The influence of gas type and temperature was investigated with a 5 mm particle. All tests, except the ambient air trials, were performed in the glove box under nitrogen and argon gas environments with a controlled temperature of 23°C and 65°C, while the RH was maintained below 3%. Ambient air trials were carried out under laboratory conditions, where the RH was approximately 38%. After the cup temperature was maintained for 30 minutes, it was removed from the shaker, and while insulated, the manual shaking was commenced. The effect of relative humidity was investigated

with 1.2 and 2.5 mm particles under a nitrogen blanket inside the glove box for a range of 10-75% RH.

2.2.2 Multiple-particle approach

The second approach included the charging behaviour of multiple LLDPE resin particles against a stainless-steel cylindrical cup coated with the same resin particles smaller than 0.5 mm (Figure 2.3b). For each trial, 2 g batches of particles with an average diameter of 0.78 mm were shaken inside the coated cup. These particles were obtained by sieving particles from the same LLDPE resin between 0.71 mm and 0.85 mm sieves. This selection simulates the contact conditions in a fluidized bed, where bulk particles of similar size interact with smaller particles (< 0.5 mm) that typically adhere to the fluidization column wall. A new batch of particles was used in each trial. The trials were performed under argon and nitrogen conditions only. Temperatures tested include 23°C and 65°C, while the RH was maintained below 3%. For the high temperature shake tests, the cup was fixed to an orbital shaker and heated until the desired temperature of 65°C was reached and maintained for 30 minutes. While maintaining a constant temperature, the cup was shaken at 900 RPM for 20 minutes.

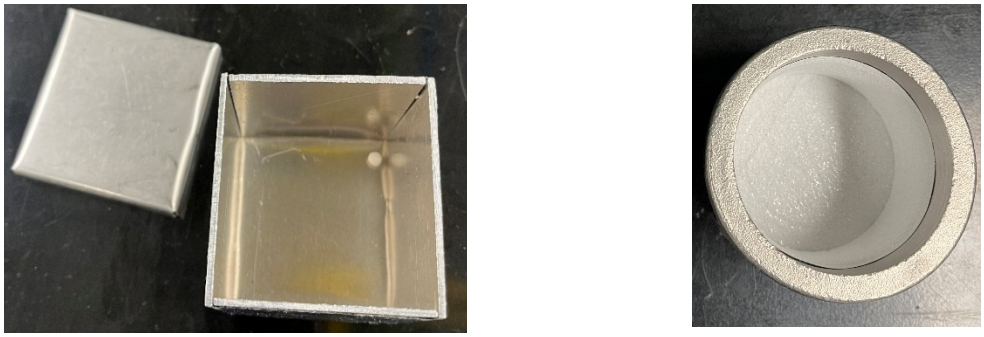

(a) (b)

Figure 2.3: (a) Cubical aluminum shaking cup, and (b) stainless-steel cylindrical cup coated with particles of size < 0.5 mm.

2.3. Results and discussion

The charge accumulation and saturation of LLDPE resin were investigated with varying gas type, relative humidity, and temperature.

2.3.1 Effect of gas type

Single-particle shake tests were performed under different gas environments to examine how the surrounding gas influences charge development. Figure 2.4 presents the charge evolution of a single 5 mm particle shaken in an aluminum cup under ambient air (RH ~38%), and nitrogen argon (RH < 3%) atmospheres. In all conditions, the particles developed a net negative charge upon contact with the aluminum container wall. This behavior is consistent with the lower work function of aluminum (~4.08 eV) [31] relative to polyethylene (~5.3 eV) [32], which drives electron transfer from the metal to the polymer.

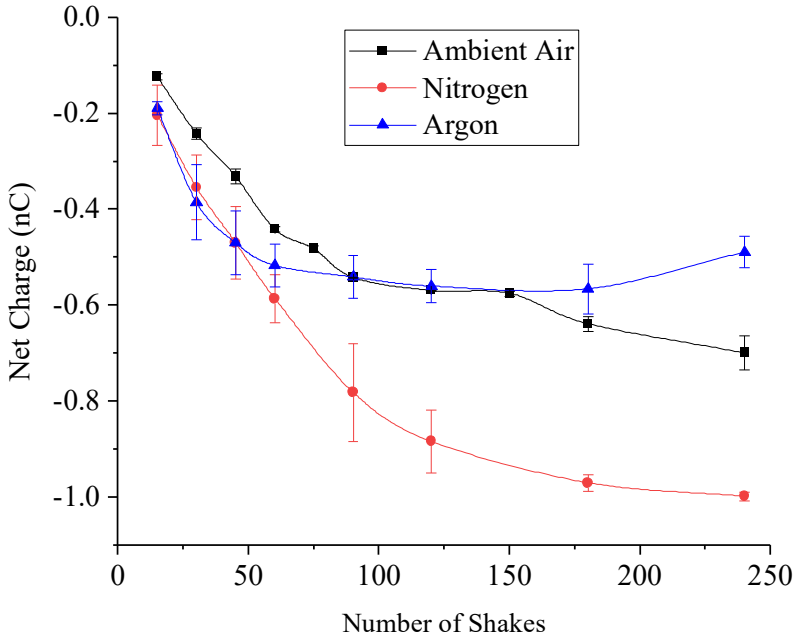

Figure 2.4: Net charge generated on the single 5 mm LLDPE particle when shaken in the aluminum cup under ambient air (RH ~38%), argon (RH < 3%), and nitrogen (RH < 3%) at 23°C.

In ambient air and nitrogen, the charge magnitude gradually increased with the number of shakes and appeared to plateau around 180 shakes before decreasing slightly at 240 shakes. However, in argon, the saturation charge was reached much earlier, closer to 50 shakes, with a value approximately 50% smaller than that in nitrogen. The smaller saturation charge measured under argon can be directly related to argon's smaller dielectric strength relative to nitrogen, as discussed earlier. This property allows argon to ionize at lower electric fields, enhancing charge dissipation

during particle-wall collisions and reducing the extent of charge accumulation on the LLDPE resin surface. Furthermore, it can be noted that the reduction in saturation charge in ambient air at (~38% RH) closely resembles that seen in argon. This is consistent with the effect of humidity discussed earlier, where adsorption of moisture on the hydrophilic aluminum wall surface provides a conductive pathway for charge dissipation of the LLDPE surface upon particle-wall contacts.

2.3.2 Effect of Temperature

To examine how temperature governs charge accumulation, especially under different gases, shaking experiments were conducted under nitrogen and argon at elevated temperatures using both single and multiple particles. The single-particle tests emphasize polymer-metal contacts, whereas the multiple-particle tests are dominated by particle-particle interactions, as detailed in Section 2.2. For the single particles, it is seen from the results in Figure 2.4 that the single 5 mm LLDPE particle reached its saturation charge by 240 shakes, hence, this number of shakes was chosen for investigating the influence of temperature. Figure 2.5 presents the net charge measured on a single 5 mm LLDPE particle after 240 shakes in an aluminum cup under nitrogen and argon at 23°C and 65°C. Under nitrogen, increasing the temperature resulted in an approximately 35% reduction in the saturation charge. In contrast, no measurable change in saturation charge was observed under argon between the two temperatures.

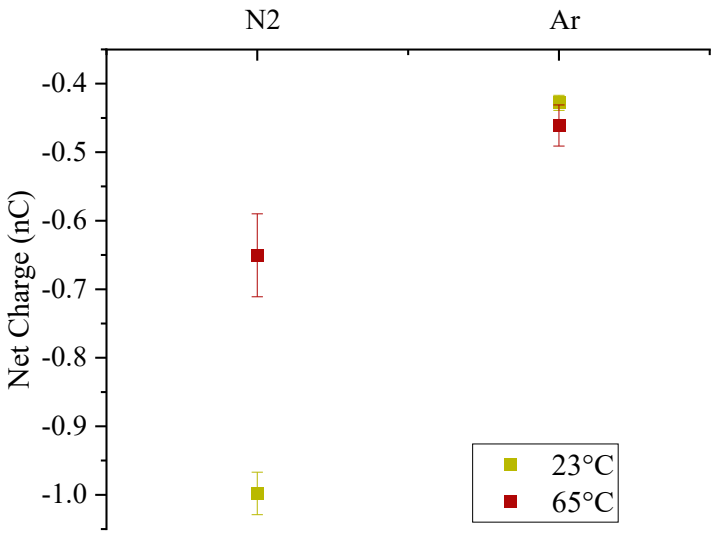

Figure 2.5: Net charge generated on a single 5 mm LLDPE particle after 240 shakes in an aluminum cup under nitrogen and argon atmospheres at 23°C and 65°C, and RH < 3%.

The influence of temperature on charging behavior for multiple particles is shown in Figure 2.6, where the specific charge (nC/g) acquired by 2 g batches of 0.78 mm LLDPE particles in a particle-coated stainless-steel cup after 20 minutes of shaking is reported for both gases and temperatures. Similar to the single-particle results, a pronounced temperature effect was observed under nitrogen, with the net specific charge decreasing by approximately 50% at 65°C compared to ambient conditions. Conversely, the saturation charge measured under argon showed no significant dependence on temperature.

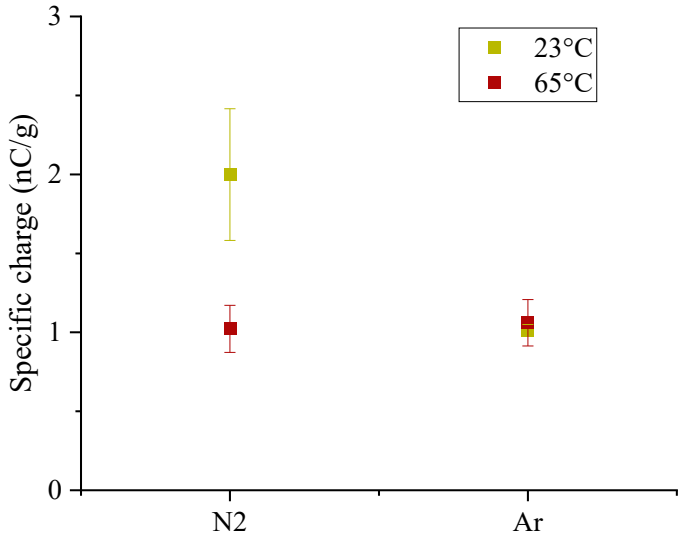

Figure 2.6: Specific charge of a 2 g batch of 0.78 mm LLDPE particles shaken in a particle-coated stainless steel cup at 900 RPM for 20 minutesunder nitrogen and argon atmospheres (RH < 3%) at 23°C and 65°C.

The results from both tests indicate that the influence of temperature on charge accumulation is gas dependent. In the case of multiple particles, charge generation occurs primarily from collisions between the larger particles and the smaller wall-coated particles, while particle-particle contacts among the larger particles contribute minimally to net charging since they are of the same material and approximately similar size. The observed polarity of the larger particles was positive, consistent with prior findings that reported larger particles tend to acquire a positive charge when contacted with smaller particles of the same material [16].

Although previous breakdown voltage studies showed that both nitrogen and argon exhibit a decrease in breakdown voltage with increasing temperature, the charge trends observed in Figure 2.5 and Figure 2.6 do not directly follow this pattern. A possible explanation for this is that charge

accumulation in argon is already limited at ambient temperature due to its inherently low dielectric strength (~0.6 kV/mm at ambient conditions [17]). Therefore, further reductions in breakdown voltage of argon with temperature have little additional impact. In contrast, nitrogen allows for a greater charge buildup at room temperature, so a possible reduction in breakdown voltage of nitrogen or lower surface resistivity or softening of PE with temperature becomes more influential in enhancing charge dissipation with nitrogen.

2.3.3 Effect of relative humidity

Similar to the effect of temperature tests discussed in the previous subsection, relative humidity tests were conducted using single particles shaken in a cubical aluminum cup for 240 shakes. Figure 2.7 presents the net charge measured on single particles of 1.2 mm and 2.5 mm shaken over a range of relative humidity levels (10-75%). The results depict a non-linear decline in charge for both particle sizes. Between 10% and 40% RH, minimal change in average particle charge is seen for both particle sizes, indicating limited moisture influence within this range. However, as RH increases beyond 40%, there is a significant reduction in charge magnitude. The results also imply an important trend that at humidities below 40%, the percent reduction in the particle's charge is independent of its size. However, at greater relative humidities, the charge decay rate depends on the particle size, and hence, the contact area. The charge trends seen in Figure 2.7 are also consistent with literature reports discussed in Section 2.1 [28-30]. These studies showed that the particle charge approaches zero at and above 75% RH. This could be possibly because even though LLDPE is hydrophobic, there still exists a possibility of moisture adsorption on its surface. This film could provide a conductive pathway for charge dissipation from PE particles upon particle-wall contacts and reduce overall charge accumulation. Extended exposure, such as the 48-hour conditioning used in this work, could allow for slow but sufficient adsorption of moisture to form a conductive film on the surface of hydrophobic PE.

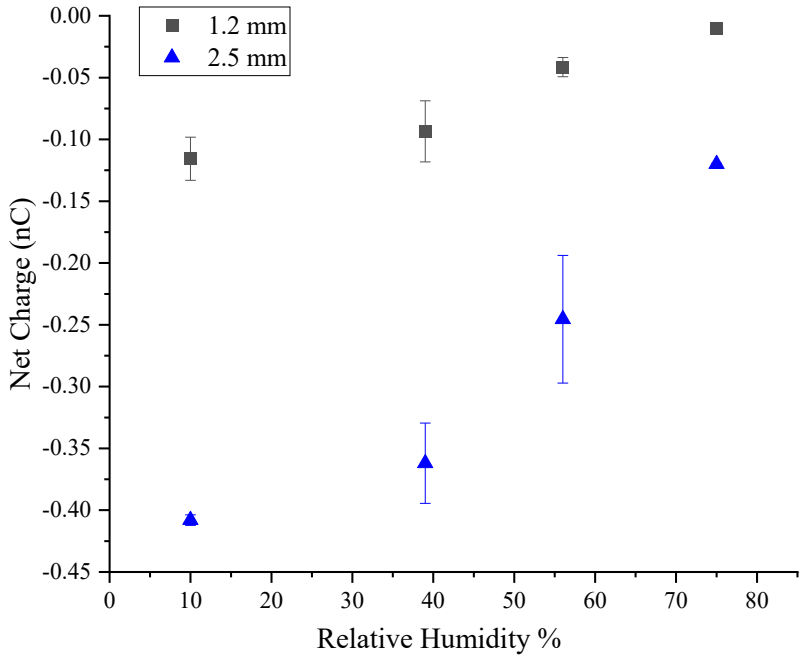

Figure 2.7: Net charge generated on single 1.2 and 2.5 mm particles when shaken in nitrogen at 4 different RH levels (10, 39, 56, and 75%) and 23°C in an aluminum cup.

Additionally, increasing the relative humidity under a nitrogen blanket effectively transforms the gas environment into a nitrogen-water vapor mixture, which can alter the gas discharge characteristics. As mentioned earlier, the maximum charge density attainable on insulating polyethylene particles is ultimately constrained by the electrical breakdown in the surrounding gas. Several studies [33-39] which measured breakdown voltage for humidified air and nitrogen, have reported that the breakdown voltage does not vary monotonically with RH. Most reports indicate that breakdown voltage initially increases with RH due to enhanced electron attachment by water vapor molecules; however, the maximum increase observed from the papers was around 6% [33-36]. In contrast, some studies have also reported a slight decrease in breakdown voltage with increasing RH for both air and nitrogen environments [37-39]. Overall, these findings suggest that RH exerts an uneven and limited influence on the breakdown characteristics of the nitrogen. Considering these reports and the present results, changes in gas breakdown behavior with RH are unlikely to be the dominant mechanism governing the observed charge dissipation.

Moreover, although aluminum surfaces exhibit only a small change in work function with humidity (typically ≤ 0.2 eV) [40], the polyethylene experiences larger effective work function

reductions due to local water structuring and surface dipoles [29]. The smooth and monotonic reduction in charge with RH is consistent with the surface-potential equalization model described by Cruise et al. [28]. So, it is possible that the charge difference may be due to leakage-dominated behavior, where the combined influence of enhanced surface conductivity due to adsorbed moisture and the change in effective contact potential occurs.

2.4. Conclusions

This study examined how gas type (i.e., argon vs nitrogen), temperature, and relative humidity influence charge accumulation in polyethylene by bench-scale shake tests. It was found that RH seems to help dissipate charges and reduce the overall charge held by the particle as observed in the single-particle trials in ambient air (RH ~38%). Experiments for a single particle across a broader RH range revealed that the charge saturation remains relatively stable from 10% to 40% RH, beyond which a decline occurs. Polarity of the charge gained by LLDPE particles seems to be dependent on the size of the particles, with larger particles exhibiting a greater fractional increase in charge dissipation between successive humidity levels compared to smaller particles, as the charge decay rate depends on the particle size and hence, the contact area. Furthermore, the most probable mechanism of charge saturation under increasing relative humidity is the change in surface potentials and conductivity, leading to charge dissipation. It is possible that there is a limited effect of changes in breakdown voltage under increasing relative humidity. The results published in this study also attempt to establish a relation between dielectric strength and charging behaviour observed in solids under continuous collisions. Argon showed a stronger impact on the charge accumulation through triboelectrification relative to nitrogen. Moreover, for both the single- and multiple-particle shaking trials, charge accumulation in argon was consistently lower than in nitrogen, attributed to argon's lower dielectric strength, which promotes faster charge dissipation. Charge accumulation results also highlighted a gas-dependent response to temperature. At a higher temperature (65°C), the charge magnitude in both the single- and multiple-particle cases decreased for nitrogen but remained nearly unchanged for argon, suggesting that charge accumulation in argon is already limited under ambient temperature and thus less sensitive to further influence by temperature elevation. However, measurement of breakdown voltage variation for both gases within the 23-65°C range could also provide further insight into the results observed. These findings have both practical and computational implications. Industrially, they support the use of argon to reduce static charge buildup and fouling

in gas-phase polymerization reactors. On the modeling side, the data provides valuable inputs for computational frameworks that couple electrostatic charging with gas-solid interactions.

Acknowledgements

Financial support from Univation Technologies, LLC (USA) and the Natural Sciences and Engineering Research Council of Canada (NSERC) is acknowledged with gratitude.

References

[1] K. S. Choi, K. T. Moon, J. H. Chung, X. Bi, and J. R. Grace, "Electrostatic hazards of polypropylene powders in the fluidized bed reactor," in *2011 IEEE International Conference on Industrial Engineering and Engineering Management*, Singapore, Singapore: IEEE, Dec. 2011, pp. 995–999. doi: 10.1109/ieem.2011.6118065.

[2] G. Hendrickson, "Electrostatics and gas phase fluidized bed polymerization reactor wall sheeting," *Chemical Engineering Science*, vol. 61, no. 4, pp. 1041–1064, Feb. 2006, doi: 10.1016/j.ces.2005.07.029.

[3] T. E. Nowlin, *Business and Technology of the Global Polyethylene Industry*. 2014. doi: 10.1002/9781118946039.

[4] A. Giffin and P. Mehrani, "Effect of gas relative humidity on reactor wall fouling generated due to bed electrification in gas-solid fluidized beds," *Powder Technology*, vol. 235, pp. 368–375, Feb. 2013, doi: 10.1016/j.powtec.2012.10.037.

[5] J. Hou, J. R. Grace, and X. Bi, "Effect of gas properties on particle charging and wall fouling in gas-solids fluidized beds," *Powder Technology*, vol. 421, p. 118419, May 2023, doi: 10.1016/j.powtec.2023.118419.

[6] J. Hou, J. R. Grace, and X. Bi, "Effect of fluidizing gases, humidity, and grounding on particle charging dynamics in gas-solids fluidized beds," *Chemical Engineering Science*, vol. 306, p. 121279, Mar. 2025, doi: 10.1016/j.ces.2025.121279.

[7] N. Sridhar and P. Mehrani, "Utility of argon as a static charge and wall fouling suppressant in atmospheric gas-solid fluidized beds," *Powder Technology*, vol. 442, p. 119880, Jun. 2024, doi: 10.1016/j.powtec.2024.119880.

[8] W. O. Moughrabiah, J. R. Grace, and X. T. Bi, "Effects of pressure, temperature, and gas velocity on electrostatics in gas−solid fluidized beds," *Ind. Eng. Chem. Res.*, vol. 48, no. 1, pp. 320–325, Jan. 2009, doi: 10.1021/ie800556y.

[9] M. I. Nimvari, A. Sowinski, and P. Mehrani, "Effect of temperature on triboelectrifcation of polyethylene particles in a pilot-scale pressurized gas-solid fluidized bed," *Powder Technology*, vol. 405, p. 117524, Jun. 2022, doi: 10.1016/j.powtec.2022.117524.

[10] W. D. Greason, "Investigation of a test methodology for triboelectrification," *Journal of Electrostatics*, vol. 49, no. 3–4, pp. 245–256, Aug. 2000, doi: 10.1016/S0304-3886(00)00013-9.

[11] I. A. Harris, M. X. Lim, and H. M. Jaeger, "Temperature dependence of nylon and PTFE triboelectrification," *Phys. Rev. Materials*, vol. 3, no. 8, p. 085603, Aug. 2019, doi: 10.1103/PhysRevMaterials.3.085603.

[12] S. Jantač, L. Konopka, and J. Kosek, "Experimental study of triboelectric charging of polyethylene powders: Effect of humidity, impact velocity and temperature," *Advanced Powder Technology*, vol. 30, no. 1, pp. 148–155, Jan. 2019, doi: 10.1016/j.apt.2018.10.017.

[13] M. I. Nimvari, A. Sowinski, and P. Mehrani, "Investigation of the role of temperature on contact electrification of polyethylene particles," *Powder Technology*, vol. 433, p. 119236, Jan. 2024, doi: 10.1016/j.powtec.2023.119236.

[14] H. Tao and J. Gibert, "Measuring gas discharge in contact electrification," *Nat Commun*, vol. 14, no. 1, Dec. 2023, doi: 10.1038/s41467-023-43721-1.

[15] J. Cross, *Electrostatics: principles, problems and applications*. Bristol: Hilger, 1987.

[16] D. J. Lacks and T. Shinbrot, "Long-standing and unresolved issues in triboelectric charging," *Nat Rev Chem*, vol. 3, no. 8, pp. 465–476, Jul. 2019, doi: 10.1038/s41570-019-0115-1.

[17] K. P. Brand, "Dielectric strength, boiling point and toxicity of gases - different aspects of the same basic molecular properties," *IEEE Trans. Elect. Insul.*, vol. EI-17, no. 5, pp. 451–456, Oct. 1982, doi: 10.1109/tei.1982.298489.

[18] T. Matsuyama and H. Yamamoto, "Charge relaxation process dominates contact charging of a particle in atmospheric conditions," *J. Phys. D: Appl. Phys.*, vol. 28, no. 12, pp. 2418–2423, Dec. 1995, doi: 10.1088/0022-3727/28/12/005.

[19] T. Matsuyama and H. Yamamoto, "Charge-relaxation process dominates contact charging of a particle in atmospheric condition: II. The general model," *J. Phys. D: Appl. Phys.*, vol. 30, no. 15, pp. 2170–2175, Aug. 1997, doi: 10.1088/0022-3727/30/15/008.

[20] T. Miura and I. Arakawa, "Gas discharge caused by triboelectricity around a contact during friction between insulators," *IEEE Trans. Dielect. Electr. Insul.*, vol. 14, no. 3, pp. 560–565, Jun. 2007, doi: 10.1109/TDEI.2007.369513.

[21] T. Miura, "Observation of charge separation and gas discharge during sliding friction between metals and insulators," *J. Phys.: Conf. Ser.*, vol. 646, p. 012057, Oct. 2015, doi: 10.1088/1742-6596/646/1/012057.

[22] X. Liu and S. Sundaresan, "The effect of gas on tribocharging of particles in a vibrated bed," *Powder Technology*, vol. 401, p. 117272, Mar. 2022, doi: 10.1016/j.powtec.2022.117272.

[23] E. Sili and J. P. Cambronne, "A new empirical expression of the breakdown voltage for combined variations of temperature and pressure," Mar. 2012, doi: 10.5281/ZENODO.1079916.

[24] S. Uhm, S. J. Jung, and H. S. Kim, "Influence of gas temperature on electrical breakdown in cylindrical electrodes," *Journal of the Korean Physical Society*, vol. 42, pp. S989–S993, Feb. 2003.

[25] R. Massarczyk, P. Chu, C. Dugger, S. R. Elliott, K. Rielage, and W. Xu, "Paschen's law studies in cold gases," *J. Inst.*, vol. 12, no. 06, pp. P06019–P06019, Jun. 2017, doi: 10.1088/1748-0221/12/06/P06019.

[26] A. V. Borodulina, O. V. Minakova, and S. L. Veber, "Breakdown voltage in argon, nitrogen, and sulfur hexafluoride gases as a function of temperature," *Russ J Coord Chem*, vol. 48, no. 7, pp. 452–455, Jul. 2022, doi: 10.1134/S1070328422070028.

[27] H. Yu, N. Huang, and L. Xie, "Effects of relative humidity on contact electrification in granular system," *Journal of Electrostatics*, vol. 135, p. 104092, Jun. 2025, doi: 10.1016/j.elstat.2025.104092.

[28] A. Schella, S. Herminghaus, and M. Schröter, "Influence of humidity on tribo-electric charging and segregation in shaken granular media," *Soft Matter*, vol. 13, no. 2, pp. 394–401, 2017, doi: 10.1039/C6SM02041K.

[29] J. Kolehmainen *et al.*, "Effect of humidity on triboelectric charging in a vertically vibrated granular bed: Experiments and modeling," *Chemical Engineering Science*, vol. 173, pp. 363–373, Dec. 2017, doi: 10.1016/j.ces.2017.08.006.

[30] R. D. Cruise, K. Hadler, S. O. Starr, and J. J. Cilliers, "The effect of particle size and relative humidity on triboelectric charge saturation," *J. Phys. D: Appl. Phys.*, vol. 55, no. 18, p. 185306, May 2022, doi: 10.1088/1361-6463/ac5081.

[31] J. R. Rumble, Ed., *CRC handbook of chemistry and physics*, 102nd edition 2021-2022. Boca Raton London New York: CRC Press, 2021.

[32] D. Song and P. Mehrani, "Mechanism of particle build-up on gas-solid fluidization column wall due to electrostatic charge generation," *Powder Technology*, vol. 316, pp. 166–170, Jul. 2017, doi: 10.1016/j.powtec.2017.01.031.

[33] E. Kuffel, "Influence of humidity on the breakdown voltage of sphere-gaps and uniform-field gaps," Proc. IEE A Power Eng. UK, vol. 108, no. 40, p. 295, 1961, doi: 10.1049/pi-a.1961.0060.

[34] Z. Zhao et al., "Evolutions of streamer dynamics and discharge instabilities under repetitive pulses in humid air," Plasma Sources Sci. Technol., vol. 32, no. 12, p. 125011, Dec. 2023, doi: 10.1088/1361-6595/ad0d08.

[35] M. Radmilović-Radjenović, B. Radjenović, Ž. Nikitović, Š. Matejčik, and M. Klas, "The humidity effect on the breakdown voltage characteristics and the transport parameters of air," Nuclear Instruments and Methods in Physics Research Section B: Beam Interactions with Materials and Atoms, vol. 279, pp. 103–105, May 2012, doi: 10.1016/j.nimb.2011.10.053.

[36] B. S. Paraselli, "Measurement of air breakdown voltage and electric field using standad sphere gap method", Accessed: Feb. 23, 2025. [Online]. Available: https://core.ac.uk/reader/53188100

[37] F. Cai, B. Zhou, and J. Xue, "Influence of moisture on the insulation characteristics of nitrogen," Journal of International Council on Electrical Engineering, vol. 8, no. 1, pp. 51–56, Jan. 2018, doi: 10.1080/22348972.2018.1471864.

[38] R. W. Macpherson, M. P. Wilson, I. V. Timoshkin, S. J. Macgregor, and M. J. Given, "Impulsive flashover characteristics and weibull statistical analysis of gas-solid interfaces

with varying relative humidity," IEEE Access, vol. 8, pp. 228454–228465, 2020, doi: 10.1109/ACCESS.2020.3046088.

[39] J. T. Krile, A. A. Neuber, J. C. Dickens, and H. G. Krompholz, "DC flashover of a dielectric surface in atmospheric conditions," IEEE Trans. Plasma Sci., vol. 32, no. 5, pp. 1828–1834, Oct. 2004, doi: 10.1109/TPS.2004.835483.

[40] J. R. Middleton, A. J. Scott, R. Storey, M. Marucci, and M. Ghadiri, "Prediction of the effective work function of aspirin and paracetamol crystals by density functional theory─a first-principles study," *Crystal Growth & Design*, vol. 23, no. 9, pp. 6308–6317, Sep. 2023, doi: 10.1021/acs.cgd.3c00218.

Chapter 3 Dielectric Strength of Argon, Nitrogen, and Their Binary Mixtures at Elevated Pressures and Temperatures

Talha Mukarram Syed, Mohsen Isaac Nimvari, Poupak Mehrani

Department of Chemical and Biological Engineering, University of Ottawa,

161 Louise Pasteur, Ottawa, ON K1N 6N5, Canada

Manuscript to be submitted to the Journal of Electrostatics

Abstract

In this work, the breakdown voltage of pure argon, pure nitrogen, and their binary mixtures containing 25, 50, 75, and 90 vol.% argon was measured at temperatures of 25, 70, and 110°C (± 2°C) and pressures ranging from 101.3 to 2600 kPa. Breakdown voltages were measured using a parallel-plate electrode configuration housed in a high-pressure chamber equipped with heating. Breakdown voltages were normalized by the effective electrode gap to account for thermal expansion. For both pure gases, dielectric strength increased nonlinearly with pressure, consistent with high *pd* Paschen behavior. Temperature effects on dielectric strength were modest between 25 and 110°C, with argon exhibiting a larger relative decline with temperature compared to nitrogen. At both pressures, gas mixtures exhibited strong nonlinear behavior, with argon additions as small as 25 vol.% to nitrogen causing a ~40% reduction in dielectric strength compared to pure nitrogen, but gradual reductions between intermediate mixtures. Temperature effects for gas mixtures were minimal between 25 and 70°C, mirroring trends observed for pure gases.

Keywords: Dielectric strength, Breakdown voltage, Paschen law, Nitrogen-argon mixtures, High-pressure discharges, Triboelectrification

3.1 Introduction

Triboelectrification commonly occurs in gas-solid handling and processing systems because particles frequently collide with one another and with surrounding surfaces. In some systems, this phenomenon can lead to operational difficulties, making its effective mitigation essential. Industrial gas-solid polyethylene fluidized bed reactors, which typically operate at pressures up to 2600 kPa and temperatures between 70-110°C, are a clear example of systems where mitigating triboelectrification is essential. In these reactors, repeated contacts between polymer and catalyst particles with each other and with the reactor wall lead to adherence of highly charged particles to the reactor walls, also known as sheeting [1]. In mitigating triboelectrification effects, argon's ability to suppress static charge buildup has been reported in several systems , including gas-solid fluidized beds [2-4]. The reason is argon's considerably lower dielectric strength compared to other gases. At 20°C and 1 atm, argon exhibits a breakdown strength of approximately 0.6 kV/mm compared with 3.4 kV/mm for nitrogen [5]. This difference is particularly relevant in triboelectric systems, where the gas dielectric strength limits the maximum charge a solid can attain. For instance, in gas-solid fluidized beds, particle charge upon collision and, as they separate, develop a growing potential difference. When this potential exceeds the gas breakdown threshold, ionization occurs, and the resulting ion-electron pairs dissipate the surface charge of the fluidizing particles [6]. Gases with lower dielectric strength, such as argon, therefore, ionize at lower field strengths and more effectively limit charge accumulation, leading to a reduced saturation charge compared to nitrogen or air. In recent studies, we have demonstrated that incorporating argon into the fluidizing medium has consistently reduced charge buildup in fluidized beds [7, 8].

The dielectric or breakdown strength of a gas is a concept that has been extensively studied in literature for many years. A foundational contribution is the Paschen law, developed in 1889 by Friedrich Paschen [9], which states that

$$V_B = \frac{Bpd}{\ln(Apd) - ln\left\{\ln\left(1 + \frac{1}{\gamma}\right)\right\}} \qquad \text{(Eq. 2.1)}$$

where p represents gas pressure and d is the distance between electrodes. A and B are gas-specific constants. γ is the secondary electron emission coefficient, influenced by factors such as the cathode work function and the ionization potential of the gas. Representative values of A, B, and the valid reduced electric field ranges (E/P) for some common gases are provided in Table 3.1.

Table 3.1: Values for A and B and their range of validity for different gases [9].

Gas	***A*** **(Torr.cm)$^{-1}$**	***B*** **(V/Torr.cm)**	***E/P*** **(V/Torr.cm)**
Air	14.6	365	100-800
Nitrogen	12	342	100-600
Argon	13.6	235	100-600
Hydrogen	5.1	138.8	20-600

Graphically, the Paschen law yields the well-known Paschen curve (Figure 3.1), which is unique to each gas but retains a characteristic shape featuring a distinct minimum at $(pd)_{min}$. To the left of this minimum, the breakdown voltage increases because reducing pressure decreases the number of molecules available for ionization. In this region, the breakdown voltage decreases sharply with pressure. Beyond the minimum, the increased molecular density shortens the electrons' mean free path. The mean free path refers to the average distance an electron can travel before colliding with a gas molecule. The reduced mean free path translates into a rise in collision frequency, restricting the energy electrons can acquire between impacts, thereby elevating the breakdown voltage with increasing pressure [9].

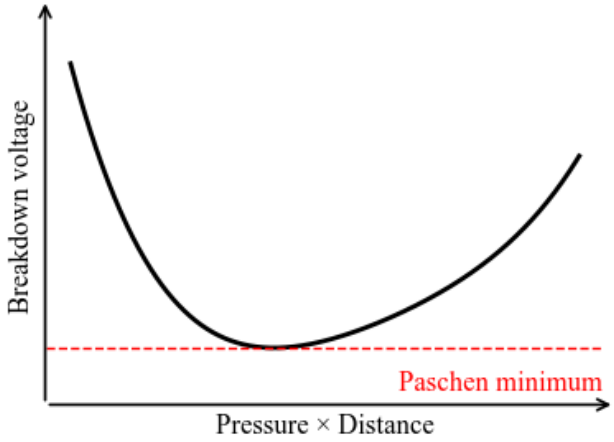

Figure 3.1: General Paschen law trend.

The Paschen law emerges from Townsend's breakdown theory [9-11]. In this model, free electrons initially present in the gap are accelerated by the applied electric field and collide with neutral gas molecules. If they collide with an energy that exceeds the ionization energy of the gas, additional electrons and positive ions are generated, eventually leading to an electron avalanche. For a self-sustaining avalanche to occur, electrons must acquire sufficient energy between collisions, which is governed by the electric field strength and the mean free path. If the mean free path is too short, frequent collisions prevent electrons from gaining ionizing energy. If it is too long, collisions and thus ionization events become too infrequent to sustain the cascade. Townsend formalized this behavior through two parameters: the first ionization coefficient, α, representing the number of ionizing collisions per unit distance, and the secondary electron emission coefficient, γ. The criterion for the Townsend theory to hold is given by

$$\alpha d = ln\,(1 + \frac{1}{\gamma}) \qquad \text{(Eq. 2.2)}$$

where α is the first ionization coefficient, γ is the secondary electron emission coefficient, and d is the gap distance.

The Townsend theory, however, fails at very low gaps, where electron tunnelling from cathode to anode and field emission can dominate [9, 12]. Additionally, the theory also fails at higher pressures and higher gap distances, where the electron avalanche itself generates an electric field strong enough to sustain further ionization. As electrons advance toward the anode, slower positive ions accumulate behind them, creating localized electric fields at the avalanche head. If the avalanche becomes densely populated with charges, this localized field can even exceed the applied electric field and give rise to secondary avalanches, which eventually form a conductive stream between the anode and cathode. The criterion for which mechanism becomes significant is provided by the Meek-Raether criterion, given below [9-11].

$$\alpha d \sim 18 - 21 \qquad \text{(Eq. 2.3)}$$

The markedly different dielectric strength of argon and nitrogen can be understood in terms of their distinct molecular properties. Argon, being monoatomic, lacks rotational and vibrational modes, so electron-atom collisions primarily lead to electronic excitation or ionization. On the other hand, nitrogen is a diatomic molecule with numerous low-energy vibrational and rotational modes that efficiently absorb electron energy without contributing to ionization [10, 13]. As a result, a larger fraction of the energy from the collisions in nitrogen is diverted into non-ionizing processes, requiring higher electric fields to sustain breakdown. Due to these reasons, argon has larger ionization coefficients and ionization efficiency than nitrogen, resulting in a lower dielectric strength [14].

In the case of gas mixtures, the breakdown behavior deviates significantly from that of the pure components, even at low additive concentrations. This sensitivity arises because each species introduces distinct ionization potentials and molecular excitation pathways. Consequently, in the context of Paschen law, the effective gas-dependent parameters *A* and *B* for a mixture cannot be inferred directly from those of the pure gases and must instead be determined empirically. In the context of Ar-N_2 mixtures, experimental studies on their breakdown behavior remain limited, and existing works have primarily focused on argon-rich compositions developed for plasma and sputtering applications. Chiad et al. [15] investigated Ar-N_2 mixtures at sub-atmospheric pressure (0.6 mbar) using stainless-steel parallel-plate electrodes. They reported an abrupt rise in

breakdown voltage upon nitrogen addition for mixture ratios of 2.5:1 and 1:1. This increase was attributed to additional energy-loss channels associated with nitrogen's vibrational, rotational, and dissociative modes. Similar trends were reported by Omar et al. [16], who observed an increasing breakdown voltage with higher nitrogen concentration in Ar-N_2 (5:3 & 1:1) mixtures using cylindrical electrodes of aluminum, copper, and stainless steel. Again, the behavior was attributed to enhanced non-ionizing energy dissipation in nitrogen-rich mixtures. Additionally, in a study by Radmilović-Radjenović et al. [17], gas discharges in microgaps were examined using molybdenum electrodes for various gases, including Ar-N_2 mixtures containing 2% and 5% nitrogen in argon. Their results showed that even small additions of nitrogen led to a significant increase in breakdown voltage relative to pure argon, while further increasing the nitrogen content from 2% to 5% produced only a marginal additional effect.

Temperature, although not explicitly mentioned in the Paschen law, exerts a strong influence on the breakdown behavior of gases. As temperature increases, the average kinetic energy of gas molecules and free electrons rises, enhancing collision frequency and increasing the probability that an electron acquires sufficient energy to ionize neutral molecules. At constant pressure, the resulting decrease in gas density lengthens the mean free path between collisions, allowing electrons to gain more energy from the applied field before impact. Collectively, these effects reduce the voltage threshold required to initiate ionization, thereby lowering the breakdown voltage [18]. This temperature dependence has been captured empirically by classical corrections such as the Peek and Dunbar models (see Figure 3.2), which modify Paschen's law using ideal-gas assumptions [18, 19]. The Peek model introduced a voltage correction proportional to T_0/T, where T_0 is the ambient temperature, and T is the new temperature. This lowers the curve from the original Paschen curve at room temperature. In the Dunbar correction, the pressure term is adjusted by a factor of T_0/T, pushing the curve to the right for higher temperatures. Uhm et al. [20] studied the variation in breakdown voltage with temperature for air, nitrogen, and oxygen over 27-300°C using cylindrical electrodes. They observed that the breakdown voltage consistently reduced with temperature for all gases. A similar trend was also observed by Massarczyk et al. [21] for neon, nitrogen, argon, and xenon between -193°C and 22°C at 1atm in a pin-plate setup. However, their trends suggested that the magnitude of breakdown voltage reduction in the same temperature range was different for different gases. Borodulina et al. [22] also reported a gas-specific declining trend

for breakdown voltage with temperature, where they found nitrogen's breakdown voltage to decrease by nearly 50% between -193°C and 22°C, compared with 36% for argon in a parallel-plate electrode setup. Galli et al. [19] investigated the combined influence of pressure and temperature on argon breakdown voltage up to 1 MPa and 400°C using a stainless-steel spherical electrode setup. Their results showed that, regardless of pressure, the breakdown voltage of argon decreased from 20°C to about 100°C but began to rise again above 200°C. This reversal was attributed to the excessive increase in electron drift velocity at very high temperatures, leading to more frequent collisions that prevent electrons from gaining sufficient energy between impacts to ionize neutral atoms.

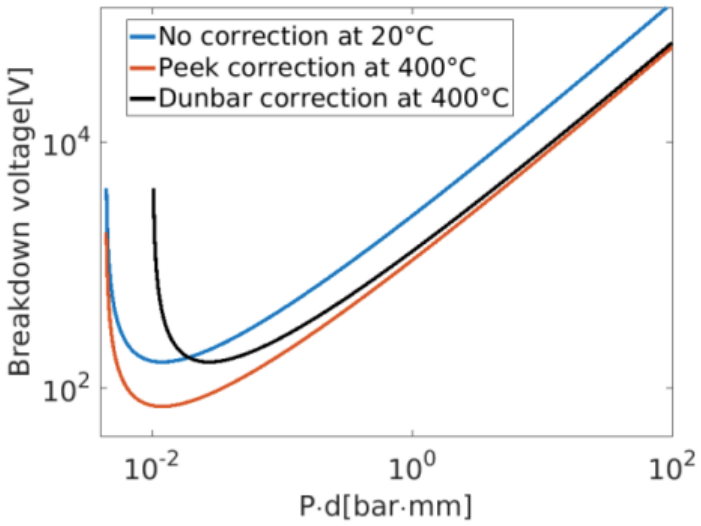

Figure 3.2: Peek and Dunbar corrections at 400°C plotted along with the standard Paschen curve (copied from *[19]*).

Despite the importance of dielectric strength in governing charge dissipation within polyethylene gas-solid fluidized bed reactors, systematic breakdown voltage data for argon, nitrogen, and their binary mixtures under conditions relevant to industrial polyethylene fluidized bed operation remain limited. Existing studies for these gases have generally been conducted at pressures well below 2600 kPa, at temperatures outside the operational range of interest, or have examined temperature effects only for individual gases rather than comparing argon, nitrogen, and their mixtures. As a result, the literature lacks a coherent understanding of how breakdown voltage

varies for the aforementioned gases at elevated pressures and temperatures. To address this gap, the present work measures the breakdown voltage of argon, nitrogen, and their binary mixtures at 25, 70, and 110°C over pressures from 101.3 kPa up to 2600 kPa. These results provide a quantitative insight into the extent to which dielectric strength influences static charge generation and accumulation in polyethylene fluidized bed reactors and related triboelectric environments.

3.2 Materials and methodology

The gas breakdown was measured in a 50 mm diameter stainless-steel test chamber, 90 mm long, with a pressure rating of up to 20.8 MPa and having three outlets. (Figure 3.3a, Figure 3.4). Two stainless-steel round parallel plate electrodes were mounted inside the chamber, with each electrode having a diameter of 25.4 mm, and the inter-electrode gap was fixed at 1.065 mm, measured using precision feeler gauges (Figure 3.3b, c). One electrode was electrically grounded and served as the anode, while the opposing electrode was left ungrounded and functioned as the cathode. The chamber was fitted with gas inlet and outlet lines, as well as a K-type thermocouple and a pressure gauge. The thermocouple was positioned above the electrode region, away from the chamber walls, to monitor the internal gas temperature.

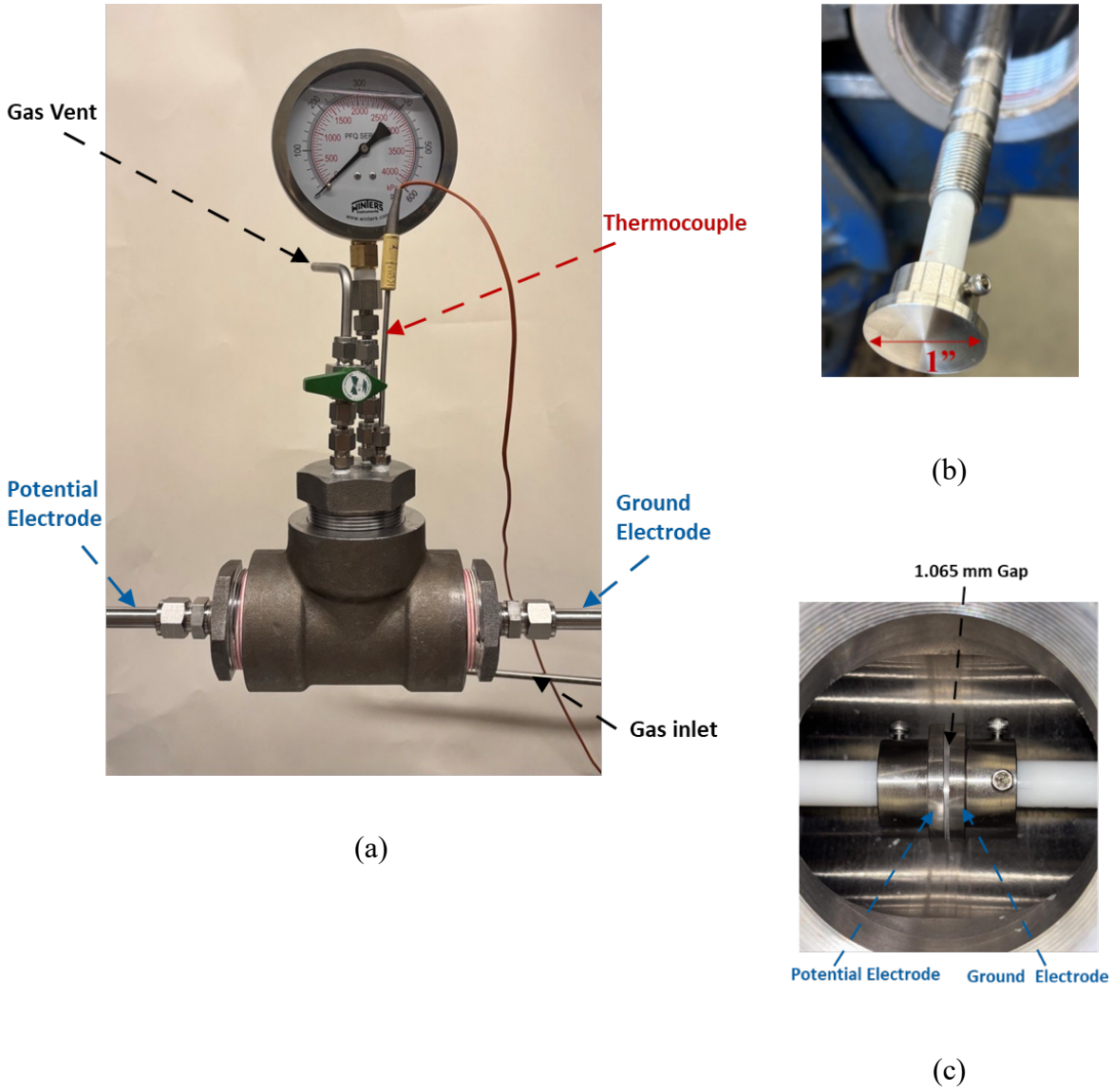

Figure 3.3: Images of the (a) test chamber with mounted electrodes, (b) plate electrode, and (c) parallel-plate electrodes setup in the test chamber.

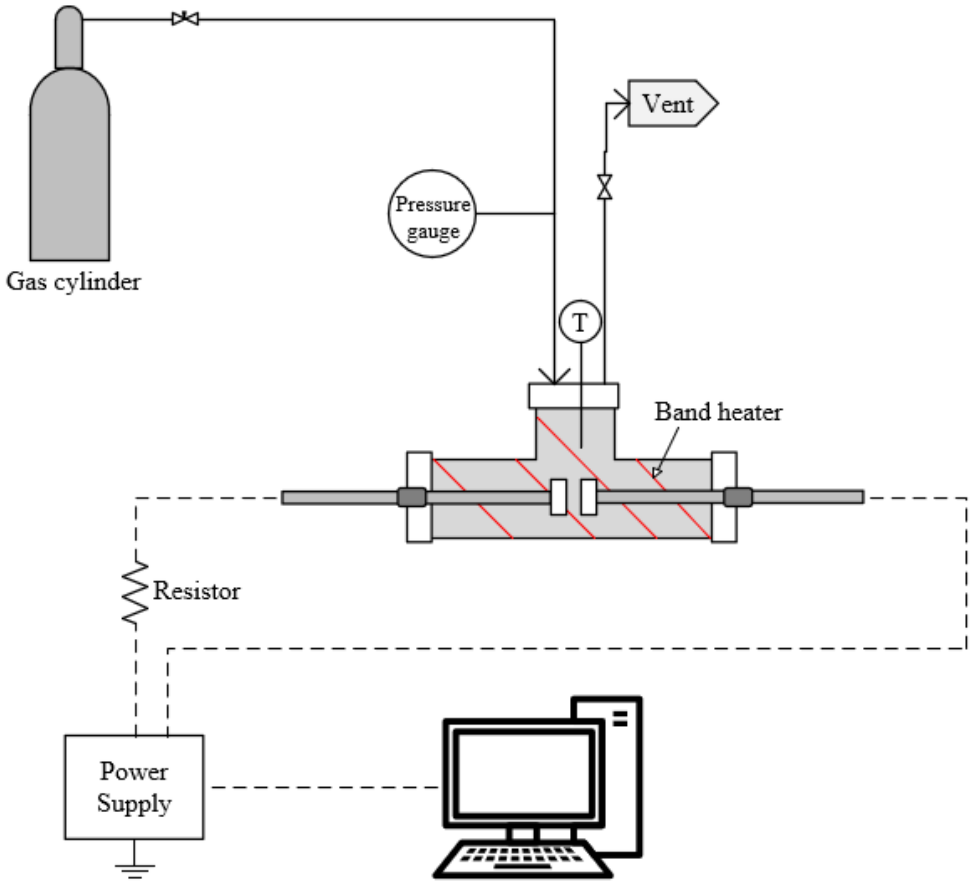

Figure 3.4: Schematic of the breakdown voltage measurement apparatus.

Argon and nitrogen gases were supplied from individual cylinders (99.9% purity) and introduced into the chamber through needle valves, which were used to control gas flow and establish desired Ar-N_2 mixtures directly inside the chamber based on the gases' partial pressures. For elevated-temperature experiments, band heaters were wrapped around the body of the chamber. The assembly was also insulated to minimize heat loss. The temperature in the chamber was maintained within a tolerance of ± 2°C. Breakdown measurements were conducted for pure nitrogen, pure argon, and their binary mixtures containing 25, 50, 75, and 90 vol.% argon. For the pure gases, experiments were performed over pressures ranging from 101.3 to 2600 kPa and at temperatures of 25, 70, and 110°C. For the gas mixtures, testing was limited to pressures of 101.3 and 2600 kPa, and temperatures of 25 and 70°C.

A high-voltage DC power supply (UltraVolt HV Rack series) was used to apply voltage across the electrode gap. The power supply could deliver up to 40 kV with a maximum output current of 100 μA. The high-voltage output was connected to the ungrounded electrode with a current-limiting resistor connected in series to prevent excessive current flow following electrical breakdown. The power supply was interfaced with a computer, enabling real-time monitoring and recording of the applied voltage and discharge current using the LabVIEW software throughout each test.

Before each measurement, the chamber was purged to remove residual gases and contaminants. The chamber was filled with the test gas to 2000 kPa and evacuated by applying suction through the outlet valve; this fill-evacuate cycle was repeated at least three times. After purging, the chamber was filled with the test gas to the desired operating pressure. For elevated-temperature experiments, the band heaters were activated at this point, and the chamber temperature was monitored using the LabVIEW software. The temperature was raised to the target value, after which the heaters were switched off, and the system was allowed to thermally stabilize before testing. The total heating and stabilization time for each trial was approximately 30 minutes. Once the desired testing conditions were achieved, the voltage from the power supply was increased at a constant ramp rate of 50 V/s, with the applied voltage and discharge current continuously monitored during this time. The gas breakdown was identified by a sudden increase in discharge current accompanied by a sharp drop in the applied voltage. Each experimental condition was tested a minimum of three times to ensure reproducibility. Additionally, repeated measurements were not conducted consecutively or even on the same day. Moreover, for gas mixture experiments, the gas filling order was alternated between repetitions.

3.3 Results and discussion

Since breakdown voltage is highly sensitive to the inter-electrode spacing, it was necessary to first quantify changes in the electrode gap arising from thermal expansion during elevated-temperature experiments. The electrode gap was initially set to 1.067 mm at room temperature (25°C), after which the chamber was heated to 120°C while the gap distance was measured at discrete temperatures. The system was then allowed to cool back to 25°C, with gap measurements repeated at the same temperature points. Figure 3.5 shows the variation of the inter-electrode gap as a function of temperature. The gap distance decreases approximately linearly with increasing temperature due to the thermal expansion of the stainless-steel electrodes, effectively reducing the

separation between the plates. The linear fit obtained from this testing was subsequently used to correct the effective electrode gap during high-temperature breakdown measurements.

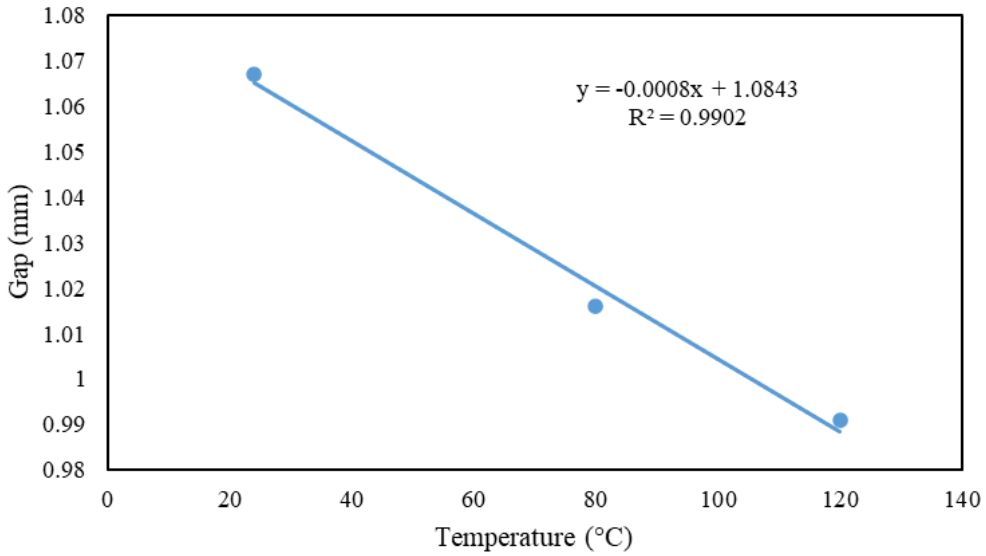

Figure 3.5: Variation of inter-electrode gap as a function of temperature.

Figure 3.6 presents the variation of normalized breakdown voltage, expressed as dielectric field strength (V_B/d), with pressure for pure argon and nitrogen at 25, 70, and 110°C. Normalizing the breakdown voltage by the effective electrode gap accounts for thermal expansion effects and allows direct comparison across temperatures. For both gases, the dielectric strength increases with pressure, consistent with Paschen-type behavior. At elevated pressures, the increased gas density shortens the electron mean free path, limiting the energy that electrons can gain between collisions, and thereby requiring higher electric fields to initiate ionization [9, 10]. However, the increase is non-linear, with the rate of increase diminishing at higher pressures.

The influence of temperature on dielectric strength is comparatively less significant across the investigated pressure range. For nitrogen, a slight decrease in dielectric strength is observed as temperature increases from 25 to 110°C at all pressures. Argon exhibits a similar qualitative trend, with a marginally more pronounced temperature dependence at elevated pressures, although the absolute changes remain small and comparable for both gases. However, this behavior contrasts with previous studies conducted at much lower pressures [21, 22], where nitrogen showed a larger

relative decline in dielectric strength with temperature compared to argon. Importantly, at pressures of 101.3 and 2600 kPa, which are conditions most relevant to the fluidized bed fouling experiments conducted in our earlier work [7, 8], the dielectric strength for both gases shows negligible variation between 25 and 70°C, with overlapping error bars indicating no statistically significant temperature effect. This reduced temperature sensitivity could be attributed to the high-pressure regime investigated in this study, in which the electron mean free path is primarily governed by pressure rather than temperature, causing collision and ionization processes to be largely pressure dominated, with diminished influence of temperature on breakdown behavior.

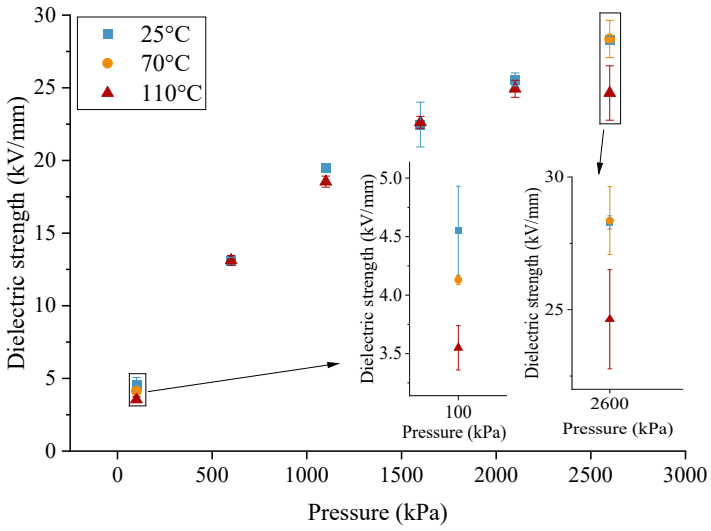

(a)

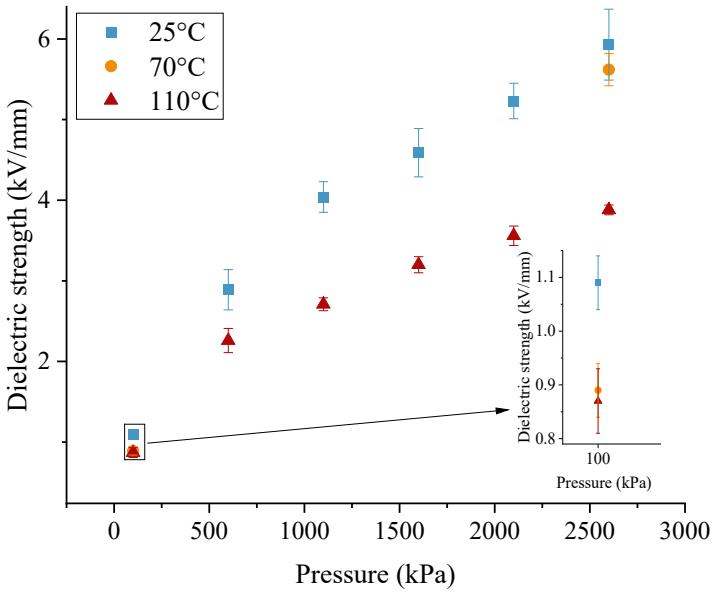

(b)

Figure 3.6: Variation in dielectric strength with different pressures and temperatures for (a) pure N_2 and (b) pure Ar.

Figure 3.7 presents the breakdown voltage data for pure nitrogen and pure argon plotted as a function of the pressure-gap product (*pd*), together with the corresponding theoretical Paschen

curves calculated using the gas-dependent constants *A* and *B* values from Table 3.1 [9]. The investigated *pd* range in this study lies beyond the Paschen minimum, where breakdown voltage is expected to increase with pressure. At lower *pd* values, the experimental breakdown voltages for pure nitrogen are in close agreement with the theoretical Paschen curve, but progressively deviate at higher values. A similar trend is observed for pure argon, although the deviation from the theoretical prediction is more pronounced across the investigated *pd* range. For both gases, the experimentally measured breakdown voltages are consistently lower than those predicted by the ideal Paschen relationship. The increasing deviation between experimental and theoretical breakdown voltages at higher *pd* values can be attributed to the limited validity range of the Paschen parameters *A* and *B* used in the theoretical calculations. These parameters are reported to be applicable over a reduced electric field range of approximately 100-600 V/Torr.cm, as listed in Table 3.1 [9]. However, in the present study, the reduced electric field values derived from the experimental data fall well below this range, spanning approximately 14-60 V/Torr.cm for nitrogen and 2-15 V/Torr.cm for argon over the investigated conditions. As pressure increases, the experimental *E/P* values progressively move away from the validity range of the literature parameters. The deviation is clearly more pronounced for argon, resulting in a larger deviation from the theoretical Paschen curve for argon compared to nitrogen. Nonetheless, the experimentally measured breakdown voltages for argon are consistent with values reported in the literature. For example, Norman et al. [11] measured the breakdown voltage of argon using spherical stainless-steel electrodes at pressures up to 1000 kPa and room temperature, and reported values that agree well with those obtained in the present study at comparable *pd* conditions.

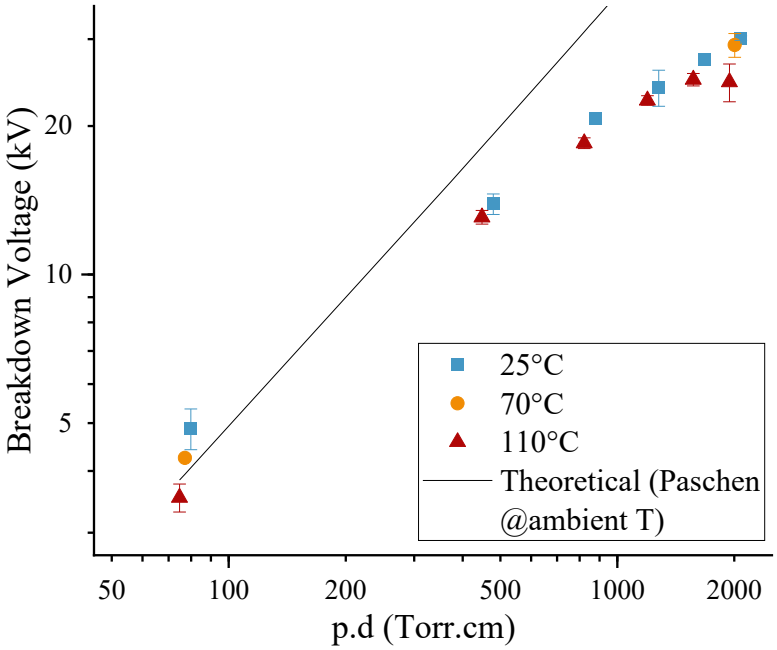

(a)

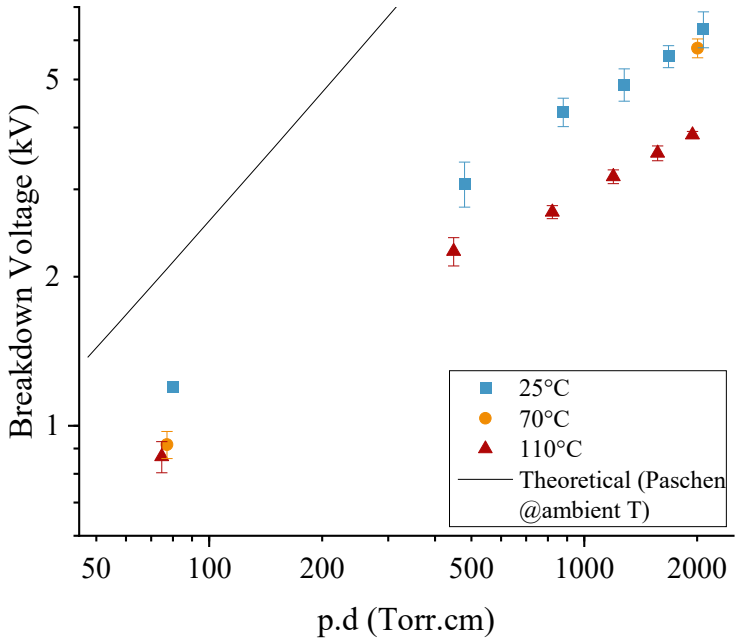

(b)

Figure 3.7: Experimental results plotted alongside the theoretical Paschen curve for (a) pure N_2 and (b) pure Ar.

Figure 3.8 shows the variation of dielectric strength of nitrogen and argon gas mixture as a function of argon concentration at 25, 70, and 110°C for pressures of 101.3 and 2600 kPa. At both pressures, a pronounced change in dielectric strength is observed as the gas composition transitions away from pure nitrogen or pure argon, indicating a strong sensitivity of breakdown behavior to even small additions of the additive gas species. This nonlinear, step-like deviation in dielectric strength from pure-gas behavior is particularly consistent with prior studies on Ar-N_2 gas mixtures [15-17], where small additive fractions have been shown to significantly alter breakdown behavior. Considering the conditions most relevant to industrial polyethylene fluidized bed reactor operation (2600 kPa and 70°C), changing the gas composition from pure nitrogen to 25 vol.% of argon reduced the dielectric strength by approximately 40%. This is quite promising since argon can only be added as an inert gas in the industrial reactors and in small concentrations. In contrast, the variation in dielectric strength among intermediate mixture compositions is comparatively modest, with a slight decrease observed as argon concentration increases. The sharp reduction in dielectric strength observed upon introducing argon into nitrogen can be attributed to the lower effective ionization threshold of argon atoms. This is because argon atoms are more readily ionized than nitrogen molecules and can facilitate the ionization process, thereby reducing the breakdown voltage of the mixture even at low argon concentrations. Conversely, the addition of nitrogen to argon increases dielectric strength relative to pure argon due to the introduction of additional energy-loss channels associated with nitrogen.

Moreover, the high-temperature measurements conducted between 25 and 70°C for gas mixtures containing 25 and 50 vol.% argon show no statistically significant change in dielectric strength with temperature, similar to the observation for the pure gases over the same temperature range. This is consistent with the earlier suggestion that, under the high-pressure conditions, dielectric strength might only be weakly sensitive to temperature within this interval.

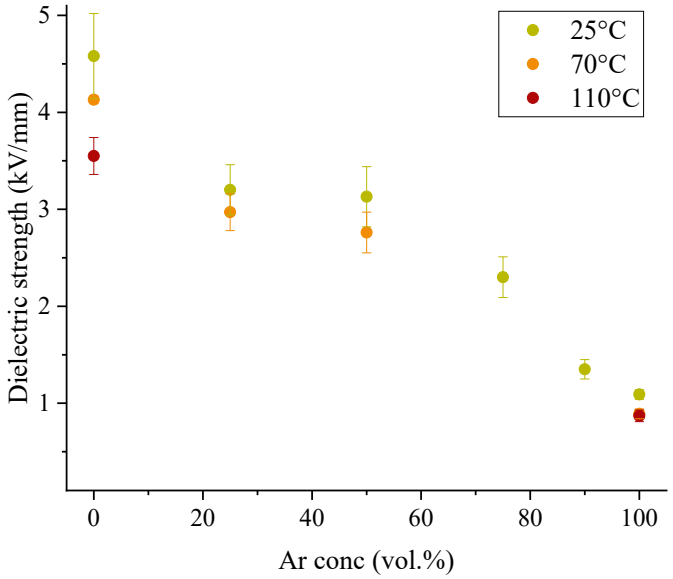

(a)

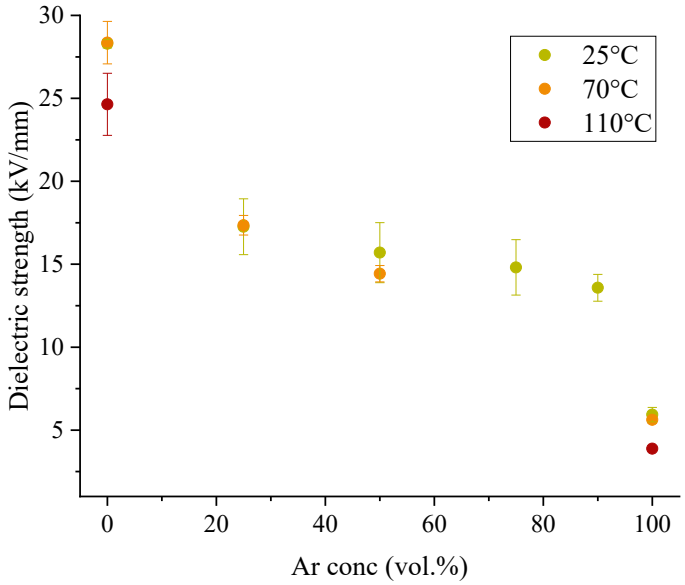

(b)

Figure 3.8: Argon-nitrogen gas mixture dielectric strength shown at different argon concentrations and temperatures, (a) 101.3 kPa and (b) 2600 kPa.

3.4 Conclusions

This study investigated the variation in dielectric strength of pure argon, pure nitrogen, and their binary mixtures across a range of compositions under elevated pressures and temperatures relevant to polyethylene gas-solid fluidized bed reactor operation. For both pure gases, dielectric strength increased with pressure in a non-linear manner, consistent with operation on the high *pd* branch of the Paschen curve, while deviations from classical Paschen predictions became more pronounced at higher pressures due to operation outside the validity range of literature Paschen parameters. Additionally, temperature effects on the gases' dielectric strength were comparatively small between 25 and 70°C at pressures of 101.3 and 2600 kPa. In the case of gas composition, small additions of argon gas caused substantial reductions in dielectric strength of the gas mixture at both pressures, while intermediate mixture compositions showed more gradual variations. Especially, changing the gas from pure nitrogen to even 25% argon at 2600 kPa and 70°C showed promising results, reducing the dielectric strength by almost 40% compared to pure nitrogen. Overall, this work provides experimentally validated dielectric strength data for Ar-N_2 systems under conditions that not only offer a mechanistic basis for the mitigation of electrostatic charge using argon in polyethylene fluidized bed reactors but also other triboelectric processes.

Acknowledgements

Financial support from Univation Technologies, LLC (USA) and the Natural Sciences and Engineering Research Council of Canada (NSERC) is acknowledged with gratitude.

References

[1] G. Hendrickson, “Electrostatics and gas phase fluidized bed polymerization reactor wall sheeting,” *Chemical Engineering Science*, vol. 61, no. 4, pp. 1041–1064, Feb. 2006, doi: 10.1016/j.ces.2005.07.029.

[2] T. M. Syed, G. M. Fernandes, N. Sridhar, and P. Mehrani, “Bench-scale tribocharging of polyethylene: Role of gas type, temperature and relative humidity,” *Journal of Electrostatics*, vol. 140, p. 104254, Mar. 2026, doi: 10.1016/j.elstat.2026.104254.

[3] T. Miura, “Observation of charge separation and gas discharge during sliding friction between metals and insulators,” *J. Phys.: Conf. Ser.*, vol. 646, p. 012057, Oct. 2015, doi: 10.1088/1742-6596/646/1/012057.

[4] X. Liu and S. Sundaresan, “The effect of gas on tribocharging of particles in a vibrated bed,” *Powder Technology*, vol. 401, p. 117272, Mar. 2022, doi: 10.1016/j.powtec.2022.117272.

[5] K. P. Brand, “Dielectric Strength, Boiling Point and Toxicity of Gases - Different Aspects of the Same Basic Molecular Properties,” *IEEE Trans. Elect. Insul.*, vol. EI-17, no. 5, pp. 451–456, Oct. 1982, doi: 10.1109/tei.1982.298489.

[6] H. Tao and J. Gibert, “Measuring gas discharge in contact electrification,” *Nat Commun*, vol. 14, no. 1, p. 8100, Dec. 2023, doi: 10.1038/s41467-023-43721-1.

[7] N. Sridhar and P. Mehrani, “Utility of argon as a static charge and wall fouling suppressant in atmospheric gas-solid fluidized beds,” *Powder Technology*, vol. 442, p. 119880, Jun. 2024, doi: 10.1016/j.powtec.2024.119880.

[8] N. Sridhar and P. Mehrani, “Utility of argon as a suppressant of triboelectrification in pressurized Gas-Solid fluidized beds,” *Chemical Engineering Science*, vol. 311, p. 121623, Jun. 2025, doi: 10.1016/j.ces.2025.121623.

[9] J. Lehr and P. Ron, *Foundations of Pulsed Power Technology*, 1st ed. Wiley, 2017. doi: 10.1002/9781118886502.

[10] J. M. Meek, J. D. Craggs, and J. M. Meek, Eds., *Electrical breakdown of gases*. in Wiley series in plasma physics. Chichester: Wiley, 1978.

[11] L. Norman, K. Silva, B. J. P. Jones, A. D. McDonald, M. R. Tiscareno, and K. Woodruff, “Dielectric Strength of Noble and Quenched Gases for High Pressure Time Projection Chambers,” 2021, doi: 10.48550/ARXIV.2107.07521.

[12] L. Trascinelli and K. L. Aplin, “Field electron emission in the atmospheric pressure range,” *Journal of Electrostatics*, vol. 127, p. 103867, Jan. 2024, doi: 10.1016/j.elstat.2023.103867.

[13] D. Berg, “The fundamentals of electric breakdown in gases,” in *1968 8th Electrical Insulation Conference*, Los Angeles, CA, USA: IEEE, Dec. 1968, pp. 53–55. doi: 10.1109/EIC.1968.7456101.

[14] A. F. Borkhari and K. Yasserian, “Influence of the hot filament on the electrical breakdown characteristics in the presence of Ar/N2,” *J Theor Appl Phys*, vol. 7, no. 1, p. 5, 2013, doi: 10.1186/2251-7235-7-5.

[15] B. Chiad, F. Kadhim, and A. Anber, “Study the Addition of Lab-Made Gas Mixing Unit with Varying of Inter-Electrode Distances on the Characterization of DC Magnetron Sputtering System,” *Open Access Library Journal*, vol. 04, no. 01, Art. no. 01, 2017, doi: 10.4236/oalib.1103269.

[16] O. F. Farag, M. M. Mansour, N. M. El-Sayed, and M. H. Elghazaly, “Mixing and cathode material effects on breakdown voltage of DC Ar glow discharge,” *Advances in App. Sci. R.*, vol. 4, no. 1, pp. 146–150, 2013.

[17] M. Radmilovic-Radjenovic, B. Radjenovic, M. Klas, A. Bojarov, and S. Matejˇcik, “The breakdown mechanisms in electrical discharges: the role of the field emission effect in direct current discharges in microgaps,” *Acta Phys. Slovaca*, vol. 63, no. 3, pp. 105–205, Jun. 2013.

[18] E. Sili and J. P. Cambronne, “A New Empirical Expression Of The Breakdown Voltage For Combined Variations Of Temperature And Pressure,” Mar. 2012, doi: 10.5281/ZENODO.1079916.

[19] G. Galli *et al.*, “Paschen’s Law in Extreme Pressure and Temperature Conditions,” *IEEE Trans. Plasma Sci.*, vol. 47, no. 3, pp. 1641–1647, Mar. 2019, doi: 10.1109/tps.2019.2896352.

[20] S. Uhm, S. J. Jung, and H. S. Kim, “Influence of gas temperature on electrical breakdown in cylindrical electrodes,” *Journal of the Korean Physical Society*, vol. 42, pp. S989–S993, Feb. 2003.

[21] R. Massarczyk, P. Chu, C. Dugger, S. R. Elliott, K. Rielage, and W. Xu, “Paschen’s law studies in cold gases,” *J. Inst.*, vol. 12, no. 06, pp. P06019–P06019, Jun. 2017, doi: 10.1088/1748-0221/12/06/P06019.

[22] A. V. Borodulina, O. V. Minakova, and S. L. Veber, “Breakdown Voltage in Argon, Nitrogen, and Sulfur Hexafluoride Gases As a Function of Temperature,” *Russ J Coord Chem*, vol. 48, no. 7, pp. 452–455, Jul. 2022, doi: 10.1134/S1070328422070028.

Chapter 4 Influence of Argon Gas Composition and Temperature on the Extent of Wall Fouling due to Static Charge in a Pressurized Gas-Solid Fluidized Bed

Talha Mukarram Syed, Poupak Mehrani

Department of Chemical and Biological Engineering, University of Ottawa,

161 Louise Pasteur, Ottawa, ON K1N 6N5, Canada

Manuscript to be submitted to the Journal of Powder Technology

Abstract

Electrostatic charging and resulting wall fouling continue to pose operational challenges in industrial polyethylene fluidized bed reactors. This study examined how the addition of argon at various concentrations and temperatures together influence particle charging and fouling behaviour in a pilot-scale polyethylene fluidized bed operated at 2600 kPa. Experiments were conducted with pure nitrogen, pure argon, and their binary mixtures (10-50 vol.% argon) at 25 and 68°C. An increase in argon concentration consistently reduced charge generation within the bulk particles and decreased both the mass and charge of the fouling layer, with argon achieving up to 85% and 70% reduction in fouling at 25 and 68°C, respectively. The higher temperature also decreased particle charging, although this effect weakened with increasing argon concentration. Notably, the elevated temperature promoted greater entrainment and reduced the charge carried by fines. Additionally, the wall fouling trends closely mirrored the measured dielectric strength of the gases under comparable conditions, reinforcing the role of gas breakdown in facilitating static charge dissipation. Overall, the results underline the strong static-mitigation capability of argon under industrially relevant operating conditions of polyethylene fluidized bed reactors.

Keywords: Fluidized bed, Polyethylene, Triboelectrification, Dielectric strength, Argon, Static mitigation

4.1 Introduction

Electrostatic charging is an inevitable phenomenon in gas-solid fluidization systems, arising from continuous particle-particle and particle-wall collisions. While often unavoidable, excessive charge accumulation in the fluidized bed can present serious operational challenges, including particle agglomeration, reactor wall fouling, and, in severe cases, electrostatic discharges that threaten process safety. In industrial operations, these problems reduce productivity and increase operating costs. The polyethylene industry provides well-documented examples where large-scale gas-phase polyethylene fluidized bed reactors experience static charge buildup that causes polyethylene and catalyst particles to adhere to the reactor wall. Due to the highly exothermic nature of the polymerization reaction, these fouled particles melt over time and form polymer "sheets". These sheets dislodge and obstruct the distributor plate and product lines, forcing unplanned reactor shutdowns. Despite numerous efforts to mitigate electrostatic charging in gas-solid fluidized beds, including polyethylene reactors [1-5], it remains a persistent issue, necessitating effective electrostatic mitigation strategies, especially under industrial operating conditions.

Several studies have investigated the influence of particle properties and operating conditions on charge generation and fouling in gas-phase polyethylene fluidized beds, including particle size distribution [6], humidity [7], gas velocity [8, 9], flow regime [10], operating pressure [8, 12] and temperature [8, 9, 13], gas type [14-16], and the addition of continuity additives [17]. Among these parameters, two factors have recently attracted growing attention, including the type of fluidizing gas and the operating temperature.

In the context of gas-solid fluidized beds, Mohsen et al. [13] examined the impact of temperature on charge generation and wall fouling in a pilot-scale polyethylene fluidized bed. They fluidized LLDPE resin as received from commercial reactors with a wide size distribution at 101.3 and 2600 kPa using nitrogen as the fluidizing gas. By increasing the operating temperature from 24 to 58°C, a reduction in wall fouling was observed at both 101.3 and 2600 kPa, coinciding with reduced charge generation; however, the magnitude of reduction was substantially greater at 2600 kPa. The reduced charge generation was linked to a decrease in the volume resistivity of polyethylene with increasing temperature, enabling enhanced charge leakage. Based on the stronger fouling and charge generation reduction observed at 2600 kPa, where smaller bubbles increase the frequency

of particle-particle contacts, the authors further concluded that temperature predominantly influences particle-particle interactions rather than particle-wall collisions. In a related work, Moughrabiah et al. [8] employed collision ball probes to measure the cumulative charge of 600 μm LLDPE particles at different axial locations in a pilot-scale fluidization column at 379 kPa. They reported that particle charge increased steadily over time at 20°C, but remained constant at 60°C, indicating suppressed charging at elevated temperatures. The same group later extended their study to binary mixtures of fine (25-50 μm) and large (425-600 μm) glass beads fluidized at 414 kPa across 20-75°C [12]. Their results confirmed that electrostatic charge decreased with temperature, and above 70°C, a polarity reversal was observed. Moreover, while the charge of entrained fines declined with increasing temperature, the mass flux of fines remained unchanged. Collectively, these studies suggest that higher temperature reduces electrostatic charging in fluidized beds primarily through enhanced charge leakage and influenced particle-particle collisions, with particularly strong effects on the charging of fines and entrained particles.

Following their previous study, Nimvari et al. [18] investigated the influence of temperature using bench-scale shake tests with LLDPE resin at 23 and 60°C in stainless-steel cups, including a configuration where the cup wall was coated with polyethylene particles. While no significant temperature effect was observed for the uncoated steel cup, a clear reduction in charge magnitude was reported for the coated configuration at elevated temperature. They also conducted resistivity measurements where a decline in the volume resistivity of polyethylene and nylon films at 60°C was observed, suggesting increased charge carrier mobility and enhanced charge leakage at higher temperatures. Additionally, Harris et al. [19] examined contact electrification between nylon and PTFE over a temperature range of 24-78°C under controlled humidity (42-44% RH) and observed an approximately 50% reduction in saturation charge with increasing temperature. This behaviour was linked to reduced surface moisture, which limited the availability of ion-transfer species at elevated temperatures. In contrast, Jantač et al. [20] studied triboelectrification of polyethylene particles and glass beads between 22 and 90°C and reported opposing trends, where charge increased for polyethylene particles but decreased for glass beads. The authors suggested that polymer softening and increased effective contact area may enhance charging in polyethylene, whereas charge leakage dominates in more conductive materials such as glass. Together, these studies highlight the mechanisms through which temperature influences triboelectric charging.

The influence of gas type on electrostatic charging in fluidized beds has also been explored by two prior studies. Hou et al. [14] compared charge generation in HDPE and glass beads fluidized with air, nitrogen, and argon. Their results demonstrated that argon reduced the charge-to-mass ratio (Q/m) of both particle types compared to air and nitrogen. However, charge analysis in that study was based on a single sampling port, which may not have captured the full extent of charging throughout the bed, and the resulting wall fouling was not quantified. Sridhar and Mehrani [15] provided a more comprehensive evaluation by measuring both charge generation and wall fouling while fluidizing LLDPE resin using nitrogen, argon, and their binary mixtures at 101.3 kPa in a stainless-steel column. They reported that replacing nitrogen with argon reduced wall fouling by 90%, while even a 10 vol.% addition of argon to nitrogen reduced fouling by approximately 50%. Interestingly, they also demonstrated that intermittent introduction of argon into a bed fluidized originally with nitrogen produced considerable fouling reduction.

This static mitigation ability of argon stems from its lower dielectric strength relative to other gases. For instance, under ambient conditions, argon's dielectric strength is roughly 0.6 kV/mm, compared with about 3.4 kV/mm for nitrogen [21]. This difference becomes especially important in triboelectric systems, where the dielectric strength of the surrounding gas limits the maximum charge attainable by a solid [22]. Matsuyama and Yamamoto [23, 24] combined experimental measurements and modeling to show that argon significantly reduced the impact charging of polymer particles such as PTFE, nylon, Delrin, and polystyrene compared to air. Their work examined the charge acquired by single particles impacting a metal plate, highlighting the role of the surrounding gas in limiting charge accumulation. Using a pin-and-disk configuration, Miura et al. [25, 26] directly visualized micro-gap discharges between metal-insulator and insulator-insulator contacts under different gases. They concluded that gas discharge events restrict the maximum charge attainable, with inert gases like argon, owing to their lower dielectric strength, being more effective in suppressing charging than nitrogen or air. Similar trends were reported by Zhang and Ciampi [27], who observed consistently lower triboelectric charging of solid carbon dioxide when rubbed against various materials in argon compared to air. In the case of gas-solid fluidized beds, this mechanism is explained by particles continuously colliding with other surfaces, where they get charged during contact, and as they separate, the potential between them increases. Once this potential surpasses the breakdown threshold of the fluidizing gas, gas ionization occurs. The ion-electron pairs that are generated during this process can dissipate the surface charge on

nearby surfaces [28]. Consequently, gases with lower dielectric strength, such as argon, undergo ionization more readily and dissipate charges at lower field strengths, leading to a lower saturation charge compared to nitrogen or air. This gas breakdown phenomenon is described by the Paschen law, which expresses the breakdown voltage as a function of the product of pressure (P) and electrode separation (d), as shown below [29]

$$V_B = \frac{Bpd}{\ln(Apd) - ln\left\{\ln\left(1 + \frac{1}{\gamma}\right)\right\}} \quad \text{(Eq. 4.1)}$$

Here, A and B are gas-specific constants, α represents the Townsend ionization coefficient, P is the operating pressure, and d is the electrode gap across which the breakdown voltage (V_B) is defined. According to this relation, dielectric strength increases with pressure until reaching a minimum, called the Paschen minimum, and then rises again [29]. This dependence of V_B on pressure has been confirmed through various studies for different gases, including helium, nitrogen, and argon [30, 31]. This implies that while argon's lower dielectric strength promotes charge dissipation, its effectiveness may diminish at elevated pressures where breakdown voltages increase. Temperature also plays an important role in modifying dielectric strength. Higher temperatures facilitate easier gas ionization, lowering the breakdown threshold and thereby further limiting the charge that particles can sustain. Several studies have confirmed this behaviour across different gases and electrode configurations. Uhm et al. [32], using cylindrical electrodes with air, nitrogen, and oxygen between 27 and 300°C, reported a consistent decrease in breakdown voltage for all gases with increasing temperature. Massarczyk et al. [31] observed a similar trend in a pin-plate setup for nitrogen, argon, neon, and xenon over -193 to 22°C, though the magnitude of the decline varied by gas, where, for instance, nitrogen had a much larger decline than argon at similar conditions. This was also shown by Borodulina et al. [33] using a parallel plates setup, where nitrogen's breakdown voltage dropped by roughly 50% between -193 to 27°C, compared to a 36% decline for argon over the same range. Likewise, Sili et al. [34] conducted breakdown voltage studies by varying temperature and pressure for a pair of stainless-steel electrodes in a Rogowski-plane electrodes configuration and demonstrated that the breakdown voltage of air decreased from about 3 kV to 1 kV as temperature increased from 50 to 100°C. Since these studies have shown that elevated temperature lowers gas dielectric strength, this mechanism could plausibly contribute to the reduction in charging and fouling observed in fluidized beds at higher temperatures [8, 13]. In

an earlier study presented in Chapter 3, we measured breakdown voltage for nitrogen, argon, and their binary mixtures at pressures up to 2600 kPa and temperatures ranging from 25 to 110°C. These measurements at 2600 kPa showed that introducing argon significantly reduced the breakdown voltage, with a decrease of approximately 40% for a 25 vol.% argon-nitrogen mixture compared to pure nitrogen. In contrast, temperature effects were more modest, where increasing the temperature from 25 to 70°C resulted in minimal changes in breakdown voltage for both pure gases and mixtures. However, between 25 and 110°C, argon exhibited a larger decline in breakdown voltage relative to nitrogen. This dataset provided quantitative insight into how gas composition and temperature influence dielectric strength under conditions directly relevant to polyethylene fluidized bed operation.

Despite these insights, the combined influence of argon concentration and temperature on the extent of charge generation and subsequent wall fouling under industrially relevant pressurized fluidization conditions has not been systematically investigated. In practice, polyethylene reactors operate at pressures of 1800-2600 kPa and temperatures between 70-110°C [2]. Hence, there is a need to study the effectiveness of argon in suppressing charge in polyethylene fluidized beds at these operating conditions. This motivates the present study, which examines the use of argon as a static mitigator in polyethylene fluidized beds at 2600 kPa and 68°C. The study analyzes charge generation, fouling mass, and fines behaviour across pure nitrogen, pure argon, and argon-nitrogen mixtures at 25°C and 68°C, and finally compares the fouling trends with the breakdown voltage trends for the gases under similar conditions. The results provide new insight into the combined effect of gas type and temperature in dictating electrostatic behaviour in polyethylene fluidized beds.

4.2 Materials and methodology

All experiments were conducted in a pilot-scale, pressurized gas-solid fluidization system (shown in Figure 4.1), extensively described in prior works from our group [11, 13, 16]. The system consisted of a 5 m high stainless-steel column with an inner diameter of 0.15 m. The column was equipped with a knife-gate valve at the bottom, modified with perforations to act as a distributor plate, and a filter bag attached at the outlet to capture entrained fines. Electrostatic charge measurements were performed using two electrically grounded Faraday cages connected to

Keithley 6514 electrometers. The top Faraday cage enclosed a filter bag to measure the cumulative charge of entrained fines, while the bottom cage collected the bulk and dislodged fouled particles.

The fluidization system operated in a closed loop, wherein the gas was introduced into the system at the start of the trial. The fluidization gases used were pure nitrogen, argon, and their binary mixtures containing 10, 25, or 50 vol.% argon. The mixtures were prepared by sequentially filling the fluidization column with the gases according to the required partial pressures. For instance, to prepare a 50% argon mixture at 2600 kPa, the system was initially filled up to 1300 kPa with nitrogen, after which argon was introduced until the final pressure of 2600 kPa was reached. The pure gases were supplied from gas cylinders with a 99.99% purity. Gas recirculation in the system was achieved by a centrifugal compressor with variable speed. An orifice plate meter situated downstream of the compressor measured the corresponding fluidizing gas flow rate. System pressure was monitored through a pressure transducer on the column. To achieve fluidization gas temperatures up to 68°C in the bed for this study, the apparatus was equipped with heating equipment, as shown in Figure 4.1. A plate heat exchanger using water at 90°C as the heating fluid was used after the compressor, followed by an inline electrical heater to directly heat the gas stream. Band heaters were wrapped over piping before the column inlet and around the column up to a height of 0.75 m. To minimize heat losses, the column and all pipelines were covered by thermal insulation. Gas temperature was monitored through two thermocouples, one located below the distributor plate (T_1) and the other (T_2) 0.75 m above it (0.35 m above the static bed height), as shown in Figure 4.1.

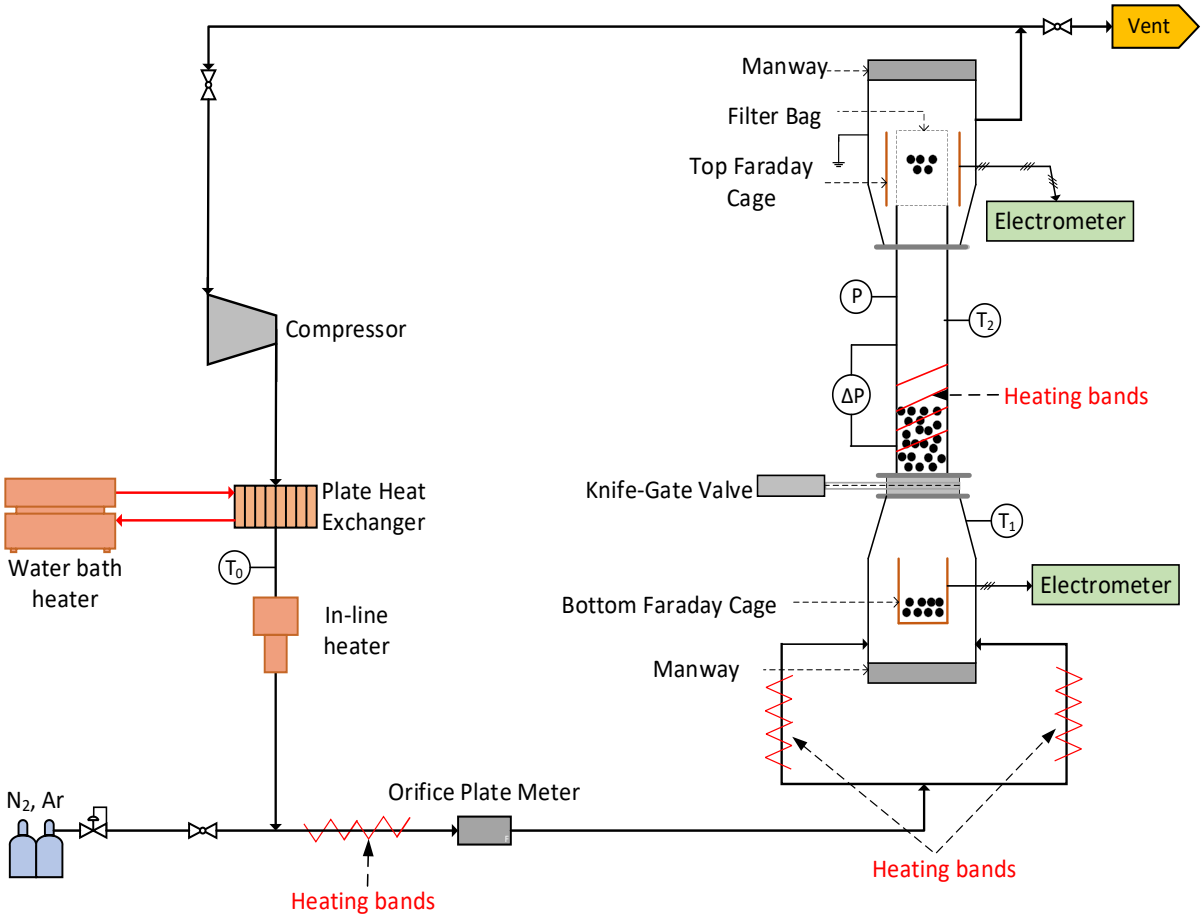

Figure 4.1: Schematic of the pilot-scale fluidization apparatus.

The minimum fluidization velocity (U_{mf}) for pure nitrogen and argon was determined experimentally at 2600 kPa by measuring the bed pressure drop across a range of gas velocities. For gas mixtures, U_{mf} was calculated as a weighted average of the individual values for nitrogen and argon according to their mixture composition. It should be noted that within the temperature range investigated in this study, the variation in U_{mf} and bed hydrodynamics was negligible. Before each trial, the system was continuously purged for 30 minutes with building air to eliminate any residual moisture and dust. A static bed height-to-column diameter (L/D) ratio of 2.7 was achieved for all trials. The particles had been neutralized to eradicate any initial charge and kept in an oven overnight to ensure moisture removal. The system was purged again, this time with the test gas through a pressurization-vent cycle, where the system was pressurized up to 100 kPa (gauge) with the test gas and vented to the atmosphere. After purging, the system was filled with the designated test gas at 2600 kPa. For high-temperature experiments, all heaters were turned on at this stage, and the gas was circulated at a velocity below U_{mf} until the thermocouple located below the

distributor plate (T_1) reached 70°C. This defined the preheating stage, which lasted about 45 minutes. Once the preheating was complete, the gas velocity was increased to $1.5U_{mf}$, initiating bubbling fluidization. Each run was conducted for 60 min, and the fluidization was monitored through the LabVIEW engineering program. A new batch of particles was used for each trial. Each operating condition was repeated at least twice to verify reproducibility. Due to the large scale of the apparatus, precise temperature control was challenging; hence, the bed temperature was maintained within a tolerance of ± 2°C.

During fluidization, entrained fines were captured in the top filter bag, and their cumulative charge was recorded by the top Faraday cage. At the end of the run, the compressor was shut down, and the system was depressurized. The bulk particles were released into the bottom Faraday cage by opening the knife-gate valve, where their net charge and mass were recorded. After this, the fouled particles on the column wall were dislodged into the bottom Faraday cage by inserting a narrow tube from the top of the column, with compressed air flowing through it. These fouled particles were classified into three regions based on their location in the column (as shown in Figure 4.2): (1) Fouling-Bottom (distributor plate to the static bed height), (2) Fouling-Top (static bed height to ~0.40 m above it), and (3) Freeboard (rest of the column up to the exit). From the particles collected in each region (bulk, fouling, and fines), samples were taken for size distribution analysis using the Malvern Mastersizer 2000.

The solid particles used in this study were the linear low-density polyethylene (LLDPE) resin, directly received from a commercial polyethylene reactor. The properties of the resin are summarized in Table 4.1.

Table 4.1: Properties of the LLDPE resin used.

Size distribution (μm)	20-1500
Sauter mean diameter (μm)	920
Particle density (kg/m³)	918

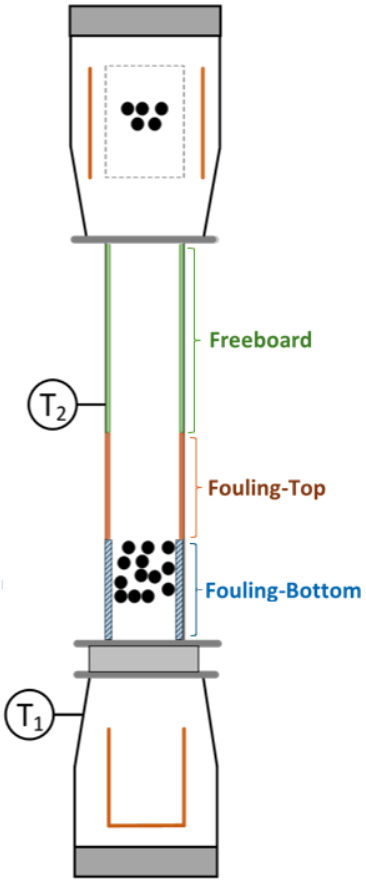

Figure 4.2: Schematic of the fluidization column depicting the fouling classification regions.

4.3 Results and discussion

Accurate control of the gas temperature in the bed was essential for the quantitative evaluation of the temperature influence on the solids' electrostatic behaviour inside the fluidized bed. Figure 4.3 presents the temperature profiles from the two thermocouples. To reiterate, T_1 is the thermocouple located below the distributor plate, and T_2 is the one placed above the static bed height. The sharp increase in T_1 at the start of the experiment corresponds to the onset of fluidization at $1.5U_{mf}$. Thereafter, both thermocouples exhibited stable readings throughout the 60-minute fluidization period. A consistent offset between T_1 and T_2 was observed, with T_2 reporting lower values. This difference arises because the hot gas below the distributor plate experiences cooling as it passes through the distributor plate. Accordingly, the actual gas temperature within the bed is best represented through T_2 since the bed quickly reaches thermal equilibrium beyond the distributor plate. The temperature profile indicates that the bed temperature approached the target temperature within 15 minutes of fluidization and remained stable for the remainder of the run.

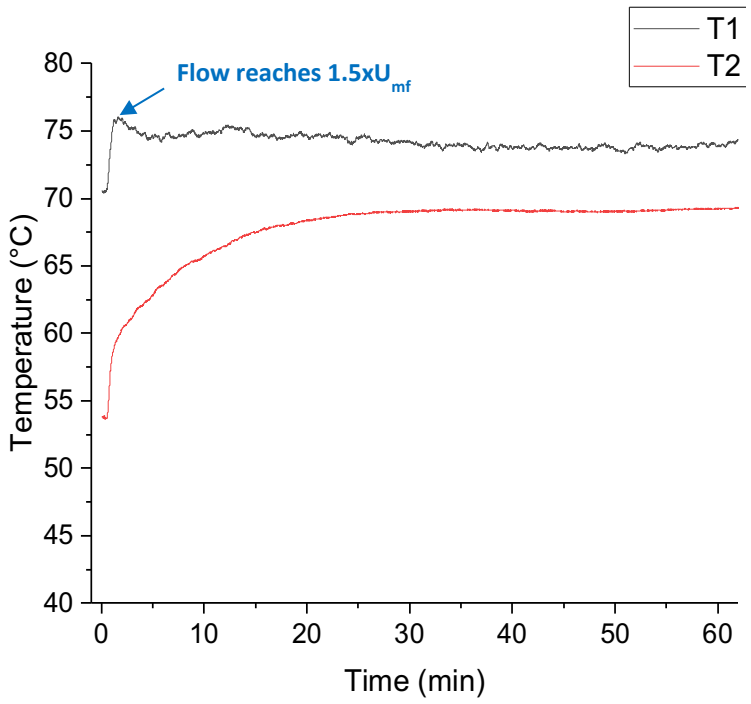

Figure 4.3: Temperature profile during a typical high-temperature fluidization trial. T_1 was measured below the distributor plate, and T_2 was measured above the static bed height.

Figure 4.4 illustrates an example of the charge-to-mass ratio (*Q/m*) for the particles collected from different regions in the column after fluidization. The particles exhibit bipolar charging, where the bulk and bottom fouling particles acquired a net negative polarity, and the top and freeboard fouling particles were positively charged. Among the negatively charged particles, the bulk that had a dp_{50} of 600 µm displayed only small *Q/m* magnitudes, whereas, in contrast, the bottom fouling particles with a dp_{50} of 300 µm acquired much larger negative *Q/m* values, strong enough for electrostatic forces to overcome drag and gravity, enabling their adhesion to the column wall. The net positively charged top and freeboard fouling particles with $dp_{50} < 300$ µm, also exhibited higher *Q/m* magnitudes, allowing their adhesion to the column wall while being entrained. These trends for *Q/m* and dp_{50} were consistent across all repeated trials and various operating conditions tested.

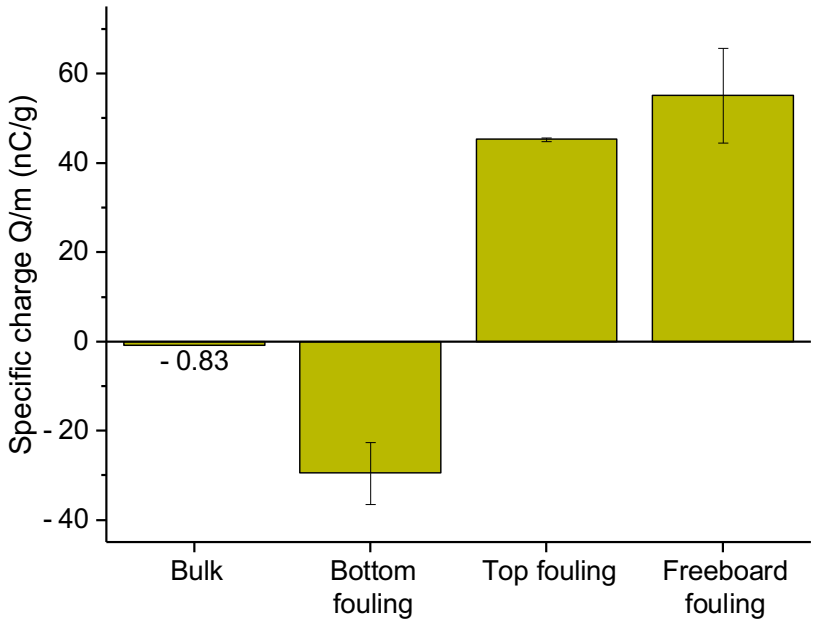

Figure 4.4: Example of charge distribution for LLDPE particles collected from different regions in the fluidized bed after fluidization with 10% argon gas at 2600 kPa and 68°C.

The observed charge bipolarity is consistent with our previous high-pressure fluidization studies [11, 13]. The polarity trend originates from the difference in work function between polyethylene (~5.3 eV) and stainless-steel (~4.5 eV) column wall [35], which favors electron transfer from the wall to the particles, imparting a negative charge to the bulk. This induces an image (opposite) charge on the column wall, leading to the accumulation of a first fouled layer of negatively charged particles. Subsequently, this layer attracts the positively charged particles from the bulk, forming a secondary layer. Smaller positively charged particles escape the bed due to their lower terminal velocities than the fluidization gas velocity, either as entrained fines or adhere to the wall in the top and freeboard regions if their Q/m is sufficiently high. It is speculated that the small particles became positively charged due to particle-particle collisions within the bed. Consequently, the escape of these particles would leave a net negative charge polarity behind that would also contribute to the migration of negatively charged particles towards the wall.

The degree of charge generation in the bulk particles under different gas compositions at 25 and 68°C is presented in Figure 4.5. As mentioned earlier, the bulk particles consist of particles large enough not to adhere to the wall and drop freely from the column after fluidization. These particles carried a negative polarity across all conditions. Pure nitrogen showed the largest negative specific

charge, while pure argon reduced the specific charge by almost 90%. At both temperatures, the mixtures followed a decreasing trend where an increase in argon concentration lowered the *Q/m* magnitude. In contrast, the influence of temperature on bulk *Q/m* for each gas type was less consistent. In most cases, a slight decrease in bulk *Q/m* when going from 25 to 68°C was observed. In others, such as 10% and 50% argon mixture gases, the bulk *Q/m* at 68°C was found to be slightly higher in magnitude.

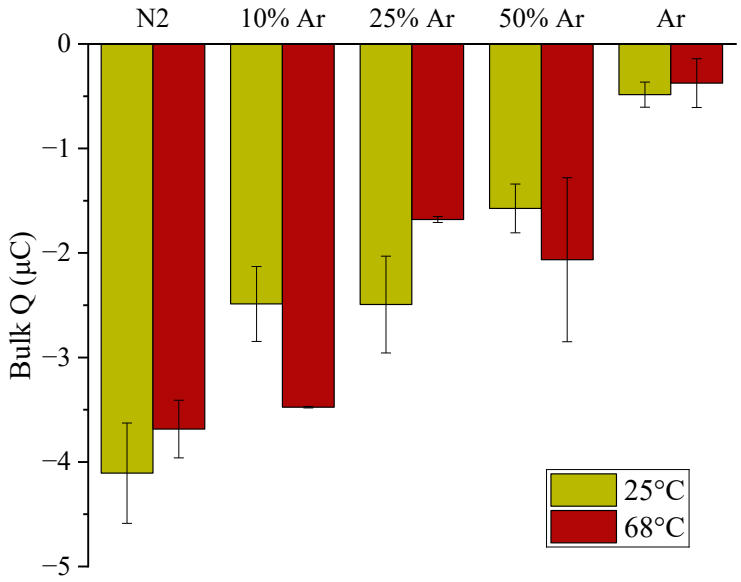

Figure 4.5: Specific charge (*Q/m*) of bulk particles at various temperatures and fluidization gases.

Figure 4.6 shows the mass and corresponding net charge of the particles collected from the bottom fouling region. A clear decline was observed between fouling charge and mass with an increase in the concentration of argon. At 25°C, the fouling mass declined by approximately 85% in pure argon as compared to pure nitrogen, while depicting a 70% decline in argon compared to nitrogen at 68°C. Even small concentrations of argon were effective, with a 10% argon mixture producing a 35% decline from pure nitrogen at 25°C. On average, the elevation of temperature also decreased fouling mass and charge for all gas types. At 68°C, for pure nitrogen, the fouling mass decreased by 55%, whereas for pure argon, the reduction was less pronounced, with a 20% decline. The charge trends closely followed the mass trends, with nitrogen producing the highest negative charges and argon the lowest, while mixtures exhibited intermediate values. Statistical analysis using Analysis of Variance (ANOVA) confirmed that both gas composition and temperature had a significant effect on fouling behavior (*P*-values found to be < 0.05), with the exception of

temperature effects in the 50% argon mixture, which was not statistically significant at the 95% confidence level. Overall, both increased temperature and argon concentration reduced bottom fouling mass and charge; however, the temperature influence diminishes with the increase in argon concentration.

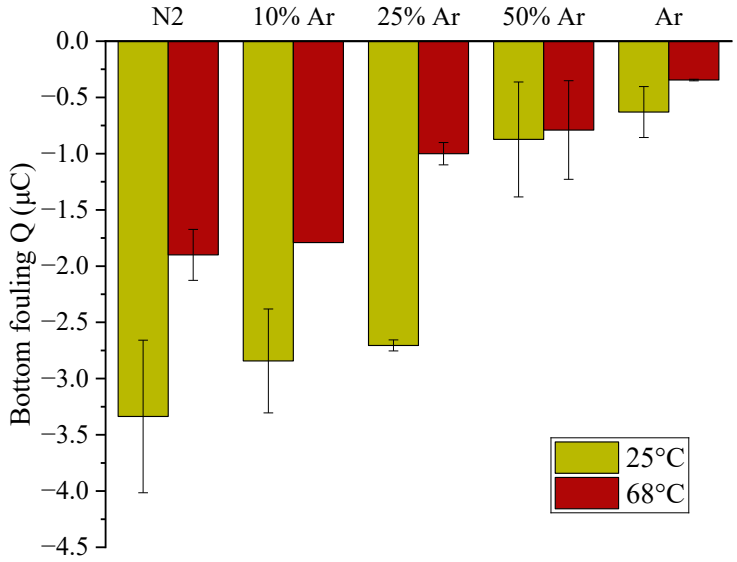

(a)

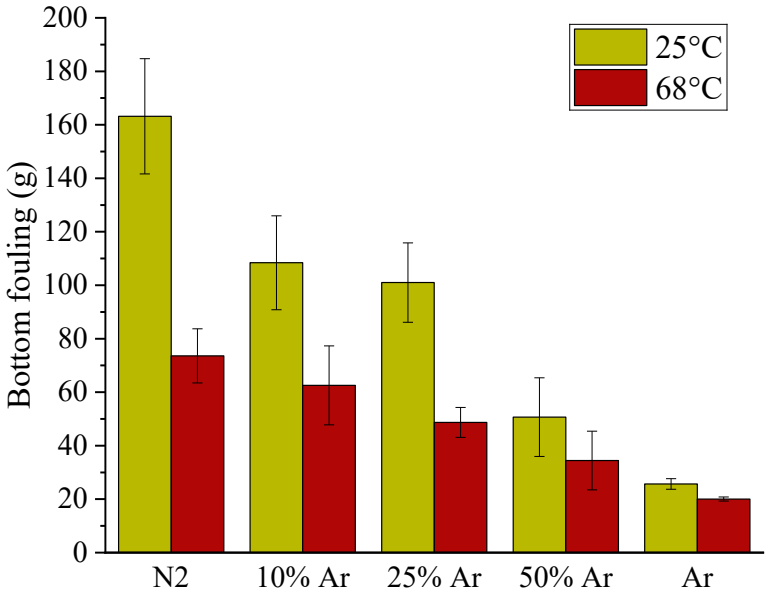

(b)

Figure 4.6: Bottom fouling (a) net charge, and (b) mass collected at different temperatures and fluidization gases.

The influence of argon concentration in suppressing charging and subsequent fouling in the fluidized bed, as seen in Figure 4.5 and Figure 4.6, was to be through argon's role in promoting gas discharge events that neutralize particle surface charge. As the particle-particle and particle-wall collisions and separations take place, local contact potentials develop between particles that behave as small electrodes in this case. When these potentials exceed the breakdown voltage of the surrounding gas, the gas ionizes and discharges, and the resulting charge carriers from the ionization process neutralize charge on the contacting surfaces. Because argon has a lower breakdown voltage than nitrogen, the threshold for gas breakdown is much lower, and hence, it was anticipated that the particle surface charge neutralization occurs more readily, limiting the maximum surface charge a particle can retain. To verify this effect, we conducted measurements of the breakdown voltage of nitrogen, argon, and their mixtures at the operating temperatures and pressures used in this study (details presented in Chapter 3). Figure 4.7 overlays the bottom wall fouling with the dielectric strength measured at 2600 kPa, plotted as a function of argon concentration at 25 and 68°C. A clear correspondence is observed between the variation in dielectric strength and the measured fouling behavior, particularly at 68°C, where both quantities decrease systematically with increasing argon concentration. This agreement verifies that gas breakdown behavior is closely linked to the extent of charge accumulation and subsequent wall fouling in the fluidized bed.

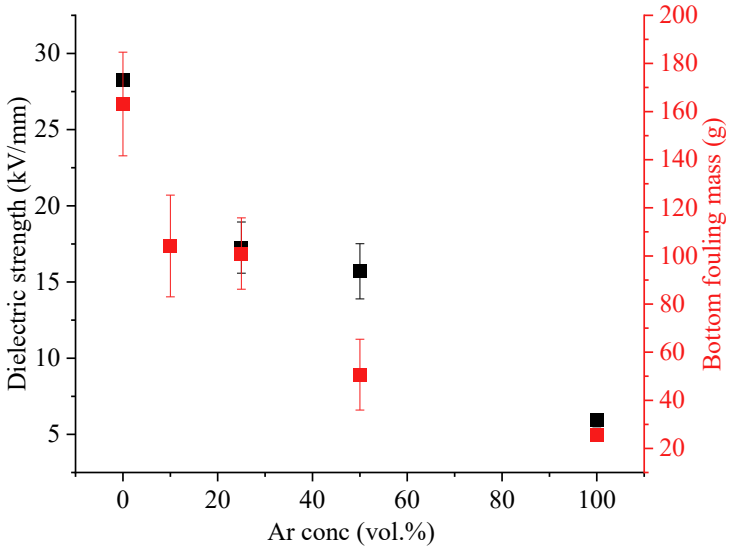

(a)

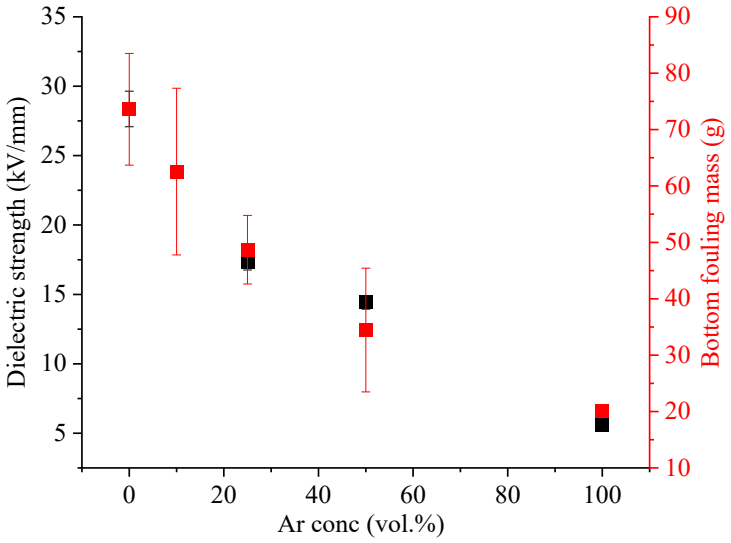

(b)

Figure 4.7: Bottom fouling mass and dielectric strength at different argon concentrations, measured at 2600 kPa and temperatures of (a) 25°C, and (b) 68-70°C.

This explains why pure argon produced the lowest charging and fouling levels in the bed (Figure 4.5 and Figure 4.6). The mixture trials followed this expectation, with fouling and charging values falling between the pure nitrogen and pure argon extremes. A small addition of argon (e.g., 10 vol.%) was already effective in reducing fouling, while higher fractions continued the trend. The trend of the particles' charge and fouling decline suggests that argon concentration governs the frequency of discharge events in the bed. This behaviour of decline in charge and fouling with increasing argon concentration was observed at both 25 and 68°C.

As mentioned by Nimvari et al. [13], one of the proposed mechanisms for the effect of temperature on charge generation involves changes in material resistivity. With increasing temperature, the volume resistivity of polyethylene decreases, allowing charge carriers to move more freely across the particle surface or through the bulk, resulting in easier charge leakage [36, 37]. At the same time, increasing temperature also reduces the dielectric strength of the gas, which would make discharge events easier. Combined, these factors could contribute to limiting the saturation charge accumulated by the particles in the fluidized bed. However, it was noted that the degree of the temperature influence was less pronounced than that of varying the argon concentration. One possible explanation is that the decline in dielectric strength, when switching from nitrogen to argon, is far greater than the reduction caused by increasing the temperature for a specific gas (e.g., nitrogen). Furthermore, the influence of temperature also diminished as the concentration of argon gas increased. This may be because argon itself is effective in suppressing most of the charge generated due to its low dielectric strength, such that elevating temperature as an additional factor has less impact under argon-rich conditions, where less charge is generated to begin with. Another possibility is that, while the dielectric strength of argon may decrease within this temperature range, the reduction may not be large enough to noticeably limit fouling. In contrast, even a modest decline in the dielectric strength of nitrogen could have a more pronounced effect, since nitrogen permits a much higher level of charge buildup to begin with.

The particles' fouling distribution along the column wall was also analyzed. Figure 4.8a shows the distribution of collected mass (fouling and fines) across the fluidization column for all gas compositions at 25 and 68°C. The results indicate that the dominant changes in fouling mass with increasing argon concentration and temperature occurred in the bottom fouling region, while the top, freeboard, and fines remained relatively constant. This is because the particle-particle and particle-wall collisions are most frequent in the bottom fouling region. Since the prerequisite for argon’s effect due to gas discharge is collision and subsequent separation of particles, the bottom region provided the most opportunity for charge mitigation through gas discharge. In this environment, particles of different sizes interact with one another. Smaller particles that gained a positive charge in collisions with larger particles are carried up with the gas, where the collision frequency is reduced. As a result, the top and freeboard regions showed weak dependence on argon concentration, consistent with our earlier findings [15, 16]. With fewer collisions in these regions, opportunities for gas breakdown and charge dissipation are limited, reducing argon’s effectiveness.

However, a closer comparison between the temperatures depicts that the combined top, freeboard, and fines mass was slightly higher at 68°C than at 25°C for each gas type. This suggests that although increasing temperature suppresses particle adhesion in the bottom fouling region, it simultaneously facilitates entrainment of smaller, charged particles, which either accumulate in the upper regions of the column or are collected as entrained fines in the filter bag. The particle size distribution of the collected fines, shown in Figure 4.8b, supports these findings as well. At the higher temperature, the fines had a larger size distribution with their dp_{50} shifted upwards compared to 25°C.

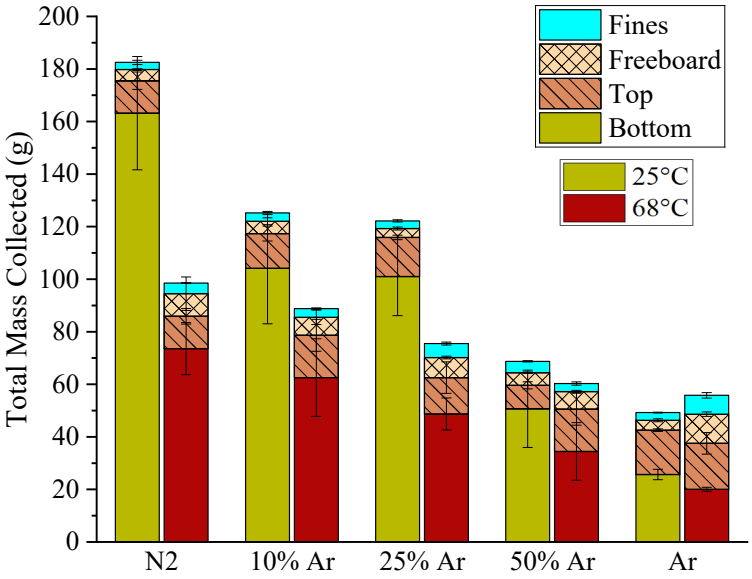

(a)

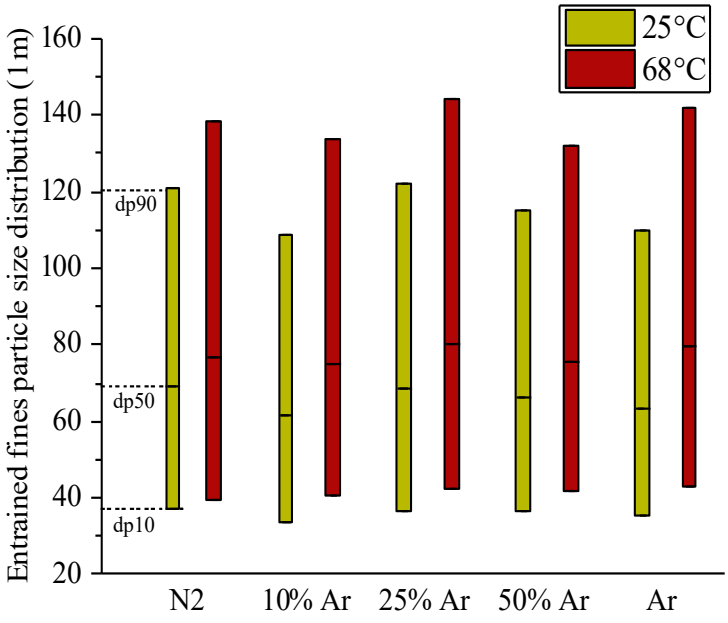

(b)

Figure 4.8: (a) Total mass collected (fouling and fines) and (b) particle size distribution of entrained fines at different temperatures and fluidization gas types.

Evaluating the cumulative charge profile of fines collected during fluidization is important, as the departure of these particles leaves behind a net charge in the bed, which can affect the extent to which particles migrate towards the column wall. As seen in Figure 4.9, at the onset of fluidization, marked by the first vertical dashed line, a sharp decline in charge was observed. This corresponds to the rapid entrainment of the smallest particles, which had not yet undergone many collisions

and initially carried a negative charge. As fluidization continued, the cumulative charge increased steadily as fine particles that had undergone collisions and acquired positive charges were entrained. This increase continues until a plateau is reached, marking the stop of gas flow at the end of 60-minute fluidization. A clear distinction was observed between the two temperatures for different gas types, where in the high-temperature trials, the rise in charge was less pronounced, and the slope was less compared to ambient temperature trials. This demonstrates that elevated temperature reduced the extent of fines charging, while argon concentration further influenced the magnitude of charge gained by the fines during the run.

As shown in Figure 4.8a and Figure 4.9, the amount of fines collected did not decline in high-temperature trials, but the charges they carried were substantially lower compared to ambient conditions. In addition, the size distribution for collected fines (Figure 4.8b) shifted upward at higher temperature, indicating that the particles that would normally remain in the bed as top or freeboard fouling particles were more easily entrained since their surface charge was reduced. This observation aligns with Nimvari et al. [13], who suggested that temperature predominantly affects particle-particle collisions. The decline in fines charge and the upward shift in size distribution support this, since smaller particles gain positive charge primarily through collisions with larger ones.

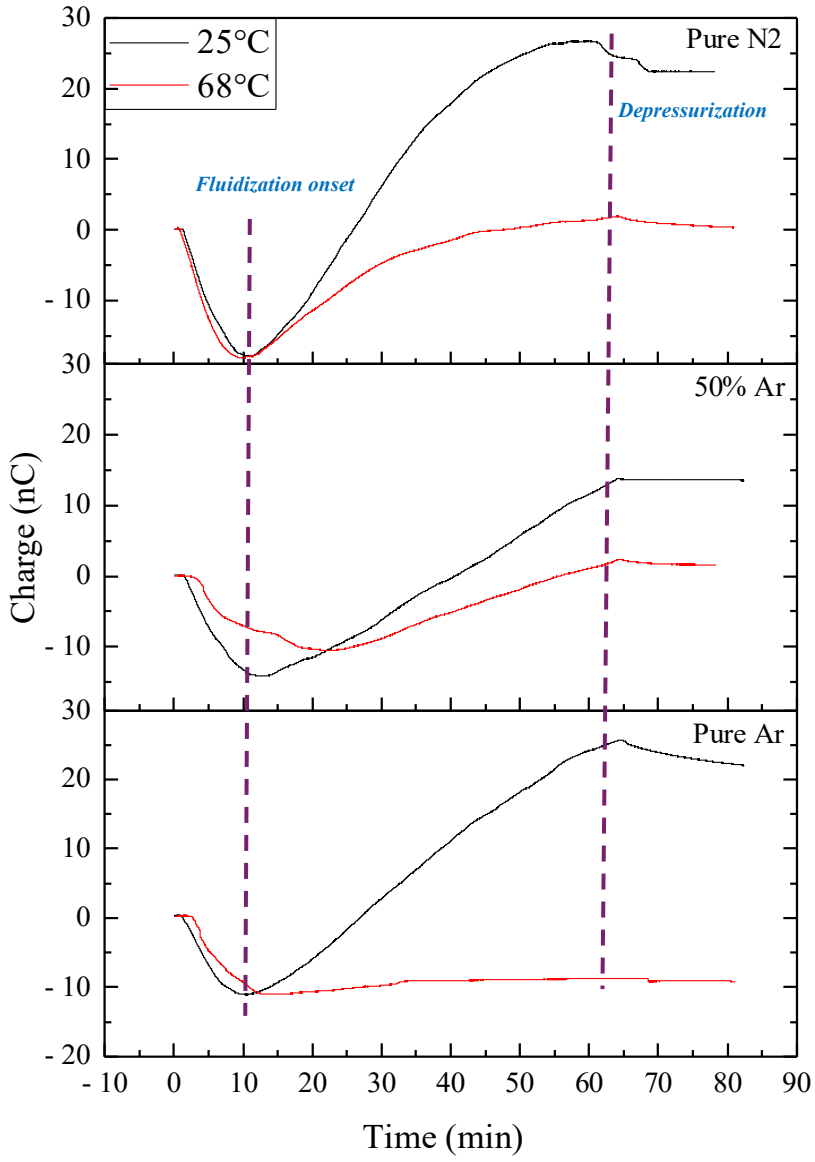

Figure 4.9: Entrained fines cumulative charge profile during 60 minutes of fluidization for pure nitrogen, 50% argon, and pure argon at two different temperatures.

Images of the fouling layer were taken after fluidization, following removal of the bulk particles and before collecting the adhered layers, to visualize deposition along the inner wall. Figure 4.10 shows representative examples for different gases at 25°C and 68°C. In the case of pure nitrogen (Figure 4.10a, Figure 4.10b), the fouled layer appeared thick and multilayered, with visible breakage along the surface. By contrast, the 50% argon (Figure 4.10c, Figure 4.10d) and pure argon (Figure 4.10e, Figure 4.10f) trials produced thinner, monolayer deposits, indicating a visible reduction in fouling.

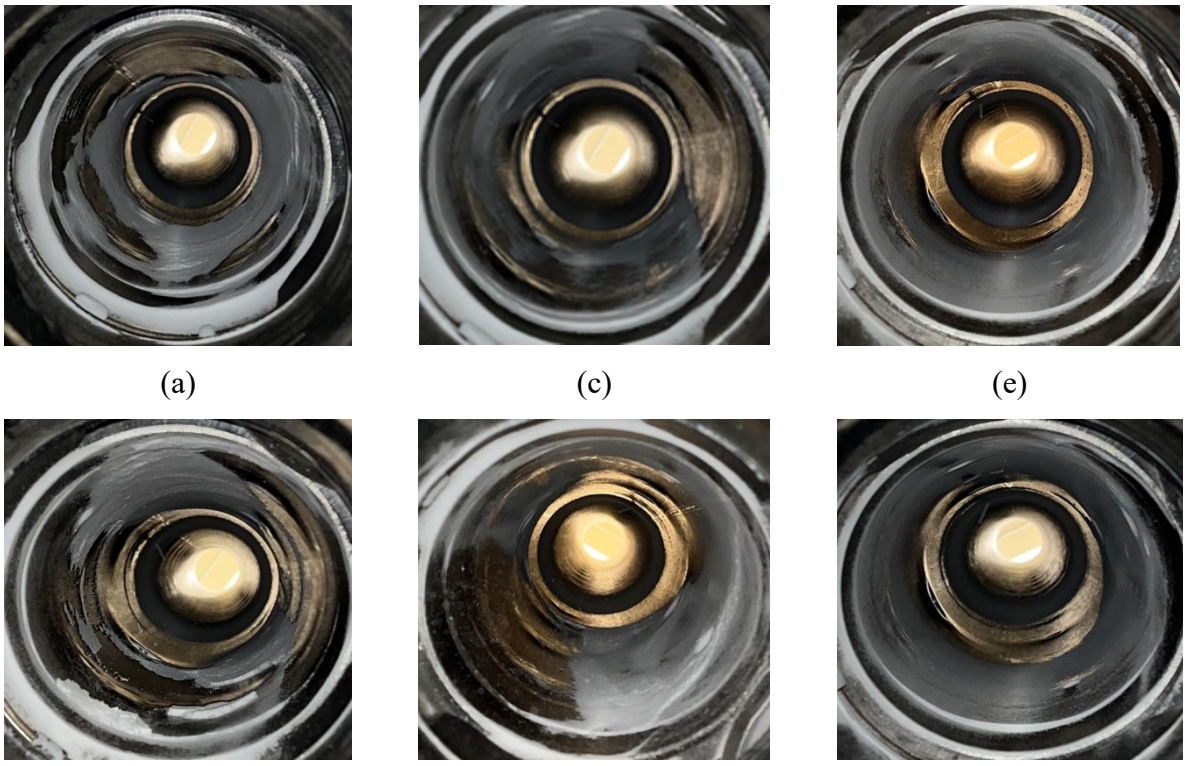

Figure 4.10: Images of the wall fouling layer taken post-fluidization for (a) N_2 at 25°C, (b) N_2 at 68°C, (c) 50% Ar at 25°C, (d) 50% Ar at 68°C, (e) Ar at 25°C, and (f) Ar at 68°C.

4.4 Conclusions

This study builds on previous work from our group by examining the combined influence of argon gas and its concentration, as well as fluidization temperature (25 and 68°C), on static buildup and column wall fouling in pressurized (2600 kPa) polyethylene fluidized beds. The results showed that increasing both argon concentration and temperature reduced the specific charge of bulk particles as well as the charge and mass of bottom fouling. However, the influence of temperature diminished as the argon fraction increased. Elevated temperature also promoted slightly greater particle entrainment, with the strongest effect observed in the charge carried by fines. The reduction in charging and fouling with argon was verified to be due to its lower dielectric strength, which facilitates gas ionization and, in turn, the fluidizing particles' surface charge neutralization. In contrast, the increases in temperature effect may be linked to a combination of decreased material resistivity and reduced gas dielectric strength, though the extent of the latter remains uncertain.

Acknowledgements

This work was financially supported by Univation Technologies, LLC, and the Natural Sciences and Engineering Research Council of Canada (NSERC).

References

[1] T. G. Song, A. S. Rhee, and G. G. Lowder, "Method for reducing sheeting and static charged during polymerization of ethylene polymers," 5391657

[2] M. G. Goode, D. M. Hasenberg, T. J. McNeil, and T. E. Spriggs, "Method for reducing sheeting during polymerization of alpha-olefns," 4803251

[3] B. D. Fulks, S. P. Sawin, C. D. Aikman, and J. M. Jenkins, "Process for reducing sheeting during polymerization of alpha-olefins," 4532311

[4] Goode, M. G. Williams, C. C. Hussein, F. D. McNeil, and T. J. Lee, "Static control in olefin polymerization," 6111034

[5] P. Mehrani, M. Murtomaa, and D. J. Lacks, "An overview of advances in understanding electrostatic charge buildup in gas-solid fluidized beds," Journal of Electrostatics, vol. 87, pp. 64–78, Jun. 2017, doi: 10.1016/j.elstat.2017.03.005.

[6] A. Sowinski, A. Mayne, and P. Mehrani, "Effect of fluidizing particle size on electrostatic charge generation and reactor wall fouling in gas–solid fluidized beds," Chemical Engineering Science, vol. 71, pp. 552–563, Mar. 2012, doi: 10.1016/j.ces.2011.11.031.

[7] A. Giffin and P. Mehrani, "Effect of gas relative humidity on reactor wall fouling generated due to bed electrification in gas-solid fluidized beds," Powder Technology, vol. 235, pp. 368–375, Feb. 2013, doi: 10.1016/j.powtec.2012.10.037.

[8] W. O. Moughrabiah, J. R. Grace, and X. T. Bi, "Effects of pressure, temperature, and gas velocity on electrostatics in gas−solid fluidized beds," Ind. Eng. Chem. Res., vol. 48, no. 1, pp. 320–325, Jan. 2009, doi: 10.1021/ie800556y.

[9] A. Sowinski, L. Miller, and P. Mehrani, "Investigation of electrostatic charge distribution in gas–solid fluidized beds," Chemical Engineering Science, vol. 65, no. 9, pp. 2771–2781, May 2010, doi: 10.1016/j.ces.2010.01.008.

[10] D. Song and P. Mehrani, "Comparison of electrostatic charge generation in gas-solid fluidized beds in turbulent versus pre-turbulent flow regime," Powder Technology, vol. 319, pp. 426–433, Sep. 2017, doi: 10.1016/j.powtec.2017.07.013.

[11] D. Song and P. Mehrani, "Effect of fluidization pressure on electrostatic charge generation of polyethylene particles," Ind. Eng. Chem. Res., vol. 56, no. 49, pp. 14716–14724, Dec. 2017, doi: 10.1021/acs.iecr.7b04056.

[12] T. A. Alsmari, J. R. Grace, and X. T. Bi, "Effects of superficial gas velocity and temperature on entrainment and electrostatics in gas–solid fluidized beds," Chemical Engineering Science, vol. 123, pp. 49–56, Feb. 2015, doi: 10.1016/j.ces.2014.10.003.

[13] M. I. Nimvari, A. Sowinski, and P. Mehrani, “Effect of temperature on triboelectrifcation of polyethylene particles in a pilot-scale pressurized gas-solid fluidized bed,” Powder Technology, vol. 405, p. 117524, Jun. 2022, doi: 10.1016/j.powtec.2022.117524.

[14] J. Hou et al., “Effect of gas properties and wall materials on particle charging in gas–solid fluidized beds,” Can J Chem Eng, vol. 101, no. 1, pp. 244–255, Jan. 2023, doi: 10.1002/cjce.24568.

[15] N. Sridhar and P. Mehrani, “Utility of argon as a static charge and wall fouling suppressant in atmospheric gas-solid fluidized beds,” Powder Technology, vol. 442, p. 119880, Jun. 2024, doi: 10.1016/j.powtec.2024.119880.

[16] N. Sridhar and P. Mehrani, “Utility of argon as a suppressant of triboelectrification in pressurized Gas-Solid fluidized beds,” Chemical Engineering Science, vol. 311, p. 121623, Jun. 2025, doi: 10.1016/j.ces.2025.121623.

[17] M. Taghavivand, A. Sowinski, and P. Mehrani, “Triboelectric effects of continuity additives and a silica catalyst support on polyethylene fluidized bed wall fouling,” Chemical Engineering Science, vol. 245, p. 116882, Dec. 2021, doi: 10.1016/j.ces.2021.116882.

[18] M. I. Nimvari, A. Sowinski, and P. Mehrani, “Investigation of the role of temperature on contact electrification of polyethylene particles,” Powder Technology, vol. 433, p. 119236, Jan. 2024, doi: 10.1016/j.powtec.2023.119236.

[19] I. A. Harris, M. X. Lim, and H. M. Jaeger, “Temperature dependence of nylon and PTFE triboelectrification,” Phys. Rev. Materials, vol. 3, no. 8, Aug. 2019, doi: 10.1103/physrevmaterials.3.085603.

[20] S. Jantač, L. Konopka, and J. Kosek, “Experimental study of triboelectric charging of polyethylene powders: Effect of humidity, impact velocity and temperature,” Advanced Powder Technology, vol. 30, no. 1, pp. 148–155, Jan. 2019, doi: 10.1016/j.apt.2018.10.017.

[21] K. P. Brand, “Dielectric strength, boiling point and toxicity of gases - different aspects of the same basic molecular properties,” IEEE Trans. Elect. Insul., vol. EI-17, no. 5, pp. 451–456, Oct. 1982, doi: 10.1109/tei.1982.298489.

[22] D. J. Lacks and T. Shinbrot, “Long-standing and unresolved issues in triboelectric charging,” Nat Rev Chem, vol. 3, no. 8, pp. 465–476, Jul. 2019, doi: 10.1038/s41570-019-0115-1.

[23] T. Matsuyama and H. Yamamoto, “Charge relaxation process dominates contact charging of a particle in atmospheric conditions,” J. Phys. D: Appl. Phys., vol. 28, no. 12, pp. 2418–2423, Dec. 1995, doi: 10.1088/0022-3727/28/12/005.

[24] T. Matsuyama and H. Yamamoto, “Charge-relaxation process dominates contact charging of a particle in atmospheric condition: II. The general model,” J. Phys. D: Appl. Phys., vol. 30, no. 15, pp. 2170–2175, Aug. 1997, doi: 10.1088/0022-3727/30/15/008.

[25] T. Miura, “Observation of charge separation and gas discharge during sliding friction between metals and insulators,” J. Phys.: Conf. Ser., vol. 646, p. 012057, Oct. 2015, doi: 10.1088/1742-6596/646/1/012057.

[26] T. Miura and I. Arakawa, “Gas discharge caused by triboelectricity around a contact during friction between insulators,” *IEEE Trans. Dielect. Electr. Insul.*, vol. 14, no. 3, pp. 560–565, Jun. 2007, doi: 10.1109/TDEI.2007.369513.

[27] J. Zhang and S. Ciampi, “The position of solid carbon dioxide in the triboelectric series,” *Aust. J. Chem*., vol. 72, no. 8, p. 633, 2019, doi: 10.1071/CH19239.

[28] H. Tao and J. Gibert, “Measuring gas discharge in contact electrification,” Nat Commun, vol. 14, no. 1, p. 8100, Dec. 2023, doi: 10.1038/s41467-023-43721-1.

[29] J. Lehr and P. Ron, *Foundations of Pulsed Power Technology*, 1st ed. Wiley, 2017. doi: 10.1002/9781118886502.

[30] X. Liu, Z. Shi, G. Yang, and X. Yan, “Experimental study on breakdown voltage of high pressure and high temperature helium gas between parallel electrodes,” *Annals of Nuclear Energy*, vol. 110, pp. 1224–1231, Dec. 2017, doi: 10.1016/j.anucene.2017.08.031.

[31] R. Massarczyk, P. Chu, C. Dugger, S. R. Elliott, K. Rielage, and W. Xu, “Paschen’s law studies in cold gases,” J. Inst., vol. 12, no. 06, pp. P06019–P06019, Jun. 2017, doi: 10.1088/1748-0221/12/06/P06019.

[32] S. Uhm, S. J. Jung, and H. S. Kim, “Influence of gas temperature on electrical breakdown in cylindrical electrodes,” *Journal of the Korean Physical Society*, vol. 42, pp. S989–S993, Feb. 2003.

[33] A. V. Borodulina, O. V. Minakova, and S. L. Veber, “Breakdown voltage in argon, nitrogen, and sulfur hexafluoride gases as a function of temperature,” *Russ J Coord Chem*, vol. 48, no. 7, pp. 452–455, Jul. 2022, doi: 10.1134/S1070328422070028.

[34] E. Sili and J. P. Cambronne, “A new empirical expression of the breakdown voltage for combined variations of temperature and pressure,” Mar. 2012, doi: 10.5281/ZENODO.1079916.

[35] D. Song and P. Mehrani, “Mechanism of particle build-up on gas-solid fluidization column wall due to electrostatic charge generation,” *Powder Technology*, vol. 316, pp. 166–170, Jul. 2017, doi: 10.1016/j.powtec.2017.01.031.

[36] M. S. Khalil and A. Gastli, “Dependence of DC insulation resistivity of polyethylene on temperature and electric field,” in *IEEE 1997 Annual Report Conference on Electrical Insulation and Dielectric Phenomena*, Minneapolis, MN, USA: IEEE, pp. 296–299. doi: 10.1109/ceidp.1997.634617.

[37] J. R. Dennison and J. Brunson, “Temperature and electric field dependence of conduction in low-density polyethylene,” *IEEE Trans. Plasma Sci*., vol. 36, no. 5, pp. 2246–2252, Oct. 2008, doi: 10.1109/tps.2008.2003443.

Chapter 5 Conclusions and Future Work

Electrostatic charge generation is a common occurrence in gas-solid systems due to repeated particle-particle and particle-surface collisions. In industrial solids handling and processing operations, this triboelectric charging can become a persistent challenge. A prominent example is gas-phase polyethylene production, where a catalytic gas-solid fluidized bed reactor is used for ethylene polymerization, and significant charge generation arises from frequent particle contacts within the bed with each other and with the reactor wall. In this environment, triboelectric charging promotes particle agglomeration and wall adhesion of highly charged particles, leading to operational issues. Wall fouling is particularly problematic because the polymerization reaction is exothermic, due to which the adhered particles can melt over time and form sheets that may detach and obstruct product or gas lines, necessitating shutdowns and maintenance with substantial operational cost. Hence, this thesis focused on evaluating an approach to reduce electrostatic charge accumulation and particle fouling in gas-solid fluidized beds. Although the study is centered on the gas-phase polyethylene fluidization process, the insights gained are relevant to a wider range of gas-phase processes in which particle charging arises from contact electrification.

Accordingly, this thesis examined the static mitigation effects of argon gas in a gas-phase polyethylene fluidized bed under industrially relevant operating conditions. Gas dielectric strength measurement, bench-scale shake tests, and gas-solid fluidization experiments were conducted to develop a systematic understanding of how argon breakdown characteristics affect charge accumulation and wall fouling in polyethylene gas-solid fluidized beds.

5.1. Conclusions

Bench-scale shake tests were used to assess electrostatic charge accumulation on LLDPE resin in different gaseous environments and temperatures. Single-particle and multiple-particle shake tests were employed to simulate charging arising from particle-wall and particle-particle interactions within the fluidized bed, respectively. At both 23 and 65°C (± 2.5°C), argon consistently resulted in lower saturation charge levels compared to nitrogen, supporting the hypothesis that gases with lower dielectric strength promote more frequent charge neutralization. However, increasing temperature led to a significant reduction in accumulated charge for nitrogen (35% in the single-particle and 50% in the multiple-particle tests), whereas the corresponding change for argon was

not statistically significant. The overall reduction in charge with temperature was attributed to enhanced charge dissipation, associated with a lower gas breakdown threshold and decreased polyethylene resistivity. The results from this study further indicated that temperature predominantly influenced particle-particle interactions rather than particle-wall contacts under shake-test conditions. The contrasting temperature effect observed between nitrogen and argon motivated a focused investigation into how dielectric strength varies with temperature for these gases, and whether gas breakdown behavior could explain the differences in charge accumulation observed at the bench scale.

A gas breakdown voltage measurement device was designed and fabricated in-house. The device included a high-pressure chamber that housed two parallel plate electrodes, one grounded and one connected to a high-voltage power supply. The chamber included band heaters and insulation to accommodate measurements at temperatures as high as 110°C. Dielectric strength measurements were performed for nitrogen, argon, and their binary mixtures over pressures from atmospheric up to 2600 kPa and temperatures of 25, 70, and 110°C (± 2°C). For all gases, dielectric strength increased with increasing pressure up to 2600 kPa, with argon consistently exhibiting a lower dielectric strength than nitrogen across all testing conditions. With respect to temperature, dielectric strength changed minimally between 25 and 70°C for all gases. The relatively weak dependence of dielectric strength on temperature between 25 and 70°C suggests that dielectric strength alone might not fully account for the pronounced temperature effects observed in nitrogen during the bench-scale charge accumulation experiments. However, when tested at 110°C for pure nitrogen and argon, a decrease relative to 25°C was observed. The magnitude of this decline varied between gases, with argon exhibiting a larger relative reduction in dielectric strength than nitrogen across the investigated pressure range. Binary argon-nitrogen mixtures showed intermediate behavior, with a reduction in dielectric strength of approximately 40% for 25 vol.% argon compared to pure nitrogen at 2600 kPa, while changes among intermediate mixture compositions were modest. Overall, this work provides experimentally validated dielectric strength data for Ar-N_2 systems under industrially relevant conditions. Additionally, the dielectric strength data produced in this study contribute to filling an important gap in the literature at elevated temperatures and pressures and can be used as a reference for future studies.

Gas-solid fluidization experiments built on the findings of the preceding studies to examine the combined effects of argon concentration and fluidization temperature (25 ± 2°C and 68 ± 2°C) on electrostatic charge buildup and column wall fouling in pressurized (2600 kPa) LLDPE fluidized beds. The results showed that increasing both argon concentration and temperature reduced charge generation and the extent of wall fouling within the bed, however, the influence of temperature diminished as the argon fraction increased. This diminished sensitivity to temperature under argon-rich conditions mirrors the bench-scale observations and suggests that argon is already effective at suppressing a large fraction of the electrostatic charge due to its low dielectric strength, such that elevating temperature provides limited additional benefit when less charge is generated to begin with. Under operating conditions of 2600 kPa and 68°C, the use of pure argon as the fluidizing gas reduced wall fouling by approximately 70% compared to nitrogen. Binary argon-nitrogen mixtures were also effective, with the addition of 25 vol.% argon resulting in an approximately 30% reduction in wall fouling at 68°C, and higher argon fractions producing progressively greater mitigation. Notably, the decrease in wall fouling with increasing argon content closely followed the dielectric strength trends of the gases, highlighting the importance of gas ionization in enabling surface charge neutralization of the fluidizing particles.

Overall, the findings of this thesis establish that argon is an effective electrostatic charge suppressor in polyethylene fluidized beds under industrially relevant temperature and pressure conditions. Additionally, binary mixtures of argon and nitrogen offer a practical balance between performance and gas consumption, making them particularly attractive for industrial applications where complete gas replacement may not be feasible.

5.2. Future Work

While this thesis demonstrates the effectiveness of argon and argon-nitrogen mixtures in mitigating electrostatic charging and fouling in polyethylene fluidized beds, further experimental work is recommended to extend and refine these findings:

1. Dielectric strength measurements could be performed for argon-nitrogen gas mixtures at 110°C, particularly at low argon concentrations below 25 vol.%. This recommendation is motivated by the significant decrease observed for the pure gases when the temperature was increased from 25 to 110°C. Building on these

measurements, future gas-solid fluidization experiments at temperatures close to 110°C could help determine whether the enhanced gas breakdown behavior at higher temperatures leads to further reductions in electrostatic charge accumulation and wall fouling. Furthermore, this could allow argon concentrations lower than 25 vol.% to achieve a comparable mitigation effect to that observed at 68°C.

2. This study focused on nitrogen, argon, and their binary mixtures; however, industrial gas-phase polyethylene reactors primarily operate with a range of process gases, including ethylene and other hydrocarbon comonomers (for instance, butene), and in some cases, hydrogen, which is used in polyethylene reactors to control polymer molecular weight. Given that these gases exhibit a wide range of dielectric strengths (e.g., 1.6 kV/mm for hydrogen and greater than 3.8 kV/mm for most hydrocarbons [1]), future work could extend to the following dielectric strength measurements, contingent on the feasibility and safe implementation of these gases in a laboratory environment.
    i. mixtures containing small concentrations of hydrogen with nitrogen, since hydrogen has a low dielectric strength and is already being used in some reactors, it could potentially have a similar static mitigation effect as argon; and
    ii. argon-based mixtures with the process gases, including ethylene.
3. The charge mitigation observed with argon is closely linked to gas ionization and the generation of charge carriers that facilitate surface charge neutralization. Building on this mechanism, future studies could explore alternative methods to enhance charge carrier generation within the gas phase, such as passive corona discharge techniques. In a study by Shoyama et al. [2], a passive electrostatic elimination cap fitted with grounded needle electrodes was installed on a silo and shown to neutralize charged polymer powders through localized corona discharge during solids handling. Similar approaches may provide supplementary pathways for electrostatic charge dissipation in gas-solid systems, provided their feasibility and safe implementation under industrial operating conditions are carefully evaluated.

References

[1] K. P. Brand, “Dielectric strength, boiling point and toxicity of gases - different aspects of the same basic molecular properties,” *IEEE Trans. Electr. Insul*., vol. EI-17, no. 5, pp. 451–456, Oct. 1982, doi: 10.1109/tei.1982.298489.

[2] M. Shoyama, Y. Osada, and C. Kwangseok, “Electrostatic neutralization of loading powder using pipe-end cap with needle electrodes,” in *2024 IEEE Industry Applications Society Annual Meeting (IAS)*, Phoenix, AZ, USA: IEEE, Oct. 2024, pp. 1–5. doi: 10.1109/IAS55788.2024.11023794.